PRESSURE- AND RATE- TRANSIENT ANALYSIS OF THE SIMULATED SINGLE AND MULTI-FRACTURED HORIZONTAL WELLS DRILLED IN SHALE GAS RESERVOIRS

A THESIS SUBMITTED TO
THE GRADUATE SCHOOL OF NATURAL AND APPLIED SCIENCES
OF
MIDDLE EAST TECHNICAL UNIVERSITY

BY

TURAL JAFARLI

IN PARTIAL FULFILLMENT OF THE REQUIREMENTS
FOR
THE DEGREE OF MASTER OF SCIENCE
IN
PETROLEUM AND NATURAL GAS ENGINEERING

SEPTEMBER 2013

Approval of the thesis:

PRESSURE- AND RATE- TRANSIENT ANALYSIS OF THE SIMULATED SİNGLE AND MULTI-FRACTURED HORIZONTAL WELLS DRILLED IN SHALE GAS RESERVOIR

submitted by **TURAL JAFARLI** in partial fulfillment of the requirements for the degree of **Master of Science in Petroleum and Natural Gas Engineering, Middle East Technical University** by,

Prof. Dr. Canan Özgen _____
Dean, Graduate School of **Natural and Applied Sciences**

Prof. Dr. Mahmut Parlaktuna _____
Head of Department, **Petroleum and Natural Gas Engineering**

Asst. Prof. Dr. Çağlar Sınayuç _____
Supervisor, **Petroleum and Natural Gas Engineering, Dept. METU**

Examining Committee Members:

Prof. Dr. Mahmut Parlaktuna _____
Petroleum and Natural Gas Engineering Dept., METU

Asst. Prof. Dr. Çağlar Sinayuç _____
Petroleum and Natural Gas Engineering Dept., METU

Can Sungu Bakiler, M.Sc. _____
Petroleum and Natural Gas Engineering Dept., METU

Asst. Prof. Dr. Ismail Durgut _____
Petroleum and Natural Gas Engineering Dept., METU

Dr. Sevtaç Bülbül _____
Petroleum Research Center, METU

Date: 26.09.2013

I hereby declare that all information in this document has been obtained and presented in accordance with academic rules and ethical conduct. I also declare that, as required by these rules and conduct, I have fully cited and referenced all material and results that are not original to this work.

Name, Last Name: Tural Jafarli

Signature:

ABSTRACT

PRESSURE- AND RATE- TRANSIENT ANALYSIS OF THE SIMULATED SINGLE AND MULTI-FRACTURED HORIZONTAL WELLS DRILLED IN SHALE GAS RESERVOIRS

Jafarli, Tural
M.Sc., Department of Petroleum and Natural Gas Engineering
Supervisor: Asst. Prof. Dr. Çağlar SINAYUÇ

September 2013, 139 pages

Nowadays, the bigger portion of produced oil and gas come from conventional resources all over the globe and these resources are being depleted in a severe manner. Over the past decade, the combination of horizontal drilling and hydraulic fracturing has allowed access to large volumes of shale gas that were previously uneconomical to produce. In recent years, they are seriously considered as supplementary to the conventional resources although these reservoirs cannot be produced at an economic rate or cannot produce economic volumes of oil and gas without assistance from massive stimulation treatments, special recovery processes or advanced technologies.

The vast increase in demand for petroleum and gas has encouraged the new technological development and implementation. With the directional drilling technology, it is possible to make use of highly deviated wellbores, extended reach drilling, horizontal wells, multilateral wells etc. Along with the technology itself simulation, reservoir characterization and the ability of future production prediction makes the development of unconventional resources a lot easier.

In this study, pressure and rate transient analysis techniques developed for hydraulically fractured reservoirs were applied for shale gas reservoirs to understand the applicability of those methods on unconventional systems. Pressure transient analysis is based on the analysis of the pressure which changes over time with variation of the fluid flow rate. For the particular analysis, fluid allowed to flow for a limited time, then well is closed and the pressure behavior is monitored and recorded in order to analyze the data. Rate transient analysis refers to production data analysis which utilizes similar concept to pressure transient analyses. It is similar to drawdown test where this drawdown period is equal to producing life of a particular field, where the flow periods are interrupted by shut-in periods, with less frequent data acquisition which is why the data quality for the analysis is not as good as for pressure transient analysis. Schlumberger Eclipse 300 simulation model was used to model the shale gas reservoir. Two commercial software tools – Saphire (Kappa) and F.A.S.T. (Fekete) that are used in petroleum engineering were applied to analyze the data. Advanced analytical models (F.A.S.T.) developed

for horizontal multi-fractured reservoirs showed some good results; however it still doesn't clear what are the actual flow regime conditions under different fracture stage and flowing conditions. In general those tools analyze the data to match either linear, bilinear or boundary dominated flow conditions. For that reason, in order to clearly understand flow regimes, rate normalized pressure derivative function was adopted along with the corrected pseudo-time function. As a result of this straight line analysis - flow regimes, fracture and reservoir permeabilities, fracture half length, fracture conductivity parameters were found under different fracture stage and flowing conditions. Under constant rate producing conditions, for single fracture case we obtained – fracture linear, elliptical, radial and late time effects, however for multi-fracture example, elliptical flow regime was masked due to close fracture spacing and additionally compound linear flow parallel to hydraulic fractures were exhibited. Under constant bottom-hole pressure producing conditions, for single fracture case we obtained pseudo-steady state flow showing pressure depletion in the stimulated reservoir region, radial flow, boundary dominated flow conditions, while for multi-fracture case we additionally observed compound linear flow regime.

Keywords: Shale Gas, Horizontal Wells, Hydraulic Fracturing, Pressure Transient Analysis, Rate Transient Analysis

ÖZ

ŞEYL GAZ RESERVUARLARINA AÇILAN YAPAY TEKLİ VE ÇOK ÇATLAKLI YATAY KUYULARDA BASINÇ- VE DEBİ- GEÇİCİ ANALİZİ

Jafarli, Tural
Yüksek Lisans, Petrol ve Doğal Gaz Mühendisliği
Tez Yöneticisi: Asst. Prof. Dr. Çağlar SINAYUÇ

Eylül 2013, 139 sayfa

Tüm dünyada üretilen petrol ve gazın büyük bir miktarı geleneksel kaynaklardan sağlanmaktadır ve bu kaynaklar hızla tükenmektedir. Son on yılda yatay sondaj ve hidrolik çatlatma eskiden çıkarılması ekonomik olmayan büyük miktarda şeyl gazin üretimine olanak tanımıştır. Son yıllarda şeyl gaz, simulasyon, özel üretim artırma işlemleri ve gelişmiş teknoloji olmadan düşük ekonomik oranlarda üretilebilmesine rağmen geleneksel kaynaklara ek olarak görülmektedir.

Petrol ve doğal gaz üretiminde artan talep yeni teknolojilerin gelişimine ve uygulamasına teşvik etmektedir. Yönlü sondaj teknolojisi ile yüksek derecede sapan, erişimi uzayan sondaj, yatay kuyular ve çoklu yanal kuyular ve bunların benzerlerinden yararlanmak mümkündür. Gelişmiş teknolojiye ek olarak rezervuar karakterizasyonu ve üretimin tahmini metodları geleneksel olmaya kaynakların üretimini kolaylaştırmaktadır.

Bu çalışmada, hidrolik çatlak durumları için geliştirilen analiz teknikleri geleneksel olmayan sistemlerde bu yöntemlerin uygulanabilirliği anlamak için şeyl gaz rezervuar simülasyonu için uygulanmıştır. Geçici basınç analizi petrolun akış hızı varyasyonu ile zamanla değişen basınç analizine dayanmaktadır. Bu analiz için, kuyunun sınırlı bir süre için akmasından sonra, verileri analiz etmek için daha sonra kapatılır, basınç davranışı izlenir ve kaydedilir. Geçici debi analizi bir üretim analizi olup, geçici basınç analizi ile aynı benzer bir kavram kullanmaktatır. Bu düşüş dönemine benzer analizdir ve bu düşüş donemi sahanın tüm akış süresine eşitdir, daha az sıklıkla veri toplama ve kuyuların sık-sık kapanması yüzünden akışın durdurulması nedeniyle verilerin kalitesi geçici basınç analizi kadar iyi değildir. Schlumberger Eclipse 300 simülasyon modeli şeyl gaz sahasını modellemek için kullanılmıştır. Iki ticari yazılımları - Saphire (Kappa) ve petrol mühendisliği kullanılan F.A.S.T. (Fekete) verileri analiz uygulanmıştır. Yatay çok çatlaklı rezervuar için geliştirilmiş gelişmiş analitik modeller (F.A.S.T.) bazı iyi sonuçlar ortaya koydu, ancak yine de farklı çatlak sayısı ve üretim koşulları altında gerçek akış rejimi tanımlanmasını sağlamıyor. Genel olarak bu yazılımlar doğrusal, çift doğrusal ve sınır hakim akış koşullarında verileri eşleştirme üzerine kurulmuşdur. Bu nedenle, akış rejimlerinin açık bir şekilde tanımlanması için üretim üzerine normalize edilmiş basınç türev fonksiyonu ve düzeltilmiş yalancı zaman fonksionları kullanılmıştır. Bu doğrusal hat analizleri sonucunda - akış rejimleri, çatlak ve rezervuar geçirgenlikleri, yarım çatlak uzunluğu ve çatlak geçirgenliği - farklı çatlak sayısı ve üretim koşulları altında bulunmuştur. Sabit debide üretim koşulları altında, tek çatlaklı

saha için - çatlak doğrusal, eliptik, radyal ve geç zamanlı efektler, ancak çok çatlaklı örnek için - eliptik akış rejimi hidrolik çatlakların yakın aralığı nedeniyle gizlenmiştir ve ayrıca çok-çatlaklı durum için çatlaklara paralel olan karışık doğrusal akışı ek olarak sergilemiştir.

Anahtar Kelimeler: Şeyl Gaz, Yatay Sondaj, Hidrolik Çatlatma, Geçici Basınç Analizi, Geçici Üretim Analizi

To my family

ACKNOWLEDGEMENTS

All praises to Almighty Allah who has never left me alone at any time in my entire life.

I wish to express my deepest gratitude to my supervisor – Asst.Prof. Çağlar Sinayuç for his guidance, motivation and overall for this continuous support throughout the project. Asst.Pr. Sinayuç has spent endless hours with me to develop the project and at this point, words are not enough to express my graditude and appreciation to Asst.Pr. Sinayuç.

I also want to acknowledge Mehmet Cihan Ertürk for guidance and support on simulation model.

I want to acknowledge all professors and instructors, with department head, Prof. Dr. Mahmut Parlaktuna, at the top of the list for valuable courses that are taught at Middle East Technical University.

Finally, I want to express my deepest gratitude to family for their support, love and understanding which always motivates me to overcome any problem that I face in my entire life.

TABLE OF CONTENTS

LIST OF TABLES

LIST OF FIGURES

NOMENCLATURE

Abbreviations

BDF: Boundary Dominated Flow
CBM : Coalbed Methane
CFL: Compound Linear Flow
EUR: Estimated Ultimate Recovery
FFR : Fracturing Fluid Residue
HF: Hydraulic Fracture
LTR: Late time region
MFHW: Multi-Fractured Hozirontal Well
OGIP: Original Gas in Place
PSS: Pseudo-Steady State
PTA: Pressure Transient Analysis
RNP: Rate Normalized Pressure
RTA: Rate Transient Analysis
SG : Shale Gas
SRV: Stimulated Reservoir Volume
UGR: Unconventional Gas Reservoir
WBS: Wellbore Storage

Symbols

A = surface area of the matrix block, ft^2
C = wellbore storage coefficient, bbl/psi
c_f = formation compressibility, psi^{-1}
c_g = gas compressibility, psi^{-1}
c_t = total compressibility, psi^{-1}
F_{CD} = Dimensionless fracture conductivity
G_s = Gas Storage Capacity, scf/ton
J = Productivity Index
k = Permeability, md
k_f = fracture permeability, md
k_{fd} = damaged fracture permeability, md
L = Fracture spacing, ft, m

L_m = Length of a block side, ft, m
m(p) = real gas pseudopressure, psi^2/cp
P = Pressure, psia, bar
P_L = Langmuir Pressure, psia, bar
P_i = initial reservoir pressure, psia
P_{wf} = Flowing Bottomhole pressure, psia
Q = Flow rate, m^3/day
r_m = radius of the sphere, ft, m
r_w = wellbore radius, ft, m
V_L = Langmuir Volume Constant, scf/ton
w_f =Fracture width, ft, m
x_f = Fracture half-length, ft, m
μ_g = Viscositty, cp
σ =Shape factor, ft^2, m2
T = temperature, °C or °R
t = Time, hours
t_a = Corrected Pseudo-time, hours
t^*_a = Adsorption Incorporated Corrected Pseudo-time, hours
t_{Dxf} = dimensionless time based on the fracture half-length xf
Sg = Gas Saturation, dimensionless
Sw = Water Saturation, dimensionless
Z = gas deviation factor, dimensionless
α =poroelastic constant
σ_{min} = the minimum horizontal stress (in situ stress)
σ_{ob} = overburden stress
ν =Poisson's ratio
η =hydraulic diffusivity
ϕ = porosity
ϕ_f = undamaged original fracture porosity

CHAPTER 1

INTRODUCTION

In general, unconventional gas reservoirs are known to have very large hydrocarbon reserves in place, a low expected ultimate recovery, and low permeability (Schenk, 2002). Those formations are unable to provide feasible amount of gas at an economical producing rate and they need to be treated with special techniques. Horizontal and multilateral wells exhibits feasible production rates with adoption of transverse hydraulic fractures, and its increased performance should be considered in an accurate way. Assessment of unconventional gas formations is challenging work due to a number of reasons. At the first place, the shale formations in general are naturally fractured and it causes interpretation challenges as reservoir heterogeneity. Moreover, permeability of matrix system ranges within nanodarcy values and it brings an extra demand on the test design which in turn requires a very long test durations. To handle the particular issue specialized analysis techniques must be developed instead. Finally, adsorbed on the grains of organic carbon that may exist in the shale formation ultimately complicates the interpretation of such formations. For all the reasons stated above, production mechanism of UGR(unconventional gas reservoirs) are much more difficult if you compare it to conventional formations. In some cases, analysis of SG (shale gas) reservoirs may not be even feasible (Soliman, 2012).

Gringarten et al. (1974) and lately, Cinco and Samaniego (1981) suggested interpretation of well testing data of conventional formations under infinite, finite-conductivity; and uniform-flux fracture flow scenarios. To be able to handle interpretation of unconventional formations a number of methods were developed: Analytical Models, Numerical Models simulating real gas diffusion (Kappa - Saphire, Topaze, Rubis), Straight line (Flow regime) analysis etc. (Olivier Houze, 2010).

The primary work of the study is to understand applicability of the analysis methods applied for hydraulically fractured wells on unconventional formations under different fracture stage and flowing conditions. In order to reach some results, the utilization pressure- and rate- transient analysis methods were executed.

The starting point was the use Eclipse 300 model to perform simulation runs for single, two- and three- stage hydraulic fracture scenarios with steady flowing rates set to 200, 500, 1000 m^3/day. As a part of pressure transient analysis (PTA) – Kappa (Saphire) and Fekete (F.A.S.T.) software tools were implemented initially for standard finite-conductivity fracture model analysis. It was followed by some advanced models in F.A.S.T. which simulates single and multi-stage fractures in stimulated reservoir volume (SRV) and volume beyond SRV region - for gas and coalbed

methane (CBM) fluid model cases which were applied separately. The advanced models account for corrected pseudo-time function by which we were aiming to decrease deviation of rate normalized pressure (RNP) derivative function for increasing flowing rates. Afterwards, Straight Line (Flow regime) Analysis was utilized as a part of rate transient analysis (RTA). In order to perform the particular analysis, rate normalized pressure (RNP) and corrected pseudo-time functions were estimated and flow regimes from the RNP derivative using corrected pseudo-time functions. Having identified the prevailing flow regimes specialty plots were used to estimate parameters for each particular flow regime. The same procedure was implemented to 6.9 bar constant flowing bottom-hole flowing pressure data.

The production data used for interpretation in this study has the time intervals that are practically too long for a well testing analysis, however it can be used as a guide for a typical well testing interpretation of hydraulically fractured unconventional formations.

CHAPTER 2

LITERATURE SURVEY

2.1 Pressure Transient Analysis

Mainly well testing is done on an exploration well in order to take a fluid sample. Additionally reasons are to measure the initial/average reservoir pressure, estimate minimum reservoir volume, well deliverability, reservoir permeability and skin effect, and identify heterogeneities and boundaries. Well testing is based on changing the flow rate of the well, namely by closing a flowing well or an injection well respectively for buildup or falloff test. This rate change creates pressure signal in the same well or in an adjacent well by the way of interference testing. For multilayer formations, flowing rates are different for each individual layer, which can be measured with a production logging tool. Rate change is established at surface or bottom hole conditions. Wellhead shut-in is typically used for wells that are already producing, while bottomhole shut-in is a typical case for testing after drilling – Drill Stem Tests. The following types of tests exist and being implemented:

• **Drawdown test**: the bottom hole flowing pressure is used for analysis. Essentially, we are aiming to produce at constant rate conditions, however practically, drawdown data is unstable, and the analysis is rarely accurate.

• **Build-up test**: shut-in pressure data is deployed for analysis. Prior to build-up test, the well must have been flowed for sufficient time for rate stabilization. Acquired data is accurately obtained for zero – constant flowing rate flowing conditions.

• **Injection test / fall-off test**: this is the process when fluid is injected underground, and which causes bottomhole pressure increment in reservoir pressure and, it is followed by pressure drop during the fall-off period and after shut-in operation is performed.

• **Interference test and pulse test**: the bottomhole pressure is recorded in a shut-in observation well from an adjacent producer. Interference tests are applied for evaluation of connectivity between wells. For pulse testing, the active well is opened for production with a number of short flow and shut-in periods, the recorded pressure vibrations are analyzed in an observation well.

• **Gas well test**: There are two main characteristics distinguishing gas well testing from liquid one. At first place, due to the fact that gas properties has solid dependence on pressure behavior

of the reservoir and application of liquid well testing techniques is not applicable for gas well testing scenario. Addtionally, high velocity effects is typical for gas wells where an additional pressure drop is observed which is characterized with rate dependent skin term.

In order to handle pressure dependence of gasses real gas pseudopressure function is implemented (Al Hussainy et al., 1966)

$$\mathrm{m(p)} = \int_{p_0}^{p} \frac{2\mathrm{p}\times\mathrm{dp}}{\mu(\mathrm{p})\times\mathrm{z(p)}} \tag{2.1}$$

and the real gas pseudotime function (Agarwal, 1979)

$$\mathrm{t_a(p)} = \int_{\mathrm{t_0}}^{\mathrm{t}} \frac{\mathrm{dt}}{\mu\times\mathrm{c_t}} = \int_{\mathrm{p_0}}^{\mathrm{p}} \frac{(\frac{\mathrm{dt}}{\mathrm{dp}})\times\mathrm{dp}}{\mu(\mathrm{p})\times\mathrm{c_t(p)}} \tag{2.2}$$

All the equations deployed for gas well test scenario will be identical with liquid equations by implementing pseudotime and pseudopressure functions.

2.2 Shale Gas

Shale gas refers to gas which is trapped within shale beds. SG is formed by combination of

- primary thermogenic degradation of organic matter
- thermogenic cracking of hydrocarbons
- biogenic degradation

Shale looks like the slate of a chalkboard and typically has extremely low formation permeability. These shales are rich in organic carbon. Despite the fact that it is hard to extract, shale gas is essentially fairly clean and dry. This is due to thermal cracking thoughout the time. Having known the fact we can conclude on magnitude and duration of particular range of temperature in the reservoir. Withdrawn fluid will be drier for higher thermal maturity cases.

Gas is stored in shales at different forms: **Adsorbed gas** which refers to gas attached to clay particles, **free gas** that is hold within the tiny spaces in the rock or in hydraulic fractures and **solution gas** that is in dissolution form within liquid hydrocarbons. Higher free-gas content in lasts with higher initial gas production rates. That is because free gas is already in the pore space and it is much easier than that for adsorbed gas to be produced.

Over the past decade, implementation of both horizontal drilling and hydraulic fracturing opened the production window that was not previously uneconomically feasible. The production of natural gas from shale formations has rejuvenated the natural gas industry in the United States. "In 2000 shale gas provided only 1% of U.S. natural gas production; by 2010 it was over 20% and the U.S. government's Energy Information Administration predicts that by 2035, 46% of the United States' natural gas supply will come from shale gas" (Stevens, 2012).

Shale has extremely low matrix permeability, so implementation of hydraulic fracturing is required for estimation of commercial production. This is done along with horizontal drilling in order to increase the productivity of the well.

Four types of porous media exist in productive shale gas formations: nonorganic matrix, organic matrix, natural fractures, and hydraulic fractures. Organic-matter pores, which have dimensions within 5 to 1,000 nm, are of a great importance due to the fact that they hold adsorbed gases, as well as store free gases. Barnett Shale example also indicates the fact that a serious amount of free gas exist in organic matter. In comparison with conventional gas reservoirs, fluid flow in gas shales is controlled by flow mechanisms at all scales, from molecular to macroscopic. Fluid-flow mechanisms consist of the (1) free gas flow, (2) desorption, (3) diffusion, and (4) imbibition suction effects. In case of adsorption, essentially, two types of adsorption processes exist:

• **Physical adsorption or van der Waals adsorption**. Fundamentally, gas is hold in organic matter by the way of physical adsorption. Physical adsorption is simply an attraction between clay particles and gas molecules and the process itself is irreversible.

• **Chemical adsorption or chemisorption**. Chemisorption (activated adsorption) is described as a chemical interaction between gas and adsorbed substance. For the particular case adhesive forces are stronger than that of for physical adsorption. The process is also usually irreversible and original substance undergoes chemical change on desorption.

Shale mineralogy is of a great importance for evaluation of amount of gas that is physically adsorbed to shale surfaces. Due to the fact that, overall, most shale gas reserves has constant temperature, it has a negligible effect on desorption, whereas it is more sensitive to pressure change in the reservoir system. Langmuir, Brunauer- Emmett-Teller, and Freundlich isotherms are implemented to explain adsorption effects.

In our case we apply Langmuir isotherm for characterization of desorption process. Langmuir's isotherm uses the following three assumptions to describe adsorption effects:

- The adsorbant surface is in touch with solution containing an adsorbate that is strongly induced to its surface
- The surface has a specific number of spots adsorbtion of solute molecules is possible
- The adsorption is described with monolayer scenario where only one layer of molecules are attached to the surface

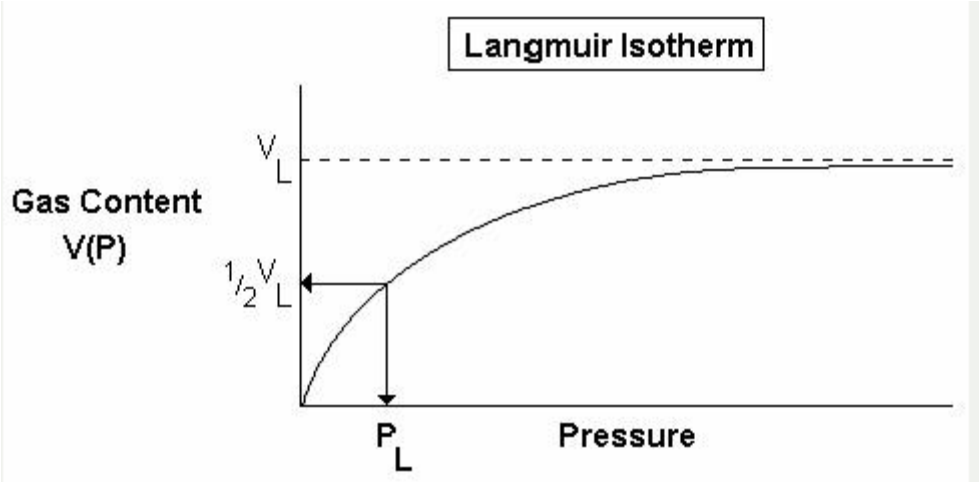

Figure 2. 1 Typical Langmuir Isotherm (Fekete Associates, 2011)

$$G_s = \frac{V_l p}{(p+P_l)} \tag{2.3}$$

The Langmuir Isotherm (Fig 2.1) shows the quantity of adsorbed gas that a saturated sample will contain at a given pressure. Decreasing pressure will cause the methane to desorb in accordance with behavior prescribed by the blue line. Gas Desorption increases in a nonlinear manner as the pressure declines.

"Imbibition suction is a phenomenon occurring in frac-water flow in tight-gas sandstones"(Bennion and Thomas, 2005). For some productive shale gas formations such as the Haynesville (Stoneburner, 2009) and Barnett less than 50% of frac water flows back when we start producing from the field. This is described as combined effects of imbibition suction and gravity segregation in fractures. Gas has a tendency to move in the upper part of the fractures,

where water stays at the bottom of the fractures. Some water can seep into shale formation during drilling and stimulation operations. A portion of this water turns into residual water in the nonorganic matrix. Imbibition suction effect can be increased due to cooling by drilling and frac water around stimulated region which in turn increases water saturation.

2.3 Naturally Fractured Reservoirs

Naturally fractured formations embody over half of known reservoirs and makes large contributions to global hydrocarbon production. These reservoirs refer to strongly heterogeneous formations that hold a highly complex network of distinct fracture groups with various spatial distribution and conductivity. It is a very challenging task to perform a characterization studies on these types of formations due to the fact that they exhibit an extreme property contrast between two domains which includes - rock matrix and fractures. These reservoirs are found sandstone, shales, and carbonate depositional environments.

Shale formation permeability ranges in such a low values that it produces gas in an extremely low rate, which makes shales to be the last source of energy for gas production. On the other hand, shales store huge amount of gas which concentrates a lot of interest on it. Producing shale beds are relatively flat and thick and they can maintain constant production for considerably long time periods.

It must be mentioned that the pore spaces are even smaller than the hydrocarbon molecules itself, which does not allow it flow through the pores. For that reason fractures are the main way to make production possible. The gas production happens in the following manner (Ahmed, 2010):

- Free gas flows from fractures,
- Gas Desoption,
- And flow of desorpted gas out of the rock matrix.

Free gas is produced at a very high rate, whereas adsorbed gas is being produced at a very low rates.

2.3.1 Behaviour of Naturally Fractured Reservoirs

Naturally fractured formations are characterized by two types of porous media: matrix and fracture and described as dual porosity reservoirs:

- Matrix porosity which refers to primary porosity φ_m
- Fracture porosity, which stands for secondary porosity φ_f

Primary porosity (φ_m) is formed when the sediment is initially deposited, for that reason, it represents original rock characteristic. It is strongly interconnected and can often be correlated with permeability since it has a strong dependence on size, geometry, and spatial distribution of the grains.

Secondary porosity (φ_f), is the consequence of post depositional geological processes. Bigger portion of such reservoirs are limestones or dolomites. Typically, secondary porosity is the result of solution and recrystallization of porous system.

Generally, matrix is porous and less permeable in comparison with fractures, whereas fractures are less porous but with high magnitude of permeability. If we do not consider the rest of the reservoir, fractures would have porosity values equal to unity, that is, they are entirely void of rock. However, fracture porosity is known to be equal to fracture and total volume ratio:

$$\varphi_f = \frac{\text{Fracture Volume}}{\text{Total Volume}} = \frac{V_f}{V_t} \tag{2.4}$$

Matrix porosity is also defined with respect to total volume., whereas, the matrix porosity values are not identical with unfractured core porosity (φcore) values that are measured in the laboratory, which is related with the following expression:

$$\varphi_m = \varphi_{core}\,(1 - \varphi_f) \tag{2.5}$$

Gilman and Kazemi (1983) noted that in naturally fractured systems, the fracture permeability k_f is given by:

$$k_f = \frac{k_e}{\varphi_f} \tag{2.6}$$

where - k_e is the effective permeability computed from PBU data. Another relationship for fracture permeability description is proposed by Poiseuille's law in the following equation:

$$k_f = 54 \times 10^9 {b_p}^2 \tag{2.7}$$

Where b_p = fracture width, inches

where it can be assumed that

$$\sum b_p = b \tag{2.8}$$

And it must be noted that neither b_p nor b is an exact representation of the fractures in a reservoir.

The two expressions above can be combined to give the correct width to be used in Poiseuille's law as:

$$b_p = \sqrt{\frac{k_e}{54 \times 10^9 \, \varphi_f}} \tag{2.9}$$

Ramirez et al. (2007) mentiones that natural fractures can increase the ultimate production from the field, but this depends upon the architecture of fractured zone. As an example, vertical and sub-vertical fractures for the reservoir with a high structural relief could increase gas segregation to crestal part of the reservoir to boost oil gas gravity drainage. However, fractures can eventuate reservoir channelization in low-permeability reservoirs, which can result in early gas and water breakthrough. Another significant characteristic of the fractures is the strongly reduced cross-sectional area available to flow.

A number of reservoir description scenarios of dual-poro reservoirs have been brought forward for simulating and elucidating the fluid flow in naturally fractured formations. Warren and Root (1963) idealized and illustrated the naturally fractured dual-poro formations by a mass of rectangular blocks, as shown in Figure 2.2.

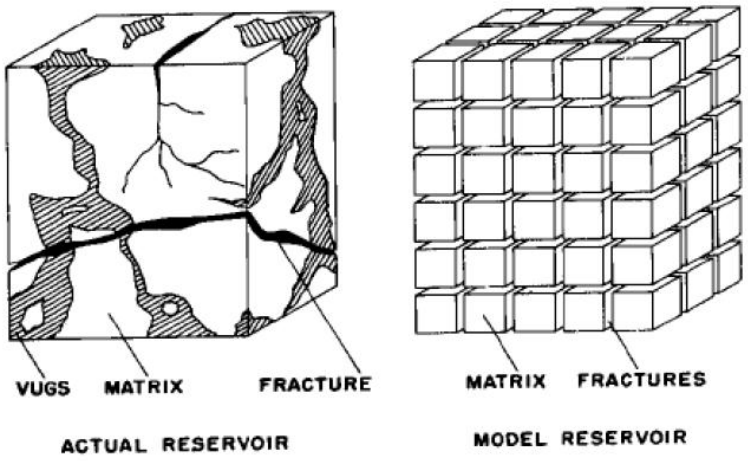

Figure 2. 2 Dual Poro system by Warren and Root (1963)

Warren and Root, in establishing their proposed model to resembled the fluid flow in idealized dual-poro system shown in Figure 2.9, exploited assumptions below:

- The rock matrix encompassing the primary porosity is homogeneous and isotropic, and it is consisted of a systematized array of similar rectangular cubes. The matrix is resembled by a high degree of storativity and lower permeability. Despite most of the hydrocarbon is stocked in matrix, an assumption has been made that fluid does not flow directly to the well, but it enters the fractures first and then flow towards the well through the fractures.
- The secondary porosity refers to system of uniform and continuous fractures that are distributed in such a way that each it is parallel to one of the principal axes of permeability. The fractures are evenly spaced with a steady width. Nonetheless, the existence of diverse fracture spacing or width along each of the axes to simulate the appropriate degree of desired anisotropy.

Warren and Roots mathematically proposed matrix–fracture transfer function "Γ" as outlined by the subsequent expression:

$$\Gamma = \sigma\left(\frac{k_m}{\mu}\right)V(p_m - p_f) \tag{2.10}$$

The shape factor "σ" is a geometric factor which is subject to the geometry and matrix–fissure system characteristic shape, and it has dimensions of a reciprocal of area and it is illustrated by the next expression:

$$\sigma = \frac{A}{V_x} \tag{2.11}$$

Kazemi (1969) advanced an extensively used relationship for resolving the shape factor found on finite-difference which is written as the following expression:

$$\sigma = 4\left[\frac{1}{L_x{}^2} + \frac{1}{L_y{}^2} + \frac{1}{L_z{}^2}\right] \tag{2.12}$$

where Lx, Ly, and Lz corresponds to matrix block dimensions. Warren and Root introduced two exclusive characteristics to describe naturally fractured dual poro system. Those parameters are called storativity ratio ω and interporosity flow coefficient λ, respectively and characterized below as the following:

a. The dimensionless parameter ω resembles the storativity of the fractures as a ratio to the total reservoir. Mathematically, it is expressed by:

$$\omega = \frac{(\phi hc_t)_f}{(\phi hc_t)_{f+m}} = \frac{(\phi hc_t)_f}{(\phi hc_t)_f + (\phi hc_t)_m} \tag{2.13}$$

Storativity values essentially ranges within 0.1 to 0.001. The second parameter λ stands for the description of fluid flow from matrix to fracture and specified as the following:

$$\lambda = (\frac{k_m}{k_f}){r_w}^2 \tag{2.14}$$

Most of the suggested models consider that the matrix–fissures system can be defined by one the following four block-shape factor geometries: Cubic matrix blocks detached by fractures with λ as given by the following relationship:

$$\lambda = \frac{60}{{L_m}^2}(\frac{k_m}{k_f}){r_w}^2 \tag{2.15}$$

where L_m stands for the length of a block side.

Spherical matrix blocks detached by fractures with λ as noted by following expression:

$$\lambda = \frac{15}{{r_m}^2}(\frac{k_m}{k_f}){r_w}^2 \tag{2.16}$$

where r_m is the radius of the sphere.

Horizontal strata matrix blocks detached by fractures with λ as given by:

$$\lambda = \frac{12}{{h_f}^2}(\frac{k_m}{k_f}){r_w}^2 \tag{2.17}$$

where h_f is the thickness of a specific fracture or high-perm layer.

Vertical cylinder matrix blocks detached by fractures with λ as given by:

$$\lambda = \frac{8}{{r_m}^2}(\frac{k_m}{k_f}){r_w}^2 \tag{2.18}$$

where r_m stands for the radius of an individual cylinder.

Warren and Root suggested the first identification method of the dual poro system, as indicated by drawdown semilog plot of Figure 2.10. The curve is characterized by two parallel straight

lines because of the two distinct porosities in the reservoir. The first one stands for the flow from fracture to wellbore. The lower transmissivity values, at later times responds to mixed effect of two porosity system. Those two lines are separated with transitional period. The first straight line corresponds to transient radial flow through the fractures, which is the reason why its slope is used to find the system permeability–thickness product. Due to the fact that the fracture storage is minimal, the fluid in the fractures is instantaneously depleted along with the rapid pressure decline in the fractures which causes further gas release from matrix to fractures and which in turn provokes a decrement in the pressure decline rate (as shown in Figure 2.3).

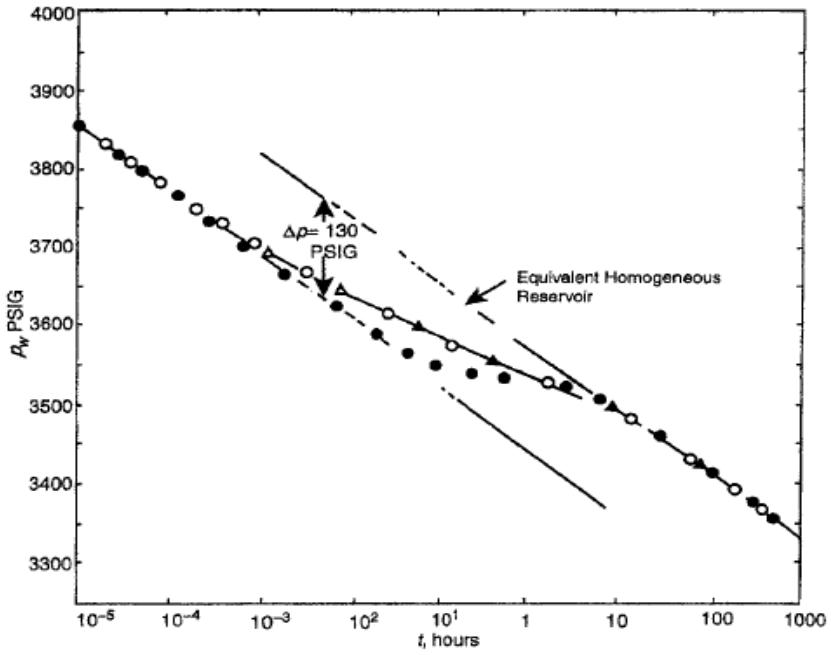

Figure 2. 3 Pressure drawdown - Warren&Root Model (Kazemi,1969)

As matrix pressure reaches pressure maintained in fractures, the pressure stabilization is observed in matrix-fracture system which stands for the second straight line on semilog plot. It must be mentioned that the first straight line can be masked by wellbore storage (WBS) effects and cannot be seen.

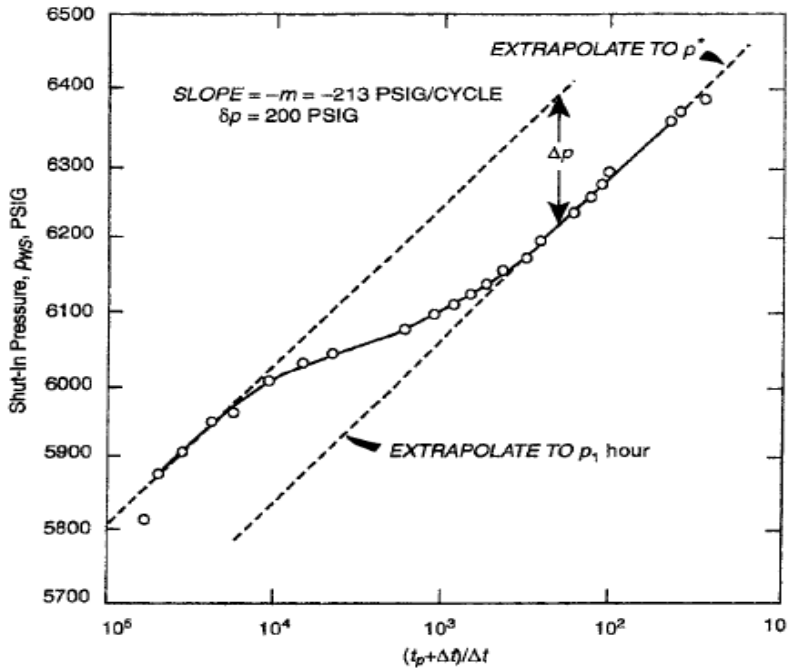

Figure 2. 4 PBU (After Warren and Root, 1963)

Consequently, only parameters defining the homogeneous behavior of a system overall k_f h can be found. Figure 2.4 resembles the BPU data. As it was shown in pressure drawdown scenario, WBS effects may mask the initial straight line on the plot. If both straight lines could be seen, permeability–thickness can be computed using the following equation:

$$(k_f h) = \frac{162.6QB\mu}{m} \tag{2.19}$$

2.3.2 Well Testing in Naturally Fractured Reservoirs

Gringarten (1987) points out that the two straight lines on the semilog plot may or may not be present depending on the condition of the well and the duration of the test. He concludes that the it is not correct to identify double-porosity behavior from semilog plot.

In semilog plot, as illustrated in Figure 2.4 the double-porosity behavior gives an S-shape curve with the initial portion of the curve exhibiting the homogeneous behavior resulting from depletion in fissures. A transitional region corresponds to interporosity flow. Eventually, the last portion shows homogeneous behavior when pressure is equalized in the reservoir when matrix contributes to production. S-shape behavior is rarely seen in highly damaged wells, and well behavior may be improperly recognized as homogeneous medium. Additionally, an analogous S-shape behavior may be revealed in irregularly bounded well drainage system cases.

Maybe the most useful way for identification of double-porosity systems is to implement a pressure-derivative method. Typically, pressure-derivative analysis is a log–log plot of rate of change of the pressure with respect to time. Its application has a number of significant advantages:

- Heterogeneities that barely seen on conventional plots are more clearly seen
- Flow regimes characteristics are strictly exhibited
- The derivative plot shows in a single graph, although many separate characteristics that would elseways require various plots.
- The derivative approach enhances the definition and quality of diagnosis analysis.

Figure 2.5 illustrates pressure derivative type curve for dual-poro system. The minimum value on the plot stands for transition period interporosity flow that is exhibited between two horizontal lines. The first line stands for radial flow originated from fractures, while the second one illustrates the total system behaviour. Figure 2.5 exhibits, at early time, the regular behavior of WBS effects which deviates from unit slope line to a maximum yielding wellbore damage. Gringarten (1987) proposes the fact that the particular shape is a result of the double-porosity behavior. So that for restricted interporosity flow, it shows to be in a “V-shape” form, while for unrestricted interporosity it has an open “U-shape” shape.

Bourdet and Gringarten (1980) introduced specialized pressure type curves based on the Warren and Root double-porosity theory which is used to analyze the well test data for dual-poro systems. They showed that double-poro behavior is a function of the following independent variables:

- p_D
- t_D/C_D
- C_De^{2s}
- ω
- λe^{-2s}

which stands for dimensionless pressure, time, and dimensionless WBS coefficient C_D as defined below:

$$t_D = \frac{0.0002637 k_f t}{[(\phi\mu c_t)_f + (\phi\mu c_t)_m]\mu r_w{}^2} = \frac{0.0002637 k_f t}{(\phi\mu c_t)_{f+m}\mu r_w{}^2} \tag{2.20}$$

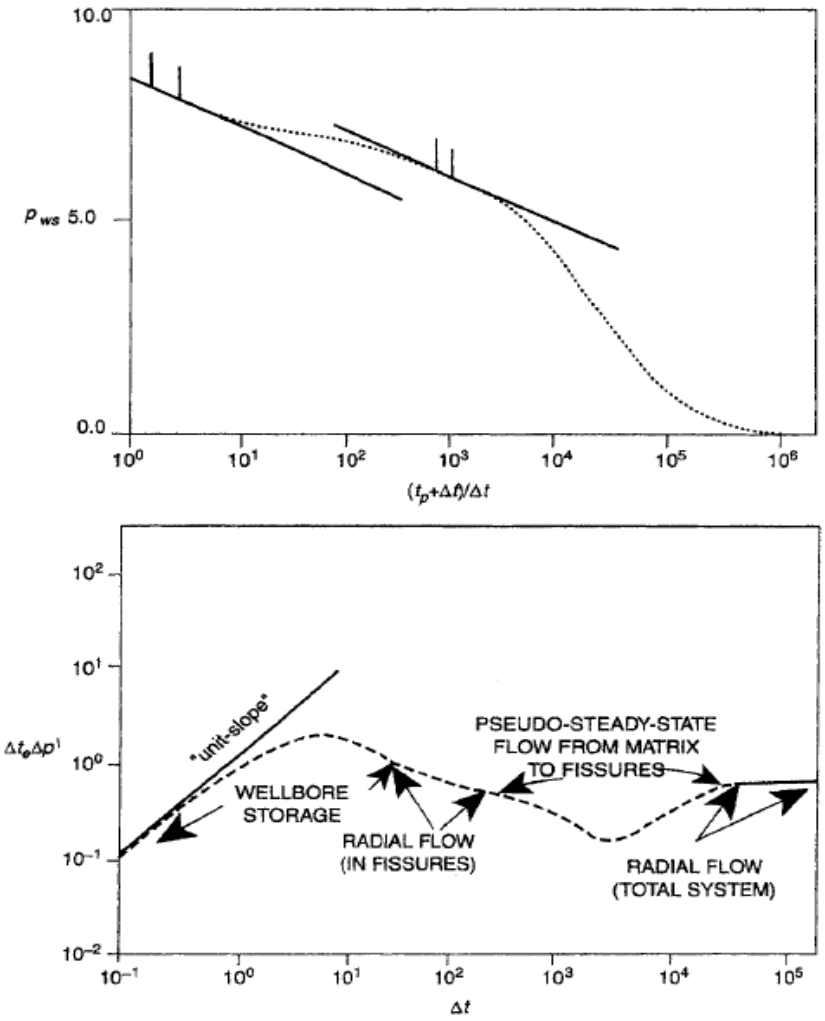

Figure 2. 5 Pressure behavior of a dual-porosity system(Ahmed, 2010)

$$p_D = [\frac{k_f h}{141.2QB\mu}]\Delta p \tag{2.21}$$

$$C_D = [\frac{0.8936}{\phi h c_t r_w{}^2}]C \tag{2.22}$$

2.4 Hydraulically Fractured Reservoirs

Tight formations and especially unconventional formations typically require hydraulic fracturing in order to gain feasible production. Hydraulic fracturing is obtained by the process of pumping a high pressure fluid into a wellbore that it exceeds its fracture limits. In most cases, a single-vertical hydraulic fracture formed that propagates in two directions from the wellbore into the formation. The fracture wings are 180° apart and they are typically similar in size and shape. Mulfracturing is the case for SG and CBM formations where a number of hydraulic fractures are propagated into the formation.

The EPA (2004) has reported the list for various applications of hydraulic fracturing:

- Boosting hydrocarbon production rates for low-perm. formations;
- Boosting hydrocarbon production rates for damaged wells;
- Joining the natural fractures to the wellbore;
- Reducing pressure drop around wellbore for sand production mitigation;
- Reducing pressure drop around wellbore for paraffin/asphaltine deposition minimization;
- Gain more area draining to the wellbore;
- Joining the full vertical extent of the productive interval to a slanted/horizontal well:

In order to choose the best candidate for stimulation treatment, the design engineer should take into account numerous parameters. The most critical properties are the following for hydraulic fracturing treatments:

- Reservoir Permeability
- In situ stress distribution
- Reservoir fluid viscosity
- Reservoir Depth & Pressure
- Skin factor

The theory and design behind hydraulic fracturing has been developed by other engineering disciplines. At this point, certain aspects, such as poroelastic theory, are unique to porous, permeable underground formations. The most crucial criterions are: Young's modulus, Poisson's ratio, and in situ stress (Ahmed, 2010).

Young's modulus is defined as "the ratio of stress to strain for uniaxial stress." The theory used to evaluate fracture extents is mainly based on linear elasticity. In order to apply this theory, Young's modulus of the formation is a critical parameter. The modulus refers to stiffness

measure of material. The more narrow fractures are the case for a solid rock when we perform hydraulic fracturing. For the lower values of stiffness, the fractures will be wider. The modulus of a particular rock type is dependent on the lithology, porosity, fluid type, and other sort of variables. Typically, Young's modulus as a function of lithology and values are shown in Table 2.1 for different rock types.

Poisson's ratio is characterized as the ratio of the relative contraction straindivided by the relative extension strain.

Table 2. 1 Typical ranges for Young'smodulus as a function of lithology (Ahmed, 2010)

Lithology	Young's Modulus (psi)
Sandstone	**$2 – 5 \times 10^6$**
Hard Sandstone	**$6 – 10 \times 10^6$**
Limestone	**$8 – 12 \times 10^6$**
Coal	**$0.1 – 1 \times 10^6$**
Shale	**$1 – 10 \times 10^6$**

Figure 2.6 illustrates the local stress state at depth for an element of formation. The stresses can be divided into the following three principal stresses:

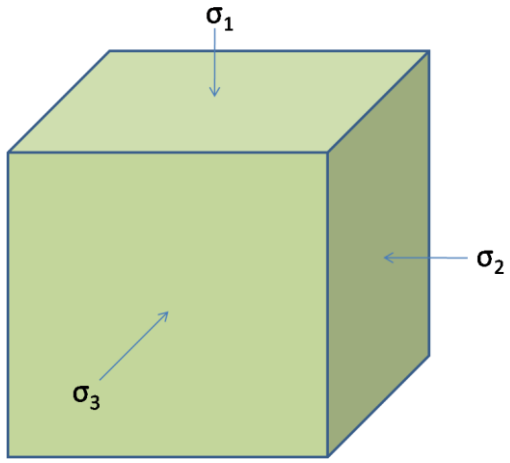

Figure 2. 6 Local in situ stress

Where $\sigma_1 > \sigma_2 > \sigma_3$. Depending on geological conditions, the vertical stress can also be the intermediate (σ_2) or minimum stress (σ_3). These stresses are normally compressive and change in magnitude throughout the reservoir, particularly in the vertical direction. The direction and magnitude of the principal stresses are important since they are used to manage:

- the pressure obligatory for creation and propagation of hydraulic fracture,
- the vertical extent and shape of hydraulic fracture,
- the direction of hydraulic fractures
- the stresses trying to crush and lodge prop agent during producing phase.

The minimum horizontal stress profile could be computed from the subsequent equation:

$$\sigma_{min} \cong \frac{v}{1-v}(\sigma_{ob} - \alpha p) + \alpha p \tag{2.23}$$

Poisson's ratio can be assessed using acoustic log data or correlations from lithology. The value of Poisson's ratio varies between 0.2 to 0.4 for coal seams. Overburden stress values are computed from density log data. Typically, the value for overburden pressure is about 1.1 psi per foot of depth. Poroelastic constant varies between 0.5 to 1.0 and "α" values generally equal to 7 for hydrocarbon reservoirs.

2.4.1 Well Testing in Hydraulically Fractured Reservoirs

Interpreation of well testing data in hydraulically fractured formations has increased complexity due to unknown stimulation characteristics. Gringarten et al. (1974) and Cinco and Samaniego (1981) suggested three transient flow models to be taken into account in such well testing data examples. (1) infinite conductivity vertical fractures – where there is no pressure drop with the hydraulic fracture and fractures are depleted instantaneously; (2) finite-conductivity vertical fractures – where there is a certain pressure drop within the fractures; (3) uniform-flux fractures.

2.4.1.1 Infinite-conductivity vertical fractures

These are highly conductive fractures which considered can be considered as an infinite. For this particular case there is no pressure drop within the fractures and flow in the fractures are considered to be instantaneous. This particular model assumes three flow regimes:

- Fracture linear flow;
- Formation linear flow;
- Infinite acting pseudoradial flow periods.

Several specialized plots are used for identification of each individual flow regime. For example, plot of pseudo-pressure versus Δt for gas production case will exhibit a half-unit slope on the early time log–log. Those flowing periods are associated with infinite-conductivity fractures, and method for diagnosis will be discussed later in this chapter.

2.4.1.2 Finite-conductivity fractures

These are the long fractures initiated by massive hydraulic fracture. The reduced permeability of fractures is due to large amount of propping agent that is used to keep the fractures open. As it was indicated before this particular model takes into account the pressure drop within the hydraulic fractures. Model considers the following four flow regimes:

- Fracture linear flow regime,
- Bilinear flow regime;
- Formation linear flow regime;
- Infinite acting pseudo-radial flow regime.

2.4.1.3 Uniform-flux fractures

A uniform-flux fracture –refers to the case when flow rate from formation into hydraulic fractures is uniform for entire fracture extent. The particular model is somehow similar to infinite conductivity fractures at some points. The main distinguishing feature is showed out at fracture boundaries. The system is characterized by a variable pressure along the fracture and essentially shows - linear and infinite acting pseudoradial flow regimes.
The general solution appears to be written in dimensionless variables. The following dimensionless groups are implemented for the sake of data analysis:

Dimensionless diffusivity: $\eta_{fd} = \frac{k_f \phi c_t}{k \phi_f c_{ft}}$

Dimensionless time: $t_{Dfx} = \left[\frac{0.0002637k}{\phi \mu c_t {x_f}^2}\right] t = t_D (\frac{{r_w}^2}{{x_f}^2})$

Dimensionless conductivity: $F_{CD} = \frac{k_f}{k}\frac{w_f}{x_f} = \frac{F_C}{k x_f}$

Dimensionless storage: $C_{Df} = \frac{0.8937C}{\phi c_t h {x_f}^2}$

Dimensionless pressure: $p_D = \frac{kh\Delta m(p)}{1424QT}$; for gas

Dimensionless radius: $r_{eD} = \frac{r_e}{x_f}$

Notice that the equations indicated above are written in terms of drawdown tests. Generally, a fracture could be classified as an infinite-conductivity fracture for the case when F_{CD} is greater than 300. The dimensionless fracture conductivity F_{CD} is defined as the ratio fracture flow capacity to the ability of the reservoir to deliver fluid to the fracture.
It must be added that fracture conductivity will reduce the well life due to following:

- Increasing stress on fracture due to increasing stress on the proppant due to decline of bottom hole flowing pressure
- Crushing of the propping agent
- Embedment of propping agent into the formation
- Non-Darcy flow effects
- Damage from fluid loss additives

The impact of the fluid flow additives on fracture permeability can be assessed by Cook's theoretical model (1973) which is expressed as the following:

$$k_{fd} = k_f(\frac{\phi_{fd}}{\phi_f})^3 \tag{2.24}$$

The productivity index J_F can roughly be estimated using the equation below:

$$J_F = J[\frac{ln(\frac{r_e}{r_w})}{ln(\frac{r_e}{0.5x_f})}] \tag{2.24}$$

There are five flow regimes, as shown conceptually in Figure 2.7, associated with the three types of vertical fractures:

- Fracture linear flow
- Bilinear flow
- Formation linear flow
- Elliptical
- Infinite acting pseudoradial flow

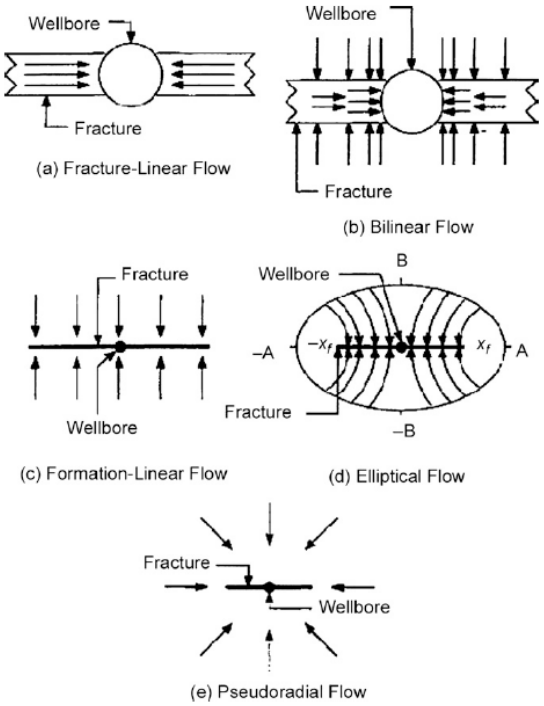

Figure 2. 7 Flow regimes in a vertically fractured well (after Cinco-Ley and Samaniego-V. 1981)

Below are specialized plots for analysis of a specific flow regime:

- Graph of Δp versus $\sqrt{time}$ for linear flow
- Graph of Δp versus $\sqrt[4]{time}$ for bilinear flow
- Graph of Δp versus ln(A+B) for elliptical flow
- Graph of Δp versus log(time) for infinite acting pseudoradial flow

2.4.1.4 Fracture linear flow

For this particular flow regime the main source of production is gas expansion within the hydraulic fractures. The data is data during for this particular flow is analyzed with Δp vs. $\sqrt{time}$ plot. Unfortunately, the particular flow regime doesn't have any practical use as it lasts in a very short tome frame. Fracture linear flow regime exists for the case when dimensionless

hydraulic conductivity exhibits values more than 300. Cinco&Samaniego (1981) observed that this fracture linear flow ends when:

$$t_{Dxf} \approx \frac{0.1(F_{CD})^2}{(\eta_{fD})^2} \tag{2.25}$$

The dimensionless pressure response at the wellbore is expressed as:

$$p_{wD} = \frac{2}{(k_f b_f)_D}\sqrt{\pi \eta_{fD} t_{Dxf}} \tag{2.26}$$

Hence for oil,

$$p_{wf} = p_i - \frac{\delta_{lfo} qB}{b_f h}\sqrt{\frac{\mu t}{k_f \phi_t c_{ft}}} \tag{2.27}$$

For gas,

$$m(p_{wf}) = m(p_i) - \frac{\delta_{lfg} qT}{b_f h}\sqrt{\frac{t}{k_f \phi_t c_t}} \tag{2.28}$$

where $\delta_{lfo}$and $\delta_{lfg}$are unit conversion constants.

2.4.1.5 Bilinear flow

Bilinear flow occurs when two different linear flows – from fractures and formation happens at the same time. The bigger portion of the fluid are originated from the formation. Actual value of the fracture conductivity can be found from this flow regime. The pressure drop within the fracture is important for the finite conductivity scenario. However, for infinite-conductivity scenario bilinear flow is not exhibited as there is no pressure drop within the fractures and they are depleted almost instantaneously. Hence, identification of bilinear flow period is of a great important, as:

- It is not possible to find a unique fracture length from well bilinear flow period data. If these data are used for fracture length determination, we will get much smaller fracture length compared to the actual one.
- The actual fracture conductivity can be found from the data corresponding to bilinear flow regime. Cinco and Samaniego (1978, 1981) suggest that change in the wellbore pressure can be described by the following expressions for the particular flow regime:

For fractured gas wells

-in a dimensionless form:

$$m_D = \left[\frac{2.451}{\sqrt{F_{CD}}}\right](t_{Dxf})^{1/4} \tag{2.29}$$

or

$$log(m_D) = log\left[\frac{2.451}{\sqrt{F_{CD}}}\right] + \frac{1}{4}log(t_{Dxf}) \tag{2.30}$$

in terms of pseudo pressure:

$$\Delta m(p) = \left[\frac{444.6QT}{h\sqrt{F_C}(\phi\mu c_t k)^{1/4}}\right]t^{1/4} \tag{2.31}$$

or equivalently:

$$\Delta m(p) = m_{bf}t^{1/4} \tag{2.32}$$

Taking the logarithm of both sides gives:

$$log[\Delta m(p)] = log(m_{bf}) + \frac{1}{4}log(t) \tag{2.33}$$

Equation 2.31 indicates that a plot of Δm(p) versus (time)$^{1/4}$ on a Cartesian scale would produce a straight line passing through the origin with a slope of bilinear flow data as:

For Gas Case

$$m_{bf} = \left[\frac{444.6QT}{h\sqrt{F_C}(\phi\mu c_t k)^{1/4}}\right] \tag{2.34}$$

or

$$F_C = \left[\frac{444.6QT}{m_{bf}h(\phi\mu c_t k)^{1/4}}\right]^2 \tag{2.35}$$

Similarly, Equation 2.32 suggests that a plot of Δp or Δm(p) versus (time) on a log–log scale would produce a quarter slope straight line and which is the diagnostic tool for identification bilinear flow regime. Plot exhibits a curvature that may concave upward or downward depending upon the value of the dimensionless fracture conductivity when bilinear flow ends. For dimensionless fracture values below 1.6, the curve will concave downward and the upward concaving behaviour is observed for the case when dimensionless fracture conductivity is more than 1.6. The upward trend is an indication of the fact that fracture tip is beginning to affect wellbore behavior. If the test has not been adequately long for bilinear flow to be ended for F_{CD} > 1.6 case, then it won't be possible to withdraw fracture length values. $F_{CD} \leq 1.6$ values are an indication of the fact that fluid flow has changed from one to two-dimensional flow regime. In this particular case, we are not able to uniquely judge on fracture length values even if bilinear flow ends during the test. Cinco and Samaniego (1978, 1981) proposes that the dimensionless fracture conductivity values can be computed from bilinear flow pressure data at which the line ends Δp_{ebf}, and using the following expression:

For Gas Case:

$$F_{CD} = \frac{1965.1QT}{kh\Delta m(p)_{ebf}} \tag{2.36}$$

The end of the bilinear flow straight line is dependent on fracture conductivity and could be computed from equations indicated below:

$F_{CD} \geq 3$ $\qquad t_{Debf} \cong \dfrac{0.1}{(F_{CD})^2}$

$1.6 \leq F_{CD} \leq 3$ $\qquad t_{Debf} \cong 0.0205[F_{CD} - 1.5]^{-1.53}$

$F_{CD} \leq 1.6$ $\quad\quad$ $t_{Debf} \cong [\frac{4.55}{\sqrt{F_{CD}}} - 2.5]^{-4}$

2.4.1.6 Formation Linear flow

This linear flow regime is the case for - $F_{CD} > 300$ scenario. As for the fracture linear flow, the formation linear flow pressure data collected during this period shows a strong correspondence with fracture length and fracture flow capacity. The following diffusivity equation describes pressure behavior corresponding to this particular flow regime, as the following:

$$\frac{\partial^2 p}{\partial x^2} = \frac{\phi \mu c_t}{0.002637k} \frac{\partial p}{\partial t} \tag{2.37}$$

The solution to above mentioned linear diffusivity equation can be used for to both fracture and formation linear flow regimes, with the solution as given in a dimensionless form as the following:

$$p_D = (\pi t_{Dxf})^{0.5} \tag{2.38}$$

or for real pressure and time, as the following:

$$\Delta p = \left[\frac{40.925QT}{hx_f}\sqrt{\frac{1}{k\phi\mu c_t}}\right] t^{0.5} \tag{2.39}$$

The particular flow regime exhibit a half-slope straight line on a log–log plot of Δp versus time, as it is indicated in Figure 2.8. Another diagnostic presentation of pressure data points is the plot of Δp or Δm(p) versus on a Cartesian scale (as shown in Figure 2.9), which would produce a straight line with a slope of m_{vf} related to the fracture length by the following equations:

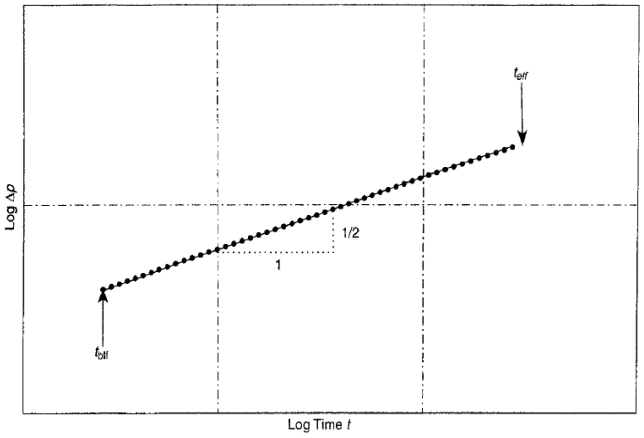

Figure 2. 8 Pressure data for a 1/2-slope straight line in a log–log graph. (AfterCinco and Samaniego, 1981)

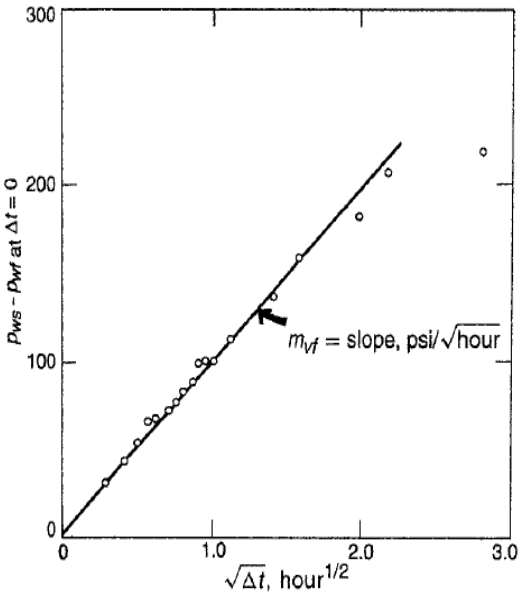

Figure 2. 9 Square-root data plot for buildup test (Ahmed, 2010)

Fractured Gas Case:

$$x_f = \frac{40.925QT}{hx_f}\sqrt{\frac{1}{k\phi\mu c_t}} \tag{2.40}$$

The straight-line relationships as illustrated by Figures 2.8 and 2.9 provide distinctive and easily recognizable evidence of a fracture. Agarwal et al. (1979) mentioned that there is a curved portion before the liner one which refers to fracture linear flow. The duration of the curved portion is a function of fracture conductivity. The beginning of formation linear flow, is closely associated with fracture conductivity and can be approximated from the following expression:

$$t_{Dblf} \approx \frac{100}{(F_{CD})^2} \tag{2.41}$$

And the end of this linear flow period end of linear is approximately defined as:

$$t_{Dblf} \approx 0.016 \tag{2.42}$$

Having known these two points we can make estimation of fracture conductivity from its specialty plot using as indicated below:

$$F_{CD} \approx 0.0125 \sqrt{\frac{t_{elf}}{t_{blf}}} \tag{2.43}$$

where t_{elf} and t_{blf} are given in hours.

2.4.1.7 Elliptical Flow

Elliptical flow is one of five distinct flow patterns around a hydraulically fractured well (Fig. 2.10) (Cinco&Samaniego, 1981). As Prats demonstrated (1961), elliptical flow geometry dominates the fluid flow in a vertically fractured well. In case of an infinite-conductivity fracture, equipressure lines are confocal eclipses with fracture tips as foci (Fig 2.10). For a finite-conductivity fracture scenario, flow geometry between the fracture tips is not elliptical because of the extra pressure drop in fracture, but flow geometry is still essentially elliptical away from hydraulic fractures.

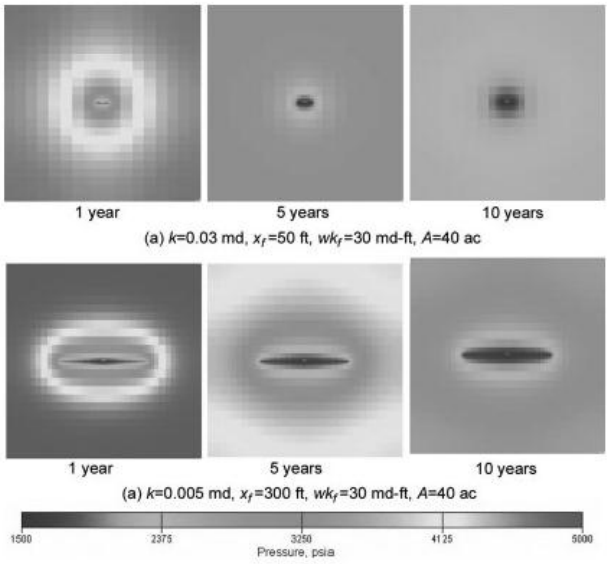

Figure 2. 10 Pressure distributions for various matrix/fracture property scenarios (Cheng, 2009)

Hale and Evers (1981) suggested an approximate unsteady-state elliptical flow solution for an infinite-conductivity fracture flowing well scenario. The particular solution models behavior of pressure transients from linear to pseudo-radial flow (Eq 2.44):

$$p_D = ln[(A + B)/x_f] \tag{2.44}$$

"A" and "B" - are the major and minor semi-axes, respectively, of the particular ellipse.

$$A = \sqrt{B^2 + {x_f}^2} \tag{2.45}$$

Hale and Evers (1981) selected t_{De} = 0.318 to specify the onset of pseudosteady-state flow, as for a linear system, whereas t_{De} is the dimensionless time defined with B as the characteristic length,

$$t_{De} = \frac{0.0002637kt}{\phi\mu c_t B^2} \tag{2.46}$$

"B" is then found by the following equation

$$\frac{B^2}{{x_f}^2} = \frac{t_{Dxf}}{t_{De}} = \pi t_{Dxf} \tag{2.47}$$

where "B" represents the depth of investigation to the formation. Having known the fact that the values of "B" is a function of time, Eq. 2.44 expresses the transient flow. In Eq. 2.47, t_{Dxf} is the time using x_f values as the characteristic length,

$$t_{Dxf} = \frac{0.0002637kt}{\phi\mu c_t {x_f}^2} \tag{2.48}$$

Fot the values of t_{De} selected to be 0.318, the "B" becomes equal to

$$B = 0.02878(\frac{kt}{\phi\mu c_t})^{1/2} \tag{2.49}$$

This t_{De} value is applicable to portray an early time elliptical flow that resembles linear flow when fracture-tip effects are not evident. Later, as fracture-tip effects become significant, the elliptical flow geometry nearly resembles radial flow. From Jones' study in 1963, the dimensionless time of t_{De} needed to gain stabilization within a defined drainage region for a radial system is equal to - 0.38. Substituting the value into the equation, we will get the following definition for "B":

$$B = 0.02634(\frac{kt}{\phi\mu c_t})^{1/2} \tag{2.50}$$

The expression of p_D is given by the following equation:

$$p_D = \frac{kh}{1422q_g(T+460)}\Delta p_p \tag{2.51}$$

Dimensionless pressure responses were estimated with modified B values (Eq. 2.50). As it was anticipated, the particular solution for linear flow is closer to Hale and Evers' solution in comparison with Riley's solution. But, due to the fact that we are going to model the elliptical flow regime, the value of t_{De} with the best match (0.38) is the preferred value in this time region. Elliptical flow exhibits a straight line on a semi-log graph of pseudo-pressure drop vs. ln(A+B). This formula is applicable for infinite-conductivity vertical fracture scenario.

Substituting the definition of dimensionlles pressure (Eq. 2.51) into Eq. 2.44, we can use the slope and x axis intercept values to find hydraulic fracture and formation permeability values as the following:

$$k = \frac{1422 q_g (T+460)}{mh} \tag{2.52}$$

and

$$x_f = exp(i) \tag{2.53}$$

The strategy to analyze the data to find formation permeability and fracture half-length is shown below as follows (procedure is iterative):

1. Take initial guesses for formation permeability and fracture half-length values.
2. Compute "A" and "B" values using Eqs. 2.45 znd 2.50, respectively.
3. Plot Δp_p vs. ln(A+B) and specify a straight line.
4. Assess formation permeability and fracture half-length using slope and x-axis intercept, respectively.
5. Update permeability and fracture half-length estimates and iterate to converge.

It must be mentioned that the computations of formation permeability and fracture half-length for a single iteration does not bear any dependence on each other.

For finite-conductivity vertical fractures (F_{CD}<300), additional pressure drop exists within the fracture. Prats showed that, for an infinite conductivity fracture, the effective wellbore radius can be assessed as the following:

$$r_{we} = \frac{x_f}{2} \tag{2.54}$$

Later on, Meyer and Jacot (2005) suggested an accurate formula as the following:

$$\frac{x_f}{r_{we}} = \frac{\pi}{F_{CD}} + 2 \tag{2.55}$$

If we apply Eq. 2.54 to a finite-conductivity fracture scenario, it yields

$$r_{we} = \frac{x_{fe}}{2} \tag{2.56}$$

where x_{fe} is the effective half-length for a finite-conductivity fracture scenario and is identical to one of the infinite-conductivity fracture. Substituting Eq. 2.55 into Eq. 2.56, we obtain the ratio, R as indicated in the following expression:

$$R = \frac{x_f}{x_{fe}} = \frac{\pi}{2F_{CDe}} + 1 \tag{2.57}$$

Consequently, the dimensionless pressure will be the following:

$$p_{pD} = ln\left[\frac{A+B}{x_{fe}}\right] = ln[(R * B + \sqrt{(R * B)^2 + {x_f}^2})/x_f] \tag{2.58}$$

For finite-conductivity fracture scenario, effective fracture half-length is then substituted into Eq. 2.44. If we define A` and B` as

$$B` = R * B \tag{2.59}$$

and

$$A` = \sqrt{B`^2 + {x_f}^2} \tag{2.60}$$

Then, p_{pD} has to be rewritten as:

$$p_{pD} = ln[(A` + B`)/x_f] \tag{2.61}$$

From the final equation we can see that elliptical flow data for a finite-conductivity fracture exhibits a straight line on a semi-log graph of Δp_p vs. ln(A`+B`). For the finite conductivity fracture scenario we have two independent iterative procedures: One for, determination of k and x_f values iteratively; and second, to find F_{CD} values iteratively. The steps in the first process are indicated below:

1. Take initial guesses for formation permeability, half-length and fracture conductivity values.
2. Calculate A` and B`values.
3. Plot Δp_p vs. ln(A`+B`) and identify a straight line.
4. Compute permeability from the slope of the straight line using Eq. 2.52, and fracture half-length values from the x-axis intercept using Eq. 2.53.
5. Update permeability and fracture half-length values, and iterate until they converge. F_{CD} values retains the same value for the convergence process of permeability and fracture half-length values. Thereinafter, as a second step we move on to determine F_{CD} iteratively:
6. Plot Δp_p vs. $t^{1/4}$ and analyze the straight line.
7. Calculate fracture conductivity from the slope of specialty plot and permeability values from the first procedure. Bilinear flow is modeled by (Lee et al. 2003):

$$p_{pD} = \frac{1.38\sqrt{\pi k x_f}}{\sqrt{w k_f}} t_{Dxf}{}^{1/4} \tag{2.62}$$

Combining equations Eq. 2.48, 2.51 and 2.62 we get:

$$wk_f = \left(\frac{443.2 q_g (T+460)}{m_b h}\right)^2 \left(\frac{1}{\phi \mu c_t k}\right)^{0.5} \tag{2.63}$$

8. Update F_{CD} and the estimated k, x_f, and wk_f values from Steps 4 and 7.
9. Repeat Steps 1 to 8 using updated values permeability, fracture half-length and fracture conductivity values until the convergence is attained.

2.4.1.8 Infinite acting pseudoradial flow

For the particular flow regime, flow behavior is identical to radial flow with a negative skin effect due to the presence of hydraulic fractures. Semilog and log–log plots of pressure vs. time is used for interpretation purposes during this regime. Below is the example of drawdown data which can be analyzed by the following equations:

$$p_{wf} = p_i - \frac{162.6 Q_o B_o \mu}{kh}\left[log(t) + log\left(\frac{k}{\phi h c_t {r_w}^2}\right) - 3.23 + 0.87s\right] \tag{2.64}$$

or in a linear form as:

$$p_i - p_{wf} = a + m\ log(t) \tag{2.65}$$

with the slope m of:

$$m = \frac{162.6 Q_o B_o \mu_o}{kh} \tag{2.66}$$

Solving for the formation capacity gives:

$$kh = \frac{162.6 Q_o B_o \mu_o}{m} \tag{2.67}$$

The skin factor s can be calculated by:

$$s = 1.151\left(\frac{p_i - p_{1hr}}{m} - log\left(\frac{k}{\phi \mu c_t {r_w}^2}\right) + 3.23\right) \tag{2.68}$$

We have to make sure that the slope is identical when preparing semilog plot for BHP vs. time, then:

$$s = 1.151\left(\frac{\Delta p_{1hr}}{m} - log\left(\frac{k}{\phi \mu c_t {r_w}^2}\right) + 3.23\right) \tag{2.69}$$

The Δp_{1hr} can be computed by the following expression:

$$m = \frac{\Delta p_{@\ log(10)} - \Delta p_{1hr}}{log(10) - log(1)} \tag{2.70}$$

If we solve the equation stated above for Δp_{1hr}, it gives:

$$\Delta p_{1hr} = \Delta p_{@log(10)} - m \tag{2.71}$$

2.5 Rate Transient Analysis (RTA) in Shale Gas Reservoirs

Rate-transient analysis (RTA) stands for production data analysis, which implements concepts similar to PTA. Some significant development for RTA method was made for conventional formations in past four decades. RTA essentially makes simplifying assumptions about reservoir, stimulation and fluid properties. For SG and CBM reservoirs, the following properties make analysis much more complex (Clarkson et al., 2012):

1. Gas desorption
2. Extremely low matrix permeability values, which is why transient flow period lasts a lot more than for conventional formations
3. Two porosity or dual-perm behavior due to the presence of natural fractures
4. Multilayer beds, and geological heterogeneities
5. Stress-dependent porosity/permeability due to presence of strongly compressible fracture pore volume
6. Shrinkage effects associated with gas desorption
7. Gas & water multiphase flow
8. Non-Darcy flow, which encompasses diffusion and slip-flow effects

Some corrections for 1, 5, 6, 7, 8 points require change in primary variables used for RTA, such as implementation of pseudo-variables that capture in fluid property adjustment of reservoir characteristic and desorption effects. If this procedure is properly implemented, data will be compatible for analysis under single-phase slightly compressible fluid conditions.

Short and long-term production characteristics for unconventional gas formations are influenced by hydraulic fracture geometry. Due to the fact that the multi-fractured horizontal wells are now essentially implemented for SG development, quantitative characterization of hydraulic fracturs shows to be of a complex manner, so that initiated fracture geometries are rarely similar to conventional “bi-wing” planar fracture geometry that is the primary assumption in conventional formations. For the case of initiation of complex geometries characterization concept of stimulated reservoir volume (SRV) (Mayerhofer et al., 2010) is implemented, which makes reservoir and stimulation characterization to be indivisible due to the fact that hydraulic fractures serve in defining the field. It is a big challenge to separate those two for the sake of characterization of the reservoir and hydraulic fracture which is impacted by any combination of completion and stimulation method applied on the field which has a key role on the type and sequence of flowing regimes that are observed, and consequently the methods implemented for analysis.

2.5.1 RTA Concept and Flow Regimes

RTA is similar to a pressure drawdown test, where the well is opened for production against known wellbore constraints for a sufficiently long time – for the whole life of the well. In conventional well-test analysis, a short drawdown period is followed by long PBU period where these test periods can be used for diagnosis of reservoir and/or hydraulic fracture properties. Those tests are essemtially conducted in a range of days in strongly controlled conditions where data acquisition is more frequent and accurate. In case of RTA, the flowing period is generally equal to producing life of a well, which may be interrupted by shut-in periods. In case of absence of downhole pressure gauges the quality and acquisition frequency is much lower in comparison with well testing analysis.

The starting point for RTA is flow-regime identification. The most common method is implementation of pressure derivative function of rate-normalized pressure (RNP) against time on a log–log plot. The use of Bourdet (Bourdet et al., 1983, 1989) method is implemented for derivative calculations. The implementation of pseudo-time function was performed in order to get data equivalent to constant rate conditions, and account for desorption and gas property changes. Having identified prevailing flow regimes in the reservoir, we can use some analysis techniques for the sake of determination reservoir characteristics. The example in Fig. 2.11 is for vertical well, infinite conductivity hydraulic fractures, completed in a bounded homogeneous tight gas reservoir. For the particular example, the following flowing regimes show out: formation linear, elliptical, pseudoradial and boundary-dominated flow regimes. If there is an additional pressure drop along the fractures occurring concurrently with formation linear flow –it gives rise to bilinear flow regime. Fracture linear flow regime can be showed out at early times for finite conductivity fracture scenario, but this flow regime is essentially too short to be seen and does not have any practical use in reality.

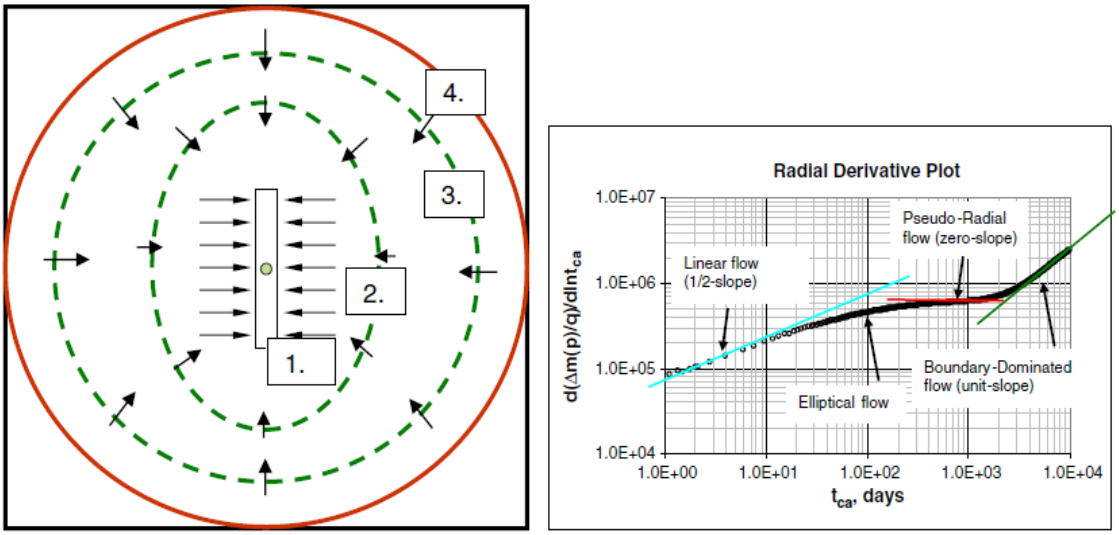

Figure 2. 11 (a) Flow-regimes associated with a slightly-stimulated vertical well subject to constant flow-rate, (b) Identification of flow-regimes for a simulated (non-stimulated) vertical dry coal well (Clarkson 2011)

Fig.2.11 is an example of constant BHP vertical well with a single-infinite conductivity hydraulic fracture, from homogeneous/isotropic tight gas reservoir simulation model. Material balance time function has been implemented to convert the constant BHP to equivalent constant rate conditions. In this particular example, three flow regimes are identified as linear, radial and boundary dominated flow (BDF) which corresponds to half, zero and unit slope respectively on the particular plot. Additionally, a transitional elliptical flow period exists showing non-linear behavior on the derivative plot between linear and radial flow regimes.

The sequence of flowing regimes is much more complicated for multi-fractured horizontal wells (MFHW) as shown in Figure 2.12a. (Chen and Raghavan, 1997; Raghavan et al., 1997). Figure 2.12 stands for an example from MFHW with multiple infinite conductivity planar fractures simulated for the same conditions as in the first example. Interference between hydraulic fractures may appear which will be observed as a BDF from log-log plot of RNP derivative. In comparison with previous example there is a possibility of observing two linear where the first corresponds to formation linear flow whereas the second one stands for compound linear flow which is an indication of the flow perpendicular to effective wellbore length (Chen and Raghavan, 1997; Raghavan et al., 1997; van Kruysdijk and Dullaert, 1989).

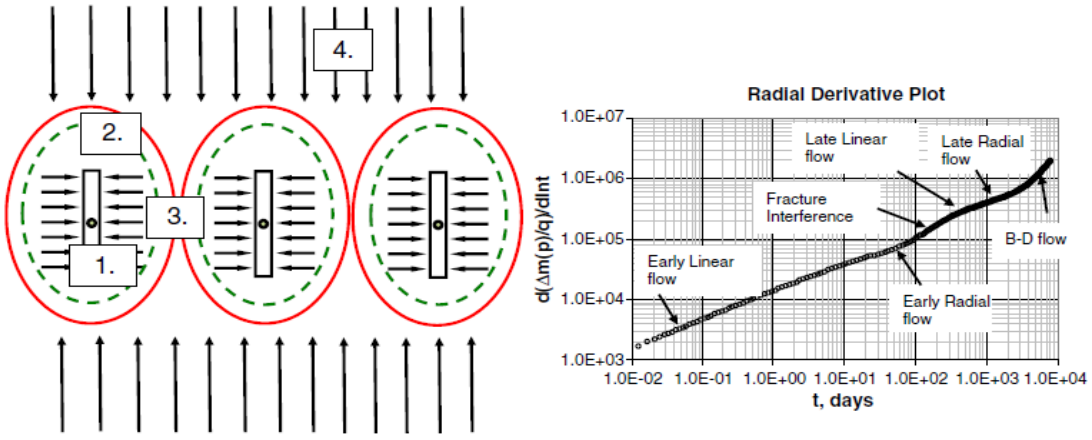

Figure 2. 12 (a) Sequence of flow-regimes for a multi-fractured horizontal well with planar infinite conductivity fractures, (b) Radial Derivative plot of MFHW (Clarkson and Beierle, 2011).

RNP derivative is used for flow regime identification (Fig. 2.12b); the results may be completely different depending on frac-spacing and reservoir characteristics. The earlier sublinear occurs as a consequence of skin effects which has either mechanical or due to flow convergence characteristics (Nobakht and Mattar, 2012). Fracture spacing is the key parameter which controls duration of early radial flow (Nobakht et al., 2012a). Simulation gridblock pressure gradients are of a great importance for visualization of flow regime sequences in the field. The primary distinguishing feature RNP derivative behavior between shales and conventional reservoirs is that there is no transitional flow regime after early linear flow.

Having identified all the prevailing flow regimes, production analysis is implemented for the sake of determining reservoir and stimulation characteristics of the well. As discussed by Clarkson and Beierle (2011) there are distinct production analysis methods that are commonly used for interpretation of unconventional gas formation as indicated below:

1. Straight-line Analysis
2. Type-curve methods
3. Analytical and numerical simulation
4. Empirical methods
5. Hybrid methods which is the combination of analytical and empirical methods

2.5.2 Straight Line Analysis

These analysis methods are identical with those that are used in PTA (Lee et al., 2003). Having identified prevailing flow regimes using RNP derivative function on log– log plot, each of those flowing regimes is analyzed using the designed specialty plots. Most of these solutions were derived for drawdown well-tests, as discussed in (Lee et al., 2003). The solution for elliptical flow regime was suggested by Cheng et al. (2009). As will be discussed below, RNP function superposition time functions are implemented for the sake of accounting variable rate/BHP production and pseudo-variables are deployed in order to handle gas property changes with respect to prevailing pressures. These transformations make eligible the use of analysis techniques that works for slightly-compressible fluid scenario.

Different flow regimes allow us to find a particular hydraulic or reservoir property. From the fracture linear flow region we can determine the product of fracture width and fracture permeability; bilinear flow-regime hydraulic fracture conductivity if we already have reservoir permeability values; from the formation linear flow, hydraulic fracture half-length can be found using the slope of linear specialty plot if we already have estimated permeability values. The elliptical flow regime analysis was recently suggested by Cheng et al. (2009). The outstanding feature of elliptical flow regime is that it does not appear as a straight-line on a semi-log RNP derivative plot, and this particular flow regime is used for the sake of estimation of hydraulic fracture half-length and reservoir permeability values. Permeability may also be extracted from slope of the radial specialty plot from the data corresponding to radial flow regime. Finally, OGIP value can be assessed from the x-intercept of the specialty plot from production data region corresponding to BDF period.

2.5.2.1 Fracture Linear Flow

On the radial derivative of rate normalized pressure function, fracture linear flow shows to be as a half-slope region for infinite conductivity fractures. For the cases when hydraulic fractures are finite conductivity the value may exceed the value of 0.5 on log-log plot. This represents early transient linear flow in the fracture system only.

$$w_f\sqrt{k} = \frac{40.93T}{m_L h(\phi\mu_{gi}c_{ti})^{1/2}} \tag{2.72}$$

where m_L is the slope obtained from the plot of $\frac{m(p_i)-m(p_{wf})}{q}$ vs $\sqrt{t_a}$, and the previous equation is used to determine the fractured permeability if other properties are known.

2.5.2.2 Bilinear Flow

It is caused by simultaneous transient flow in the fracture system and matrix.

$$\left(w_f k_f\right)^{\frac{1}{2}}(k)^{\frac{1}{4}} = \frac{443.2T}{h\sqrt[4]{(\phi\mu_{gi}c_{ti})}}\frac{1}{m_{BL}} \tag{2.73}$$

where m_{BL} is the slope obtained from the plot of $\frac{m(p_i)-m(p_{wf})}{q}$ vs $\sqrt[4]{t_a}$, (Clarkson an Beierle 2011) and if matrix permeability is known we can extract fracture conductivity values.

2.5.2.3 Formation linear Flow

This flow period appears right after transition period stated above in the case of $F_{CD} > 300$ and it is spotted as a half slope on log-log plot of radial derivative. Analysis equation is

$$\left(x_f k_f\right)^{\frac{1}{2}}(k)^{\frac{1}{4}} = \frac{443.2T}{h\sqrt[4]{(\phi\mu_{gi}c_{ti})}}\frac{1}{m_L} \tag{2.74}$$

where m_L is the slope obtained from the plot of $\frac{m(p_i)-m(p_{wf})}{q}$ vs $\sqrt{t_a}$, (Clarkson and Beierle 2011) and the previous equation is used to determine the fractured permeability if other properties are known.

2.5.2.4 Elliptical Flow

This flow period is the case for the extra-low permeability reservoirs with long hydraulic fractures. It is very practical for use as it is often the case for unconventional formations when radial flow is not achieved but there is sufficiently long elliptical flow period. This flow period corresponds to the region happening just prior to pseudoradial flow on the RNP derivative plot. This is an iterative process (discussed earlier in this chapter). Analysis equations are:

$$k = \frac{1422 q_g (T+460)}{m_E h} \tag{2.75}$$

and

$$x_f = exp(i) \tag{2.76}$$

Additionally, for finite-conductivity fracture case process includes two iterations to find 1)matrix permeability and hydraulic fracture half-length; and 2) fracture conductivity values.

$$w_f k_f = \left(\frac{443.2(T+460)}{m_E h}\right)^2 \left(\frac{1}{\phi \mu c_t k}\right)^{0.5} \tag{2.77}$$

where m_E is the slope obtained from the plot of $\frac{m(p_i)-m(p_{wf})}{q}$ vs $ln(A+B)$, (Clarkson an Beierle 2011) .

2.5.2.5 Pseudoradial Flow

The flow period shows to have a zero slope on RNP radial derivative plot. Matrix permeability and damage skin are primary deliverables from the particular flow regime data. Analysis equation are:

$$k = \frac{1637T}{m_R h} \tag{2.78}$$

and

$$s = 1.1513\left(\frac{b`_R}{m_R} - \log\left[\frac{k}{\phi \mu_{gi} c_{ti}}\right] + 3.23\right) \tag{2.79}$$

where m_R is the slope and $b`_R$ is the y axis intercept obtained from the plot of $\frac{m(p_i)-m(p_{wf})}{q}$ vs log(ta) plot (Clarkson an Beierle 2011) .

2.5.3 Pseudo-time Function

It can be analytically shown that square-root-of-time (RNP vs square-root-of-time) plot is dependent on the production rate (Fig 2.13). Depending on the production rate square-root-of-time plot may deviate from a straight line during linear flow (Morteza, 2012). Likewise, the higher the production rate the earlier the plot deviates from the expected straight line. This deviation brings to front some errors for data interpretation, especially for flow regime identification. For that reason, pseudo-time function is incorporated for data analysis. Pseudo-time is a mathematical time function that accounts for the variable compressibility(c_t) and viscosity (μ_g) of gas as well as the variable total (formation) porosity (f) with respect to time and pressure.

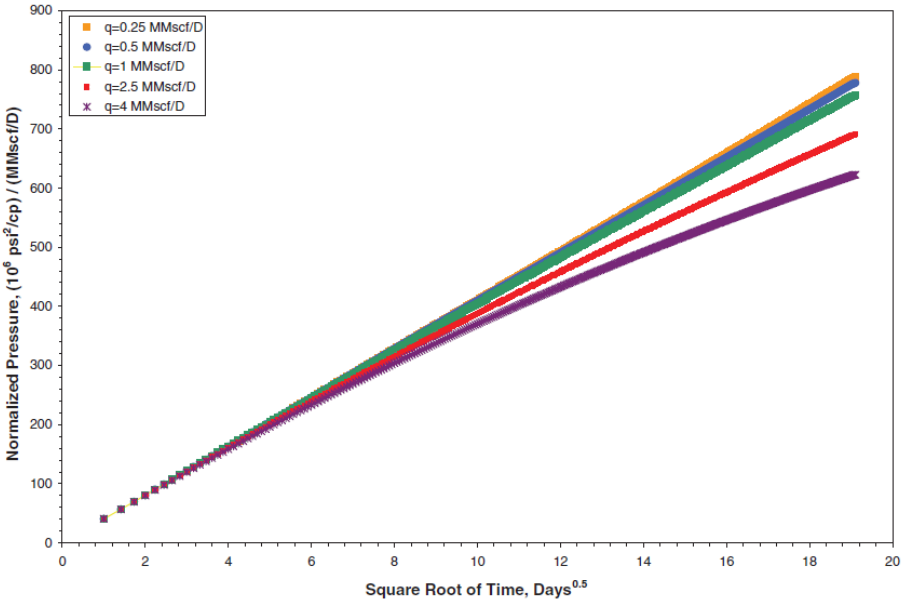

Figure 2. 13 Square-root-of-time plot for various flowing rates (Morteza, 2012)

In well testing, analytical equations are solved after making certain assumptions. In general, four assumptions are taken into account. These are:

- Total system compressibility (c_t) is constant
- Gas viscosity (μ_g) is constant
- Total porosity (ϕ) is constant
- Fluid saturations (S_g and S_w) are constant.

For gas, most of the assumptions listed above are no longer valid. Gas compressibility (c_g) varies significantly with pressure. Gas viscosity (μ_g) and gas compressibility factor also vary with pressure but not to the same degree. Pseudo-pressure and pseudo-time (t_a) are used to deal with these changing properties and linearize the flow equations for gas. With the introduction of pseudo-pressure and pseudo-time, the gas flow equation can be written in a manner similar to the liquid equation. It should be noted that the concept of pseudo-time is not susceptible to a completely rigorous solution, as is the case for pseudo-pressure, because the gas properties change with pressure, but not with time. Pseudo-time was developed by Agarwal (1980) and he characterized pseudo-time function in terms of the viscosity and total compressibility at wellbore conditions. Time function had negligible effect on late time data, and was essentially used for PBUs only. Later on, it was realized that the Agarwal definition of pesudo-time for buildups, was incompatible with BDF. Likewise, Agarwal pseudo-time definition showed to be not capable of handling the problem, due to the fact that it was using a simplified version of the total

system compressibility (c_t). Later on Blasingame has introduced a new definition of pseudo-time in order to handle depletion effects. He suggested defining pseudo-time function in terms of average reservoir pressure rather than at wellbore conditions. The new pseudo-time correction (Eq 2.80) appeared to be working under BDF conditions.

$$t_a = (\mu_g c_t)_i \int_0^t \frac{dt}{\mu_g c_t} \tag{2.80}$$

However, when transient flow prevails, the pseudo-time concept is not valid and its use can create anomalous responses. This will occur in low permeability systems or in reservoirs with irregular shapes, especially where some of the boundaries are very distant from the well. Anderson and Mattar (2005) showed that, in reservoir with significant transient flow, it was more appropriate to define pseudo-time in terms of the average pressure within the region of investigation rather than the average reservoir pressure and finally corrected pseudo-time was introduced which calculates values at reference pressure within the area of influence. The following procedure should be followed to analyze linear flow production in case of corrected pseudo-time:

1. Plot RNP vs $\sqrt{t}$ on Cartesian coordinates in order to determine the slope of the line, m
2. Using the slope determine $x_f\sqrt{k}$ value using the following equation:

$$x_f\sqrt{k} = \frac{200.8T}{mt\sqrt{(\phi\mu_g c_t)_i}} \tag{2.81}$$

3. Calculate the average pressure in the region of influence at different times using the following equation:

$$\frac{\bar{p}}{\bar{Z}^{**}} = \frac{p_i}{Z_i^{**}}\left(1 - \frac{1000B_{gi}\sqrt{(\phi\mu_g c_t)_i}}{4x0.113h\phi S_{gi}x_f\sqrt{k}}\sqrt{t}\right) \tag{2.82}$$

4. Calculate the corrected pseudo-time for constant rate production, t_a, from Equation 2.80 and by using the average pressure in the region of influence (Fig. 2.14)

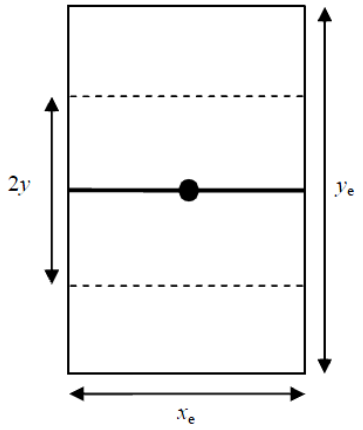

Figure 2. 14 A hydraulically fractured well in the center of a rectangular region (Morteza, 2012)

5. Plot RNP vs $\sqrt{t_a}$ on Cartesian coordinates in order to determine the slope of the line, m
6. Using new slope values calculate $x_f\sqrt{k}$ using Equation 2.81
7. Continue Steps 3-6 until $x_f\sqrt{k}$ converges.

For the sake of incorporation of complex reservoir behavior in the straight line analysis for CBM and shale gas reservoirs is through the alteration of pseudo-time function. Alterations have been made for a) adsorption (Eq 2.83),

$$t_a{}^* = (\mu_g c_t{}^*)_i \int_0^t \frac{dt}{\mu_g c_t{}^*} \tag{2.83}$$

where

$$c_t = c_g + \frac{\rho_B B_g V_L P_L}{32.0368(p_L+p)^2\phi} \tag{2.84}$$

b) non-static permeability (Eq 2.85),

$$t_a = \frac{(\mu_g c_t)_i}{k_i} \int_0^t \frac{\bar{k}(p)dt}{\overline{\mu_g c_t}} \tag{2.85}$$

and c) non-Darcy flow (Eq 2.86)

$$t_a = \frac{(\mu_g c_t)_i}{k_\infty} \int_0^t \frac{\overline{k_a}(p)dt}{\overline{\mu_g c_t}} \tag{2.86}$$

CHAPTER 3

STATEMENT OF PROBLEM

In recent years diverse analytical and numerical analyses were executed for characterization of unconventional reservoirs. Pressure transient characteristics of unconventional formations are crucial for both evaluation of fracturing treatment and overall in estimation of fracture and reservoir parameters and production forecasting of a particular field. However, ultra-low permeability is the main constraint for such analysis as it needs longer durations for well testing data. Production data of such formations is the main source that is used for the utilization of the fracture and matrix properties in this particular study.

The particular study is based on utilization of diverse well testing analysis methods for production data extracted from the shale gas simulation model. The objectives of this thesis work are: 1) to employ analysis methods established for hydraulically fractured wells to the shale gas simulation model to understand the applicability of the methods on unconventional systems; 2) compare the values found for different flowing and fracture stage conditions; 3) determine drawbacks of utilization of the conventional well testing methods on synthetic shale gas field, 4) to understand how to apply analysis techniques to handle flow regime identification

CHAPTER 4

SIMULATION MODEL

Initially, a 3D layered model grid was designed (Erturk, 2013) and petrophysical properties were assigned by Petrel. As the next step, Eclipse 300 - numerical compositional simulator, was adopted to examine scenarios of horizontal wells with multi stage hydraulic fracturing for shale gas reservoir. The 3D grid which has 32500 cartesian blocks (Nx=25, Ny=25, Nz=52) designed with four intervals having thicknesses of 5, 9, 15, 19 meters, and used for all scenarios by the way of updating the specific properties of each system. The horizontal well is designed to have 800 meters of effective length that is completed in shale gas reservoir with the thickness of 19 meters, in our particular case. Later on, one to three hydraulic fractures with 250 meters fracture half-length was designed in the model. The details for the simulation model are shown in Table 4.1.

Table 4. 1 Simulation Dataset for Shale Gas Reservoir (Erturk, 2013)

Parameters	Values	
	Matrix	Fracture
Permeability in X direction, md	0.0004	0.0004
Permeability in Y direction, md	0.0004	0.0004
Permeability in Z direction, md	0.0004	0.0004
Porosity	0.04	0.002
Net Thickness, m	9	9
Sw	0.1	
Average Reservoir Temp., C	92	
Langmuir Pressure, bar	46.89	
Langmuir Volume, m^3/kg	0.0118	
HF half-length, m	250	
HF height, m	9	
Rock Density, kg/m^3	1434	
Rock Compressibility, 1/bars	7.25E-05	

Increased permeability for the grid blocks was applied for 9 meters interval where permeabilities are set in a logarithmically decreasing manner in vertical and horizontal directions. The permeability distribution for refined grid blocks (5^{th} layer) is shown in Appendix G.

Simulation scenarios were conducted using Eclipse 300 software. Following are the key modeling parameters of studied unconventional gas resources:

- Dual Porosity System
- Natural Fractures
    - Fracture Spacing, Aperture, Length
    - Natural Fracture Orientation
- Hydraulic Fracturing
    - Fracture Half Length, Height, Width,
    - Hydraulic Fracture Distribution
- Dynamic Permeability
- Adsorption Isotherm
- Geomechanics

4.1 Dual Porosity Modeling

Shale gas reservoirs are naturally fractured systems and typically modeled as dual porosity system. In shale gas reservoirs, natural fractures are narrow and sealed owing to the pressure of the overburden rock (Gale, et al. 2007) and they must be stimulated to reactivate the natural fracture matrix. Dual porosity approach was proposed by Warren and Root to separate the flow within fractures and flow caused by contribution from the reservoir matrix (Warren & Root, 1963). The reservoir is characterized by two overlapping continua - with fracture networks serving the role of primary contribution to flow and matrix blocks which holds the role of storage. The interaction between these two continua is controlled by shape factor (σ) term that can be evaluated with typical dimensions of matrix blocks (Kazemi, 1976).

The shape factor may be expressed by analytical derivations, numerical derivations, and time-dependent functions. Several authors proposed shape factor constant but Kazemi and Gilman type of shape factor is mostly utilized in the numerical simulators since it is easy to apply. The

shape factor (σ) accounts for the matrix-fracture interface area per unit bulk volume and Kazemi has proposed the following form for σ:

$$\sigma = 4\left[\frac{1}{L^2_x} + \frac{1}{L^2_y} + \frac{1}{L^2_z}\right] \tag{4.1}$$

where Lx, Ly, and Lz are typical X, Y and Z dimensions of the blocks of material making up the matrix volume and they refer to fracture spacing in represented directions and also Lx, Ly, and Lz are thus not associated to the simulation grid dimensions.

In a dual porosity reservoir, fluids exist in two interconnected systems (Figure 4.1):

- Rock Matrix System

- Rock Fracture System

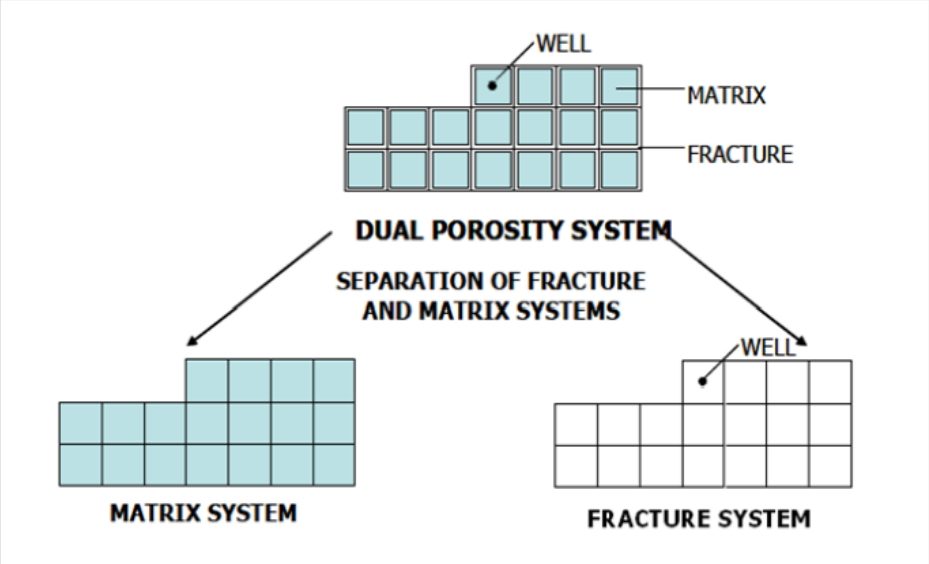

Figure 4. 1 Rock matrix-fracture system reservoir model (Nelson, 2001)

Matrix blocks are linked only by fracture system having no connection among individual matrix blocks, and thus flow occurs only within the fracture system. For the sake of modeling such systems, simulation cells are connected with each block in the geometric grid.

4.2 Hydraulic Fracture Modeling

For the sake of modeling of hydraulic fracturing on the synthetic field methods stated below were used:

- Grid refinement
- Multiply permeability
- PI Modification
- Negative Skin

An assumption made that the fractures lie in the single plane of local grid cells that approximates the real geometric fracture orientation. Grid refinement is symmetrically located within the plane of host cells and the X, Y, and Z transmissibility multipliers for all grid cells intercepted by the fracture are assigned according to the position of the grid cells since the hydraulic fracture conductivity is reduced away from the wellbore and above the perforation landing point. Grids were created distinctly for vertical and lateral well configurations. For the vertical well of shale gas and tight gas cases, the grids located in the middle layer of each zone with 5x25 blocks along I and J plane of host cells respectively. For the horizontal well of shale gas and tight gas cases, the local grids located in the middle layer of each zone with three stages 25x5 blocks along I and J plane of host cells respectively.

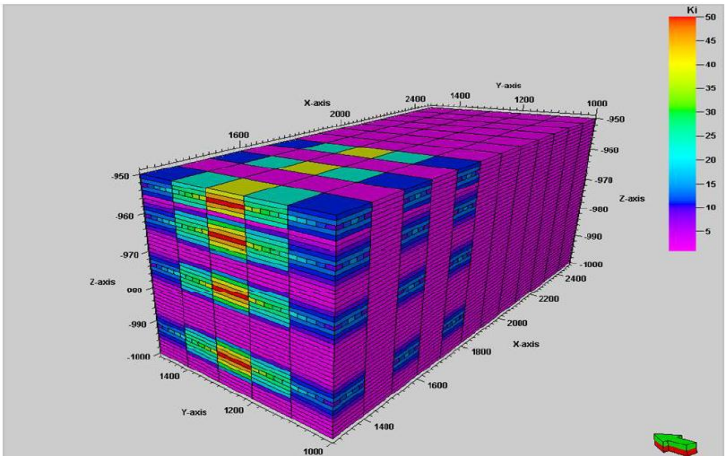

Figure 4. 2 Local Grid Refinent of Hydraulic Fractures for Multilateral Well (Mehmet Cihan Erturk, 2013)

The decreasing conductivity of hydraulic fractures of these two distinct systems in the reservoir was regulated with different permeabilities that have smaller values away from the wellbore in the horizontal and vertical directions. These arrangements are represented in the Figure 4.2 for

the horizontal completion scenario. Distance between the refined grid blocks is one grid block or 100 meters.

4.3 Adsorption Modeling

Adsorption term is defined as gas molecules that are accumulated on the surface of a reservoir rock (Montgomery et al, 2005). The amount of adsorbed gas is determined in gas volume per unit mass (for example, scf/ton) and is affected by various factors such as nature of the solid sorbent, temperature, pressure etc. In some circumstances, it has a huge impact on the gas production. The diffusive flow between the matrix and the fracture is given by adsorption or diffusion models. The adsorbed gas concentration on the surface of the rock is assumed to be a function of pressure and only described by a Langmuir Isotherm that is entered into system as a table of pressure versus adsorbed concentration.

In shale gas module of Eclipse, the pore volume of the matrix cells has a different interpretation than for an ordinary dual porosity run; it gives the shale volume of the cell, using the time-dependent sorption model. By default the porosity is set to unity minus the porosity of fracture. The cell bulk volume times the porosity then equals the shale volume.

It is possible to choose between two types of adsorption model: instant and time dependent. In our simulation cases, time-dependent sorption model was used. For the time dependent method, a simulation cell either contains free gas in a pore space or adsorbed gas in the rock. The rock is characterized by a single simulation cell and connecting simulation cell. A cell having a non-zero coal region number as set by COALNUM, it needs to specify a porosity value that corresponds to a rock fraction value. For cells having a zero coal region number the porosity value correspond to the pore volume fraction as illustrated in Figure 4.3

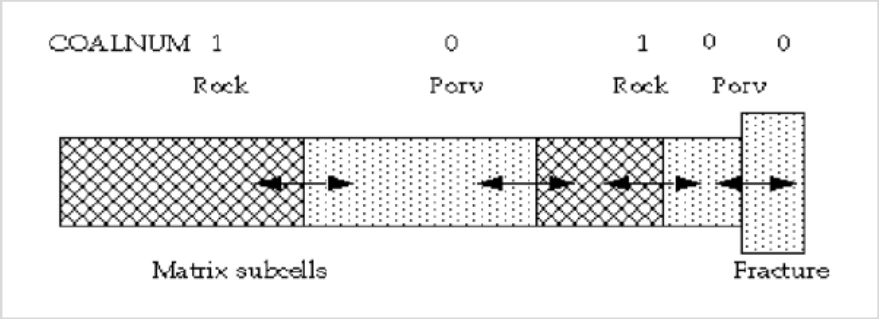

Figure 4. 3 Representation of matrix diffusion (Eclipse 2011 Manual)

If pore volume-to-pore volume connections exist, permeability values also need to be input in order to compute the transmissibility between the matrix subgrid cells. The diffusive flow between the matrix and the fracture is a function of molar density in the matrix coal/shale, matrix fracture diffusivity, rock density, diffusion coefficient, and gas saturation. In addition, the matrix fracture diffusivity depends on the cell bulk volume and the shape factor that accounts for the matrix-fracture interface area per unit volume. Often sorption time is a quantity that is easier to obtain than the diffusion coefficients. This parameter controls the time lag before the released gas enters the coal fracture system.

4.4 Compaction Effect

The permeability is critically sensitive to changes in effective stress (pore pressure) during drawdown. For the coalbed methane and shale gas cases, permeability changes as a function of pressure due to matrix shrinkage and compression process of natural fractures. As the pressure reduces during the production, overburden stress increases and permeability decreases, however pressure drop leads to desorption of gas on the surface of coal matrix and that give rises to shrinkage of matrix which enhance the width of cleats. This phenomena has been proposed by Palmer and Mansoori (1996) and illustrated in the Figure 4.4 and 4.5.

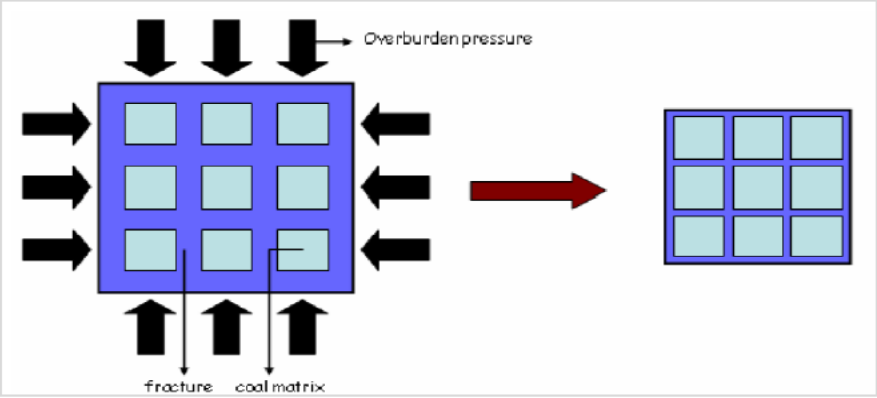

Figure 4. 4 Schematic of coal seam before cleats compression and after cleats compression (Palmer, 1996)

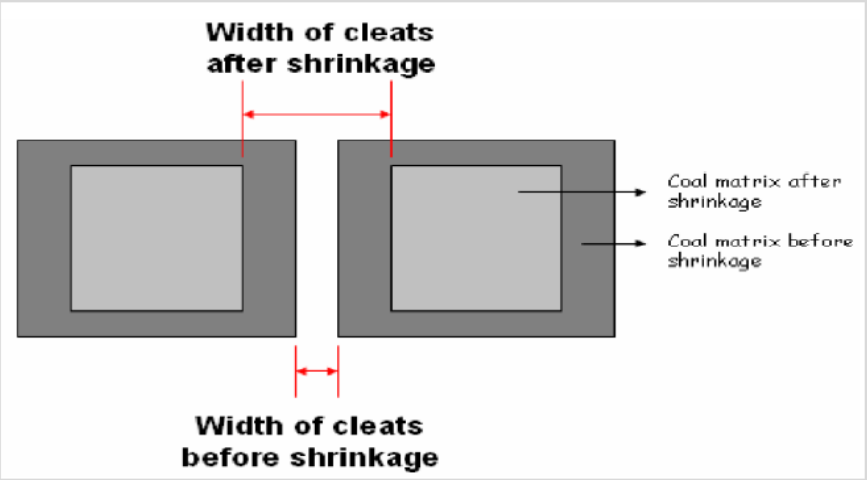

Figure 4. 5 Schematic of matrix shrinkage phenomenon (Palmer, 1996)

Palmer and Mansoori model includes the rock compaction effect on the production and it is also included in the model to account for production caused by compaction.

CHAPTER 5

METHODOLOGY

In this work, simulation model built up for production performance analysis of shale gas reservoir case with different well trajectories and completion techniques (Erturk, 2013) was used to perform simulation runs in order to get production data for pressure and rate transient analysis. The starting point was to use make constant rate production simulation runs for rates set to 1000, 500 and 200 m^3/day. In order to perform this operation in <<Shale-Horizontal-1-stg.DATA>> Eclipse 300 input data file we set the <<'MCE-1' OPEN GRAT 2* 1000 2* 6.9 / >> command on WCONPROD function tab where production rate is set to 1000 m^3/day and bottomhole flowing pressure limit is set to 6.9 bars. The same procedure was applied with 500 and 200 m^3/day for simulation runs with one and more fracture stages. Data was exported in a monthly basis for twenty years, between Jan 1, 2012 to Jan 1, 2032. Using Table 4.1 and constant rate production data from simulation several analytical methods were applied in order to obtain reservoir and stimulation parameters.

5.1 Application of Kappa-Saphire Well Testing Interpretation Software

As a part of Saphire Well Testing Interpretation tool standard gas well testing option was used for interpretation of the simulation data. As a Well Model, “Finite Conductivity Fracture” model was applied. “Two Porosity Sphere” model were implemented in order to account for three dimensional flow from matrix to natural fractures. Boundary condition was selected to be infinite for the reservoir model. It was assumed to have a single hydraulic fracture which has the length equal to the sum of all fracture stages for multiple stage hydraulic fracture scenario. “Improve” button was used to estimate the set of parameters that minimizes the sum of errors between the model and measured data by the way of non-linear regression. Under Saphire, the regression can be run either on the "log-log" or on the "simulation" (pressure history). “Simulation” regression is used when pressure data is partially available and the regression may be made on the full pressure history of the well. The “log-log” regression optimizes the fit between recorded and calculated values for the extracted flow period only and works on the delta P values only. “Log-log” regression is considered for the particular analysis as we already have full pressure history data and do not need to back calculate it again. Bourdet derivative was used as a derivative method in the software tool.

5.2 Application of Fekete F.A.S.T. Well Testing Interpretation Software

In comparison with Saphire Well Testing Interpretation tool, additionally, pseudo-time function is used to account for correction to gas properties and pseudo-pressure term is replaced by rate normalized pressure function. Utilization of the software started with Finite-Conductivity Fractures model. The key difference from Saphire Finite conductivity model is introduction of pseudo-time function which is defined in terms of average reservoir pressure. Drainage radius is defined by initial guess and used as a variable along with the matrix permeability, fracture flow capacity and fracture half-length for nonlinear regression.

Utilization Finite Conductivity Fracture case was followed by some advanced built-in analytical models which accounts for gas desorption effects and incorporates modeling of horizontal well with multiple hydraulic fractures.

5.2.1 Advanced Analytical Models

In addition to the analytical models accessed via the wizards and models menu, advanced analytical and numerical models available in the "Advanced Models" tab. The analytical models are powerful tools which can be used to history match and forecast productivity from horizontal wells that have been stimulated with multi-stage hydraulic fractures. The Advanced models use corrected pseudo time. Traditional drawdown pseudo-time is calculated at the average reservoir pressure at a specific time. However, during transient flow, it has been proposed (Anderson and Mattar, 2007) that it is more appropriate to use the average pressure within the volume of investigation. Using corrected pseudo-time is generally recommended. However, the volume of investigation calculation involves complex geometries. Models allow incorporation of adsorption parameters to better quality analysis of shale gas and CBM reservoirs. Automatic Parameter Estimation (APE) is used to estimate the set of parameters that minimizes the sum of errors between the model's rate or pressure response and the measured data. Simplex method is the only APE method available for the new analytical models in F.A.S.T. WellTestTM. In new analytical models the Bourdet derivative is the only derivative method available in the software tool. The derivative may be smoothed by changing the log-cycle fraction that is used to in the Bourdet calculation.

5.2.1.1 SRV Horizontal Multifrac (Uniform Fracs) model

This is a rectangular model that contains an inactive horizontal well fed by multiple identical and equally-spaced transverse fractures. The width of the reservoir is defined by the distance between the tips of the fractures and the length of the reservoir is defined by the horizontal well length (Fig 5.1).

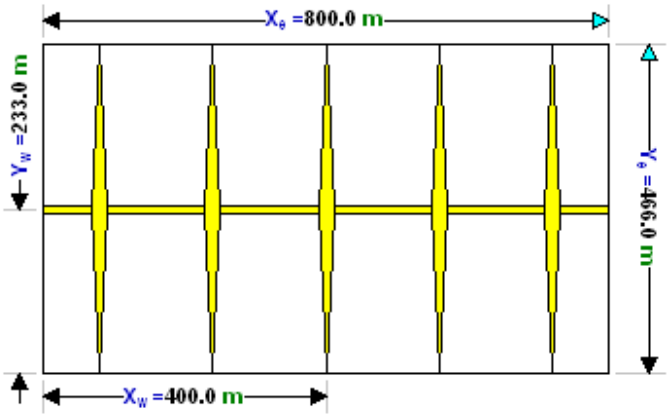

Figure 5. 1 SRV Horizontal Multifrac Model Example (F.A.S.T. Help)

The model is a simple model which calculates relatively quickly. In this model, fracture half-length is always half of Ye. Corrected pseudo-time is used for the model which assumes boundaries to be within the stimulated reservoir volume. In practice, we do have an understanding about the distance between hydraulic fractures in the field case from the sleeves set for fracture stimulation operation. At this point we can use fracture spacing information from the simulation model to account for the distance between the hydraulic fractures. The drawback of the particular analytical model is the inability to adjust fracture spacing. For single, two- and three- fracture stage cases, fracture is placed in a rectangular region with effective well length of 800 meters. Reservoir and stimulation parameters were adjusted to match recorded and calculated values on history plot. Utilization in SRV model was conducted for gas and coal-bed-methane cases where adsorption parameters (Langmuir Isotherm model) are included for both cases.

5.2.1.2 General Horizontal Multifrac (Uniform Fracs) model

The model is the most generalized model in Fekete's suite of analytical multifrac models. Individual fracture properties and fracture spacing can be specified, the wellbore can be activated, and the reservoir dimensions are not constrained by the dimensions of the completion. As a result, it calculates relatively slowly. It is a homogeneous, single-phase, rectangular reservoir model which consists of horizontal wellbore and transverse fractures. The reservoir dimensions and well position may be specified, provided the entire wellbore and all fractures fit within the reservoir boundaries. In addition, each fracture can be situated anywhere along the horizontal wellbore and configured to have a unique fracture half-length and conductivity (Fig. 5.2).

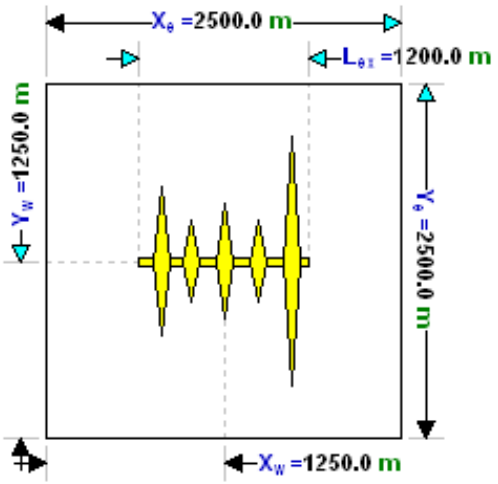

Figure 5. 2 General Horizontal Multifrac Model Example (F.A.S.T, help)

It is possible to model the combined effects of the horizontal wellbore and multiple fractures as well as the transition into middle-time flow regimes and boundary dominated flow for any number of different geometrical configurations. Depending on the configuration, it is possible to observe pseudo-radial flow regime with this model. This model also incorporates the use of corrected pseudo-time function. Corrected pseudo-time is used for the model assumes boundaries to be specified region beyond the stimulated reservoir volume. From the simulation data reservoir dimensions are set to be 2500x2500 m^2 with net pay thickness of 9 meters. Horizontal well with the length of 800 meters is then placed in the center of the rectangular reservoir, distance between multiple fractures were set to 200 meters and analysis were conducted for one-, two-, three- stage hydraulic fracture cases under 1000, 500 and 200 m^3/day production rates. Reservoir and stimulation parameters were adjusted to match recorded and

calculated values on history plot. Utilization in the model was conducted for gas and coal-bed-methane cases where adsorption parameters (Langmuir Isotherm model) are included for both cases.

5.3 Rate Transient Analysis

As a part of rate transient analysis – straight line (flow regime) analysis was applied. The starting point for the utilization corrected pseudo-time function. Initially, we applied the formula developed for formation linear flow which has not yielded any positive results so that the $x_f\sqrt{k}$ values were increasing in a non-linear form. Having known that we have fracture linear flow for our system which is followed by elliptical and radial flow periods we decided to use average pressure in the region of influence from Petrel via "Property - Geometrical Modeling - Index filter" tab in order to be able to handle several flow regimes at a time. Thereinafter, rate normalized pressure (RNP) versus natural logarithm of pseudo-time time derivative function was adopted in order to make conclusion on the prevailing flow regimes under different fracture stage and flowing conditions. Detailed analysis flow regime identification and specific analysis procedures are described below for different one-, two- and three- staged hydraulically fractured well with 1000, 500 and 200 m^3/day flowing rates.

5.3.1 Single-stage horizontal well Scenario

The starting point was the utilization of RTA on a hydraulically fractured horizontal well with 200 m^3/day production. Firstly, RNP and its derivative function were implemented (Fig 5.3a) in order to define prevailing flow regime of the system.

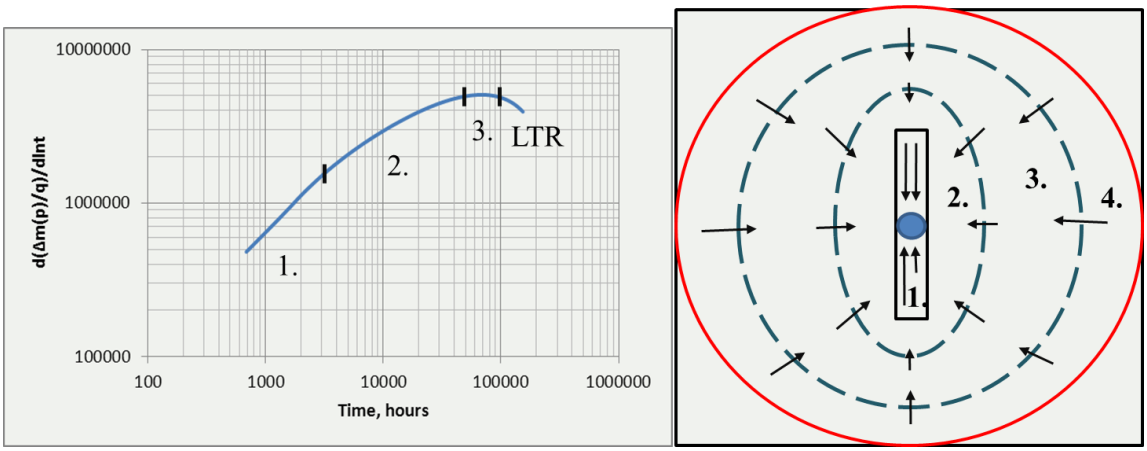

Figure 5. 3 a) RNP derivative -200 m3/day production with single-stage HF; b) sequences of flow regimes for a hydraulically fractured horizontal well 1. Fracture Linear Flow, 2. Elliptical Flow, 3. Pseudoradial flow, 4. Boundary Dominated Flow (BDF)

In this particular production case the four flow regimes for a hydraulically fractured horizontal well were observed and clearly distinguished. Linear flow period showed out to be a bit more the ½ which was an indication of finite conductivity fracture model. At this point, elliptical flow analysis for finite conductivity fracture case was performed (using Eq 2.75, 2.76 and 2.77) on the region corresponding to this flow regime (Region 2) and dimensionless fracture conductivity was found to be 0.77 which in turn supported the thoughts about the fracture linear flow regime. Production data corresponding to fracture linear flow (Region 1) regime was also analyzed from the slope of RNP and corrected pseudo-time function using Eq.2.80 for the average reservoir pressure in region of influence. Region 3 corresponds to pseudo-radial flow which is analyzed using Eq. 2.78 Late time region (LTR) shows to have an irregular behavior for boundary dominated flow. At this point, if we consider the fact that for the particular region the rate of change of RNP decreases that shows pressure support to the system which can be result of compressibility effects of the desorpted gas without any boundaries felt.

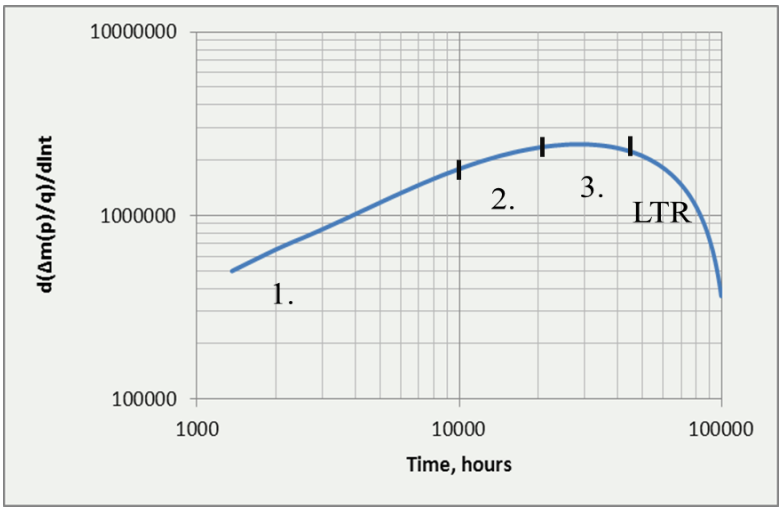

Figure 5. 4 RNP derivative -500 m3/day production with single HF

The same chart was plotted for 500 m^3/day production rate which has showed similar flow regime characteristics (Fig 5.4) where the same analysis techniques were implemented in order to find reservoir and stimulation parameters.

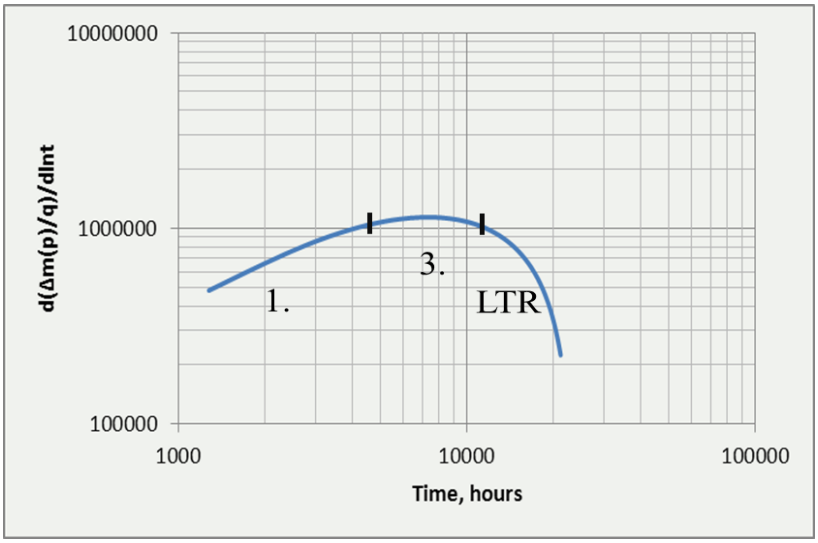

Figure 5. 5 RNP derivative -1000 m3/day production with single HF

In comparison with the previous two cases for 1000 m^3/day production has shown different flow behavior. For the particular case transitional flow (elliptical flow) period cannot be observed due to high production rates which cause higher pressure drawdowns in a hydraulically fractured horizontal well. Due to non-availability of elliptical flow period hydraulic fracture half-length values cannot be evaluated. Fracture linear and pseudo-radial flow regimes analyzed to get matrix permeability and fracture flow capacity.

5.3.2 Two-stage horizontal well Scenario

For the multi-fractured horizontal well it is expected to see the flow regimes indicated in Fig.5.6(b). From the RNP derivative plot (Fig 5.6a) we can conclude that an elliptical flow regime of individual fractures is masked due to the fact that fractures are too close. For that reason, the Region-A encompasses fracture linear and compound linear flow (CFL) which is followed by pseudoradial flow regime.

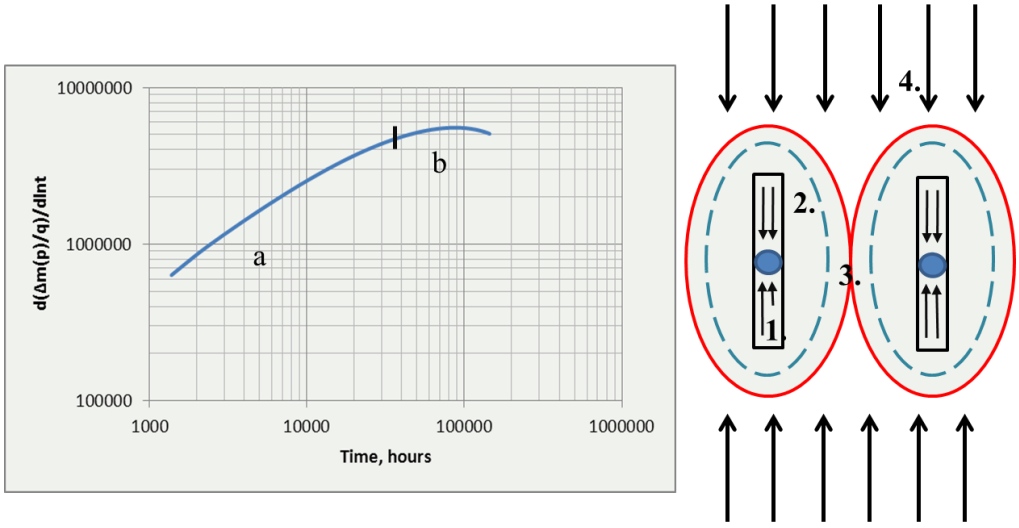

Figure 5. 6 a)RNP derivative -200 m3/day production with two-stage HF-s; b) sequences of flow regimes for multi-fractured horizontal well 1. Fracture Linear Flow, 2. Elliptical Flow, 3. Fracture Interference, 4. Compound linear flow (CFL)

Again, due to the fact of non-availability of elliptical flow regime we are unable to calculate fracture half-length. The very beginning of the linear flow data was used to analyze the data based on fracture linear flow analysis (Eq 2.72). Thereinafter, Region-B was used for pseudoradial regime analysis corresponding to this flow regime (Eq 2.78).

The procedure was deployed for 500 m^3/day production rate which has showed similar flow regime characteristics (Fig 5.7) where the same analysis techniques were implemented in order to find reservoir and stimulation parameters.

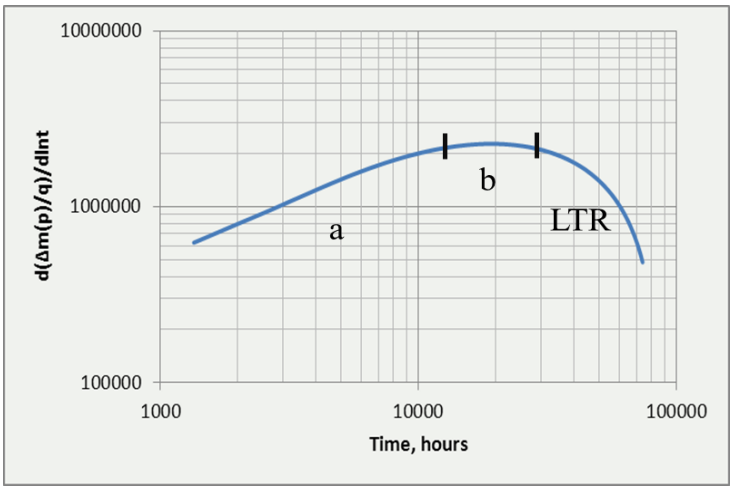

Figure 5. 7 RNP derivative -500 m3/day production with 2 HF-s

Increased production rate masks the elliptical flow regime in a severe manner. LTR corresponds to the late time region flow exhibiting pressure support due to desorbed gas.

Fig 5.8 shows RNP derivative function of horizontal well with two transverse fractures for 1000 m^3/day, daily production rate which also exhibits the similar behavior with the previous examples.

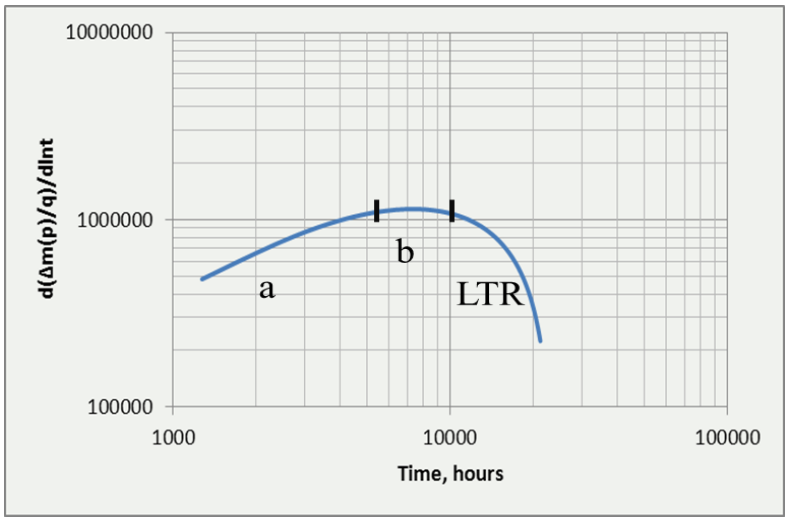

Figure 5. 8 RNP derivative -1000 m3/day production with 2 HF-s

In comparison with the previous cases pseudoradial flow regime is reached earlier due to increased production rate.

5.3.3 Three-stage horizontal well Scenario

Three stage horizontal well model production data shows similar characteristics with two stage horizontal well RNP derivative results. In all cases elliptical flow regime is masked due to close fracture spacing which makes fracture half-length calculation impossible. Region A includes fracture linear flow and CFL flow regimes which are followed by pseudoradial flow regime. The very early time data was used for fracture linear flow straight line analysis (Eq 2.72). Matrix permeability is found (Eq 2.78) from pseudoradial flow regime.

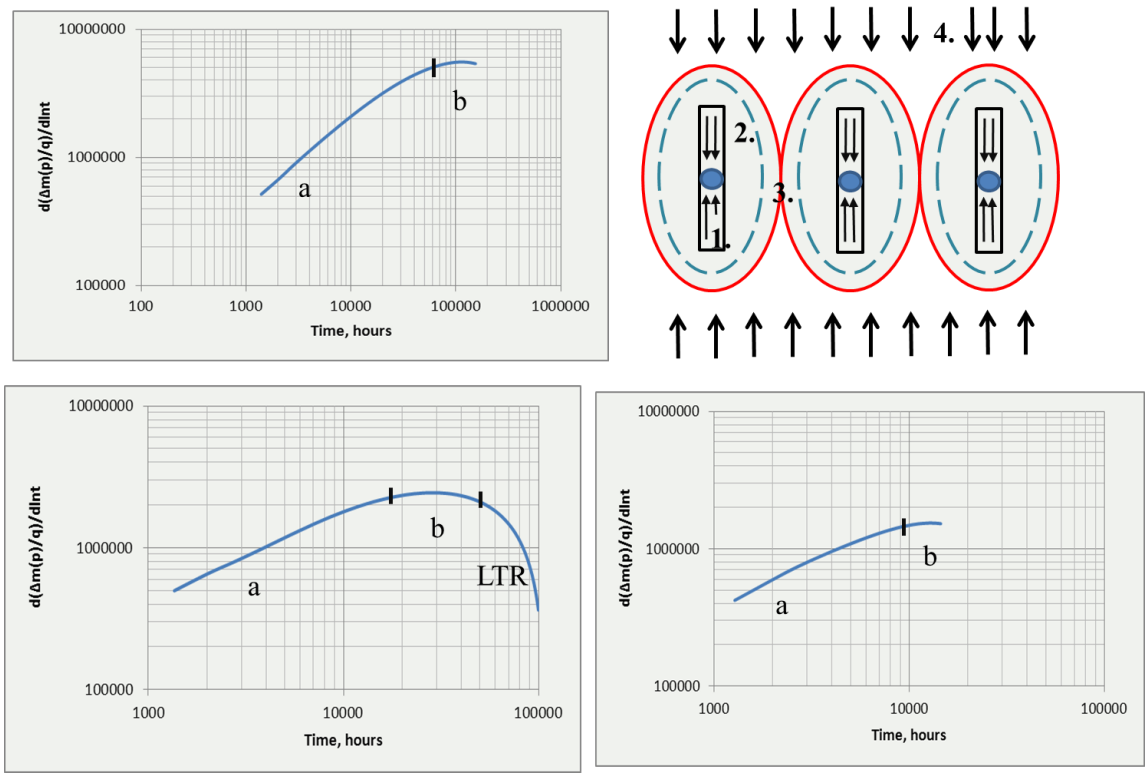

Figure 5. 9 a)RNP derivative -200 m3/day production with 3 HF-s; b) sequences of flow regimes for multi-fractured horizontal well 1. Fracture Linear Flow, 2. Elliptical Flow, 3. Fracture Interference, 4. Compound linear flow (CFL), c) RNP derivative -500 m3/day production with 3 HF-s; d) RNP derivative -1000 m3/day production with 3-stage HF

5.3.4 Constant BHP Production Example

Additionally, constant BHP simulation runs were adopted for rate transient analysis where the well bottom-hole flowing pressure limit is set to 6.9 bars.

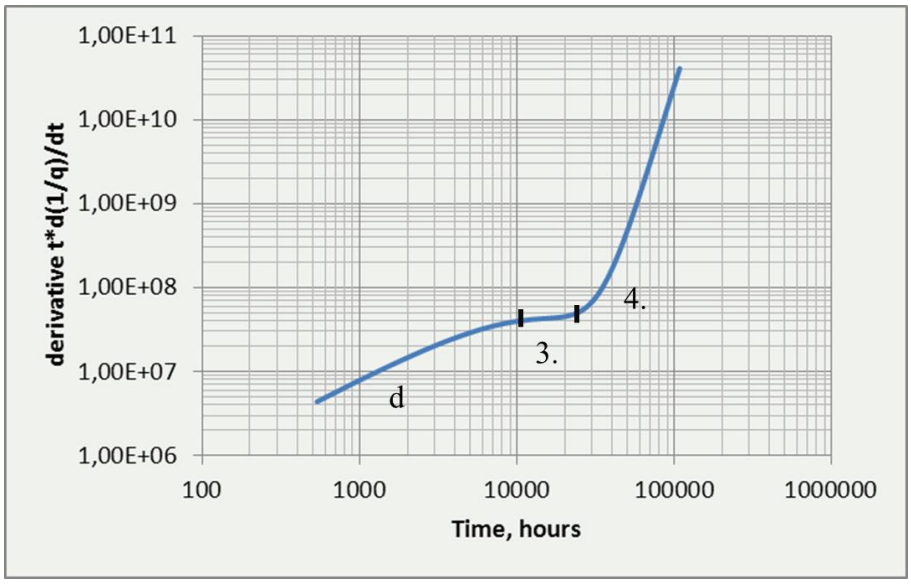

Figure 5. 10 Reciprocal rate derivative - constant BHP production with single HF

Region D on Fig. 5.10 exhibits unit slop which refers to pseudo-steady state flow which in turn is the result of pressure depletion in SRV region. With bottom hole flowing pressure set to 6.9 bars gas production starts with very high rates which deplete gas within region. The particular flow regime is followed by pseudoradial flow (3) and boundary dominated flow (4) as shown in flow regime sequence example for a single hydraulically fractured well in Fig. 5.3(b).

Thereinafter, utilization of reciprocal rate derivative was performed for two and three hydraulic fractures cases (Fig. 5.11). At early time, derivative function exhibits similar flowing regimes (regions D and region B) with the single hydraulic fracture case.

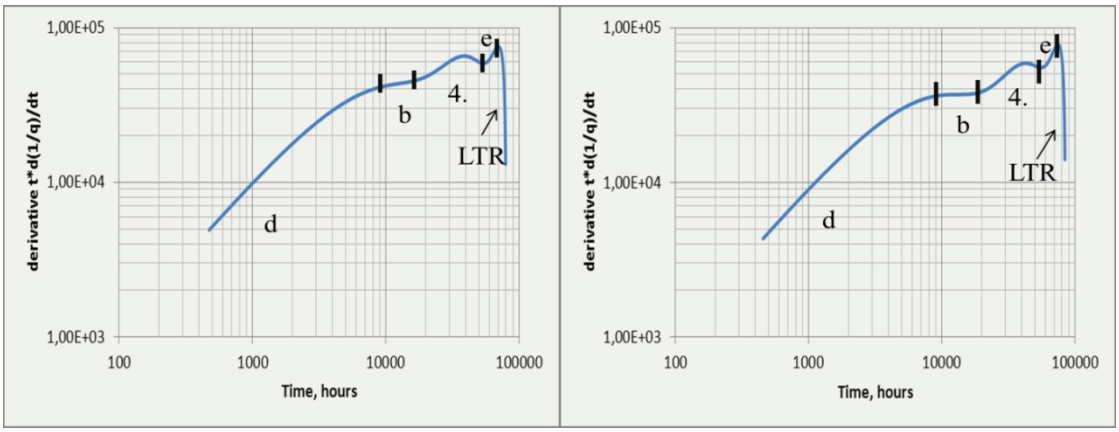

Figure 5. 11 Reciprocal rate derivative - constant BHP production with a) 2 stage, b) 3 stage

Flow then develops to compound linear flow (CFL) as shown in Fig. 5.6b and Fig. 5.9b which has the characteristic behavior (Fig 5.12) for $\frac{2x_f}{D_f} > 1$ case (Luo, 2010) which in turn is supported by the numerical model.

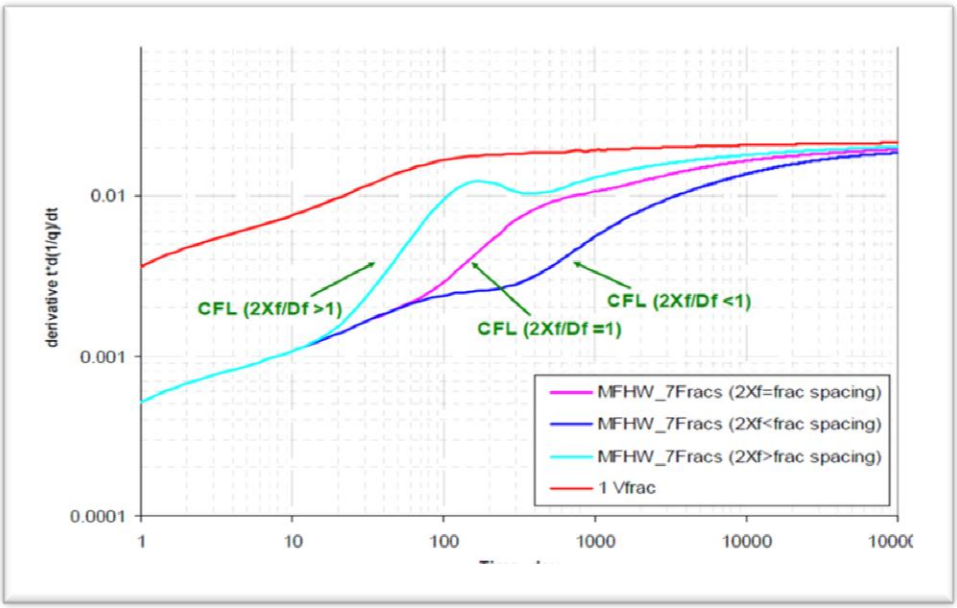

Figure 5. 12 Log-log analysis of reciprocal rate derivative for 7-stage MFHW case (Shanqiang, 2010)

In comparison with const-rate production examples for const-BHP case boundary dominated flow regime (Region E) is developed after compound linear flow. Thereinafter, late time region (LTR) effects can be observed from the reciprocal rate derivative example for both cases. Decreasing slope of LTR is an indication of gas flow to the system which may be the result of desorption in the drained reservoir system.

CHAPTER 6

RESULTS & DISCUSSION

In this part of the thesis, the results for pressure transient analysis and straight line analysis (RTA) under different fracture stage and flowing conditions are presented and discussed. Results for each specific analysis technique will separately be assessed and compared under different flowing and fracture stage conditions.

6.1 Saphire Interpretation Results

Analysis results for single stage hydraulic fracture produced under 1000 m^3/day constant rate is indicated below (Fig 6.1). The disadvantage of the tool is that the finite conductivity model has a built in analysis techniques which is based on bilinear and linear flow regimes only. Analysis is performed in such a way that model analysis line on the log-log plot was extended to find imaginary radial flow by which reservoir permeability is extracted. Then any part of the derivative corresponding to half and quarter slope were used for analysis of linear and bilinear flow periods which gives anomalous results.

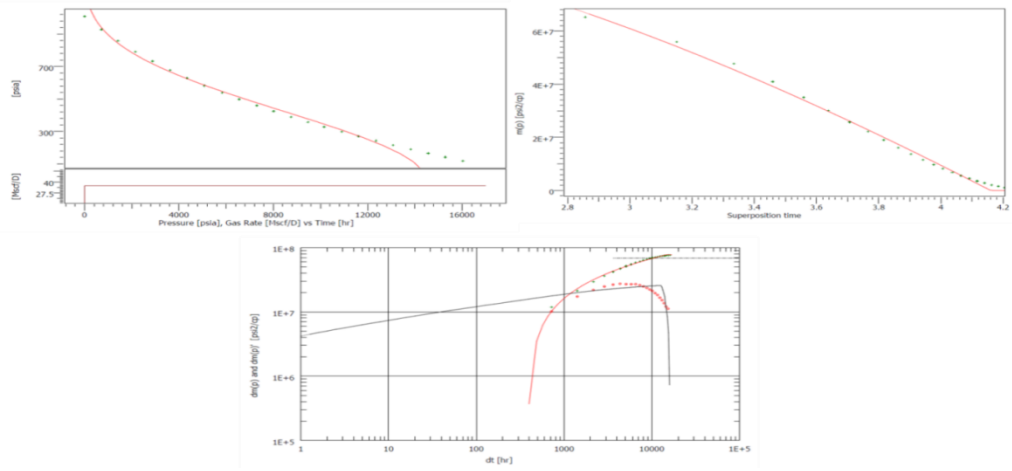

Figure 6. 1 Saphire Finite Conductivity Model for single stage hydraulic stage - 1000 m3/day production: a) history plot; b) semilog plot; c) presudo-pressure log-log derivative plot

Detailed results for different flowing rates and fracture stages are shown:

Table 6. 1 Saphire Finite Conductivity Model under different fracture stage and flowing conditions

Kappa Finite Conductivity Fracture Model		k (mD)	x_f (m)	$k_f w_f$ (mD*m)	k_f (mD)	F_{CD}
1stg	1000 m^3/d	8,16E-03	1195,12	25,79	507,73	2,64
	500 m^3/d	2,86E-03	1326,22	56,40	1110,28	14,87
	200 m^3/d	1,17E-03	1890,24	60,06	1182,3	27,16
2stg	1000 m^3/d	3,37E-03	2405,49	96,95	1908,49	11,96
	500 m^3/d	2,74E-04	4969,51	190,85	3756,96	140,16
	200 m^3/d	1,33E-04	23871,95	1118,90	22025,64	352,41
3stg	1000 m^3/d	5,98E-04	29512,2	116,16	2286,59	6,58
	500 m^3/d	4,42E-04	4634,15	527	10382,66	257,50
	200 m^3/d	4,47E-04	1868,90	257,93	5077,3	308,75

Fracture permeability (kf) numbers are calculated with an assumption of 2 inch fracture width (Table 6.1). Having known the original k (0.004 mD) and x_f (250 m) values from Table 4.1 we may conclude that the particular model is not an efficient tool to handle the particular interpretation. Function plots for single and multiple hydraulic fracture stages under different flow rates are included in Appendix A.

6.2 Fekete Interpretation Results

Results for single and multiple hydraulic fractures produced under different production rates using different analysis models are separately indicated:

6.2.1 Finite Conductivity Model Case

Analysis results for the single stage hydraulic fracture produced under 1000 m^3/day constant rate is indicated below (Fig 6.2). Values are the result of good history match, but with low tolerance

on log-log plot which is again the result of inability to recognize any flow regime other than linear and bilinear flow. Results for a total nine different analysis for single, two and three stage hydraulic fracture cases for gas production rate of 1000, 500 and 200 m^3/day for each case are shown in Table 6.2. With good initial estimates and fine tuning a very close reservoir and stimulation properties were found despite the mismatch on log-log plot. However, having known that it is possible to find several sets of parameters which yield an acceptable model match, we cannot conclude on the applicability of the particular model for the analysis.

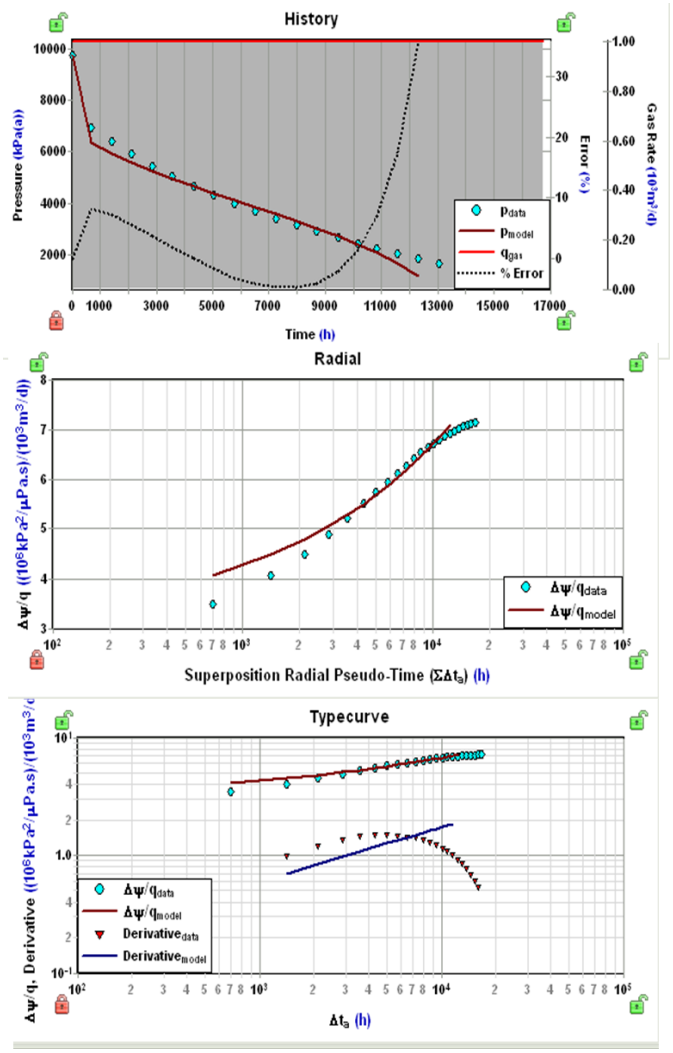

Figure 6. 2 Fekete F.A.S.T. Finite Conductivity Model for single stage hydraulic stage - 1000 m3/day production: a) history plot; b) semilog plot; c) RNP log-log derivative plot

Table 6. 2 Fekete F.A.S.T. Finite Conductivity Model under different fracture stage and flowing conditions

F.A.S.T Finite Conductivity Fracture Model		k (mD)	x_f (m)	$k_f w_f$ (mD*m)	k_f (mD)	F_{CD}
1stg	1000 m^3/d	2,62E-03	257,86	169	3326,77	250,05
	500 m^3/d	1,70E-03	191,02	147	2893,70	451,88
	200 m^3/d	9,44E-04	151,20	144	2834,65	1009,36
2stg	1000 m^3/d	7,75E-04	215,94	156	3070,87	932,25
	500 m^3/d	6,83E-04	207,23	141	2775,59	996,08
	200 m^3/d	3,69E-04	166,33	139	2736,22	2265,91
3stg	1000 m^3/d	7,34E-04	154,90	128	2519,69	1126,09
	500 m^3/d	3,00E-04	166,46	162	3197,26	3255,55
	200 m^3/d	1,88E-04	176,73	162	3195,66	4881,07

With good initial estimates and fine tuning very close values to original reservoir were found which can be the result of incorporation boundary conditions and pseudo-time function. At first look, we can conclude that the model definitely works having known the original k (0.004 mD) and x_f (250 m) values from Table 4.1. However, F_{CD} values (>300) are an indication of finite conductivity fractures, where we cannot observe any bilinear flow regime and compute fracture flow capacity ($k_f w_f$) values. Also, despite the good estimated values, the mismatch on log-log plot again shows irrelevancy of the particular model in analyzing the reservoir and stimulation properties. All the analysis plot are included in Appendix B.

6.2.2 Horizontal Multifrac SRV Gas Model Case

The total of nine analyses were performed under for single, two and three stage hydraulic fracture cases for gas production rate of 1000, 500 and 200 m^3/day for each case separately. Analysis results for single stage hydraulic fracture produced under 1000 m^3/day constant rate is indicated below (Fig 6.3).

The anticipated mismatch on the log-log plot is the result of linear and bilinear flow model as the particular advanced analytical model encompasses - bilinear, formation linear flow regimes and fracture interference effects (for multi-fractured case only).

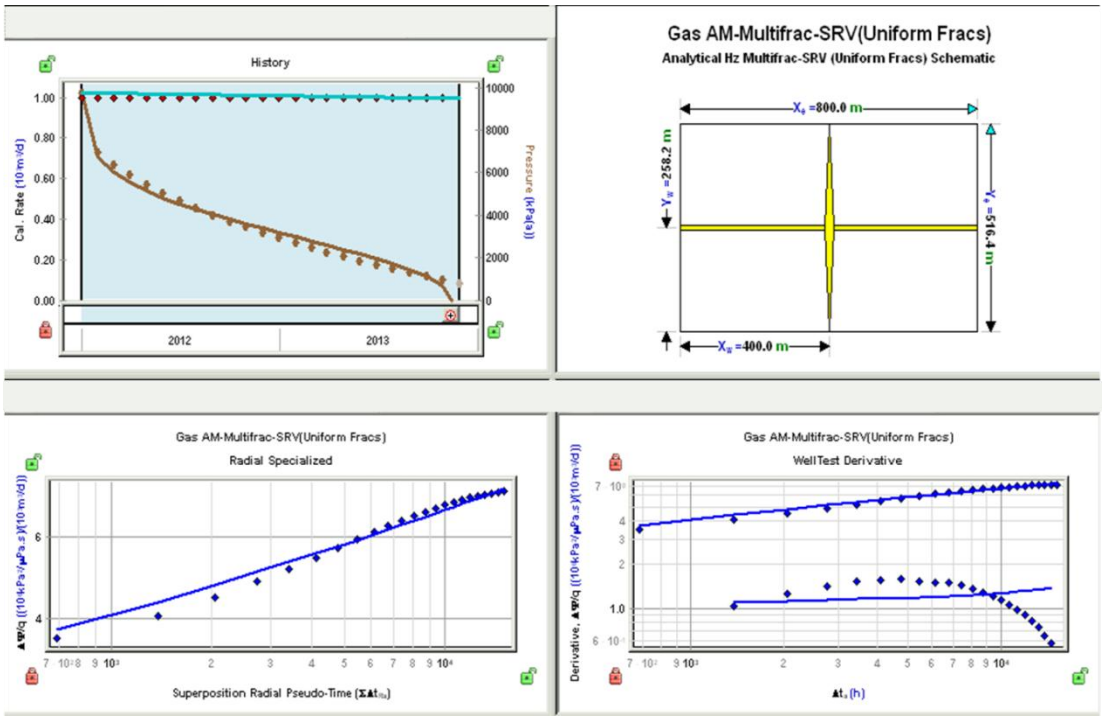

Figure 6. 3 Fekete Horizontal Multifrac SRV (Uniform Frac-s) Gas Model for single stage hydraulic stage - 1000 m3/day production: a) history plot; b) SRV model Shematic c) semilog plot; d) RNP log-log derivative plot

Results for different fracture stage and flowing conditions are indicated in Table 6.3.

Table 6. 3 Horizontal Multifrac SRV GAS Model under different fracture stage and flowing conditions

Fekete Horizontal Multifrac SRV GAS model		k (mD)	x_f (m)	$k_f w_f$ (mD*m)	k_f (mD)	F_{CD}
1stg	1000 m^3/d	6,91E-03	258,2	7,2	142,0	4,05
	500 m^3/d	4,43E-03	279,5	5,1	99,5	4,05
	200 m^3/d	1,78E-03	294,4	5,3	103,4	10,01
2stg	1000 m^3/d	3,06E-03	255,8	3,0	59,1	3,84
	500 m^3/d	1,74E-03	277,0	2,1	40,9	4,30
	200 m^3/d	9,71E-04	223,3	3,2	63,8	14,95
3stg	1000 m^3/d	2,91E-03	284,6	3,7	72,3	4,44
	500 m^3/d	1,12E-03	264,4	2,2	43,3	7,41
	200 m^3/d	1,56E-03	735,3	3,8	74,8	3,31

Having known the original k (0.004 mD) and x_f (250 m) values from Table 4.1 we may conclude that for the Table 6.3, despite the good estimates of hydraulic fracture half-length and relatively good matrix permeabilities the results for fracture flow capacity are underestimated.

6.2.3 Horizontal Multifrac SRV CBM Model Case

Additionally, using the same model (Horizontal Multifrac SRV model) CBM fluid type analyses were performed under for single, two and three stage hydraulic fracture cases for gas production rate of 1000, 500 and 200 m^3/day for each case separately. Analysis results for single stage hydraulic fracture produced under 1000 m^3/day constant rate is indicated below (Fig 6.4).

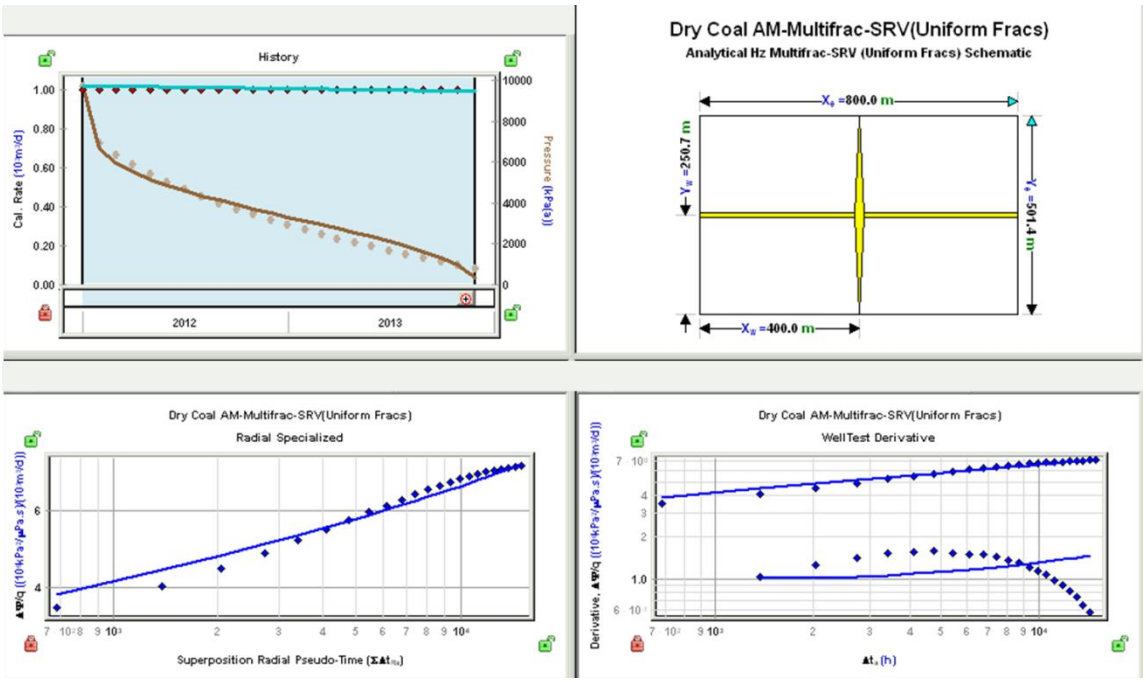

Figure 6. 4 Fekete Horizontal Multifrac SRV(Uniform Frac-s) CBM Model for single stage hydraulic stage - 1000 m3/day production: a) history plot; b) SRV model Shematic c) semilog plot; d) RNP log-log derivative plot

As it can be seen from the Fig. 6.4 - CBM case has showed the similar characteristics with the gas fluid model. Detailed results for SRV (Uniform Frac-s) CBM fluid model for all the applied production scenarios are shown in the Table 6.4.

Table 6. 4 Horizontal Multifrac SRV CBM Model under different fracture stage and flowing conditions

Fekete Horizontal Multifrac SRV CBM		k (mD)	x_f (m)	$k_f w_f$ (mD*m)	k_f (mD)	F_{CD}
1stg	1000 m^3/d	6,69E-03	250,7	7,2	141,2	4,27
	500 m^3/d	4,17E-03	266,3	5,1	100,8	4,60
	200 m^3/d	1,65E-03	264,3	5,5	109,0	12,67
2stg	1000 m^3/d	2,90E-03	236,1	2,4	47,5	3,53
	500 m^3/d	1,52E-03	286,2	1,8	35,3	4,11
	200 m^3/d	7,84E-04	261,1	3,3	65,8	16,34
3stg	1000 m^3/d	2,87E-03	283,6	4,1	80,3	5,01
	500 m^3/d	1,12E-03	251,4	1,5	29,1	5,25
	200 m^3/d	1,64E-03	869,6	3,5	69,2	2,47

The only difference between the SRV Gas Model is the lower estimated matrix permeabilities since in CBM case coal has higher volume of gas adsorpted gas for the same adsorption parameters.

6.2.4 General Horizontal Multifrac Gas Model Case

In this case produced gas is not limited to SRV and whole reservoir is simulated as if there is a gas production outside the stimulated reservoir region which allows fluid regimes other than linear and bilinear flow regimes to be developed. Analysis results for single stage hydraulic fracture produced under 1000 m^3/day constant rate is indicated below (Fig 6.5)

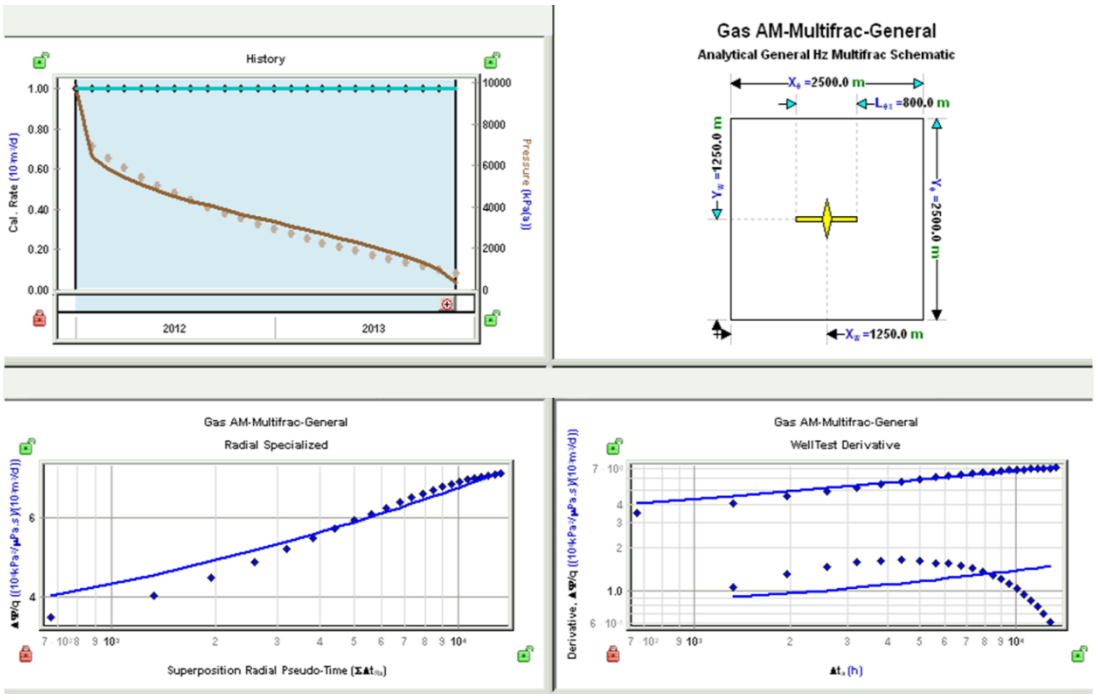

Figure 6. 5 Fekete Horizontal Multifrac General Gas Model for single stage hydraulic stage - 1000 m3/day production: a) history plot; b) SRV model Shematic c) semilog plot; d) RNP log-log derivative plot

The particular set of parameters estimated from the analysis shows mismatch on RNP log-log derivative plot which is an indication of having approximately the similar conditions with SRV Uniform Fracture model. In both cases fracture flow capacity is underestimated. In the particular model estimated reservoir permeabilities are lower than those for SRV model which is due to increased reservoir volume. However, for production rates of 200 m^3/day (one, two and three stage hydraulic fracture cases) along with the history match, a good match on the RNP log-log derivative plot were estimated (Appendix E) which is an indication of radial flow regime. Achievement of the particular flow regime is the result of low fracture flow capacity which allows radial flow regime to be developed (Table 6.5).

Table 6. 5 Horizontal General Multifrac GAS Model under different fracture stage and flowing conditions

Fekete Horizontal Multifrac General –Gas Model		k (mD)	x_f (m)	$k_f w_f$ (mD*m)	k_f (mD)	F_{CD}
1stg	1000 m^3/d	1,21E-03	238,5	1,4	27,2	4,78
	500 m^3/d	1,05E-03	289,1	1,5	28,6	4,79
	200 m^3/d	8,96E-04	118,2	0,7	13,0	6,24
2stg	1000 m^3/d	9,54E-04	292,5	1,0	20,2	3,68
	500 m^3/d	6,14E-04	287,3	0,9	16,8	4,83
	200 m^3/d	7,74E-04	235,5	0,9	18,1	5,04
3stg	1000 m^3/d	1,03E-03	246,1	1,2	23,9	4,78
	500 m^3/d	1,07E-03	190	1,2	23,0	5,73
	200 m^3/d	8,41E-04	202,1	0,7	12,8	3,83

Having known the reservoir dimensions and real field case fracture flow capacity values the conclusion can be made on inability of the particular model to sustain radial flow regime for the analysis.

6.2.5 General Horizontal Multifrac CBM Model Case

Results for the particular model are similar with those obtained in Horizontal General Multifrac Gas model. Analysis results for single stage hydraulic fracture produced under 1000 m^3/day constant rate is indicated below (Fig 6.6)

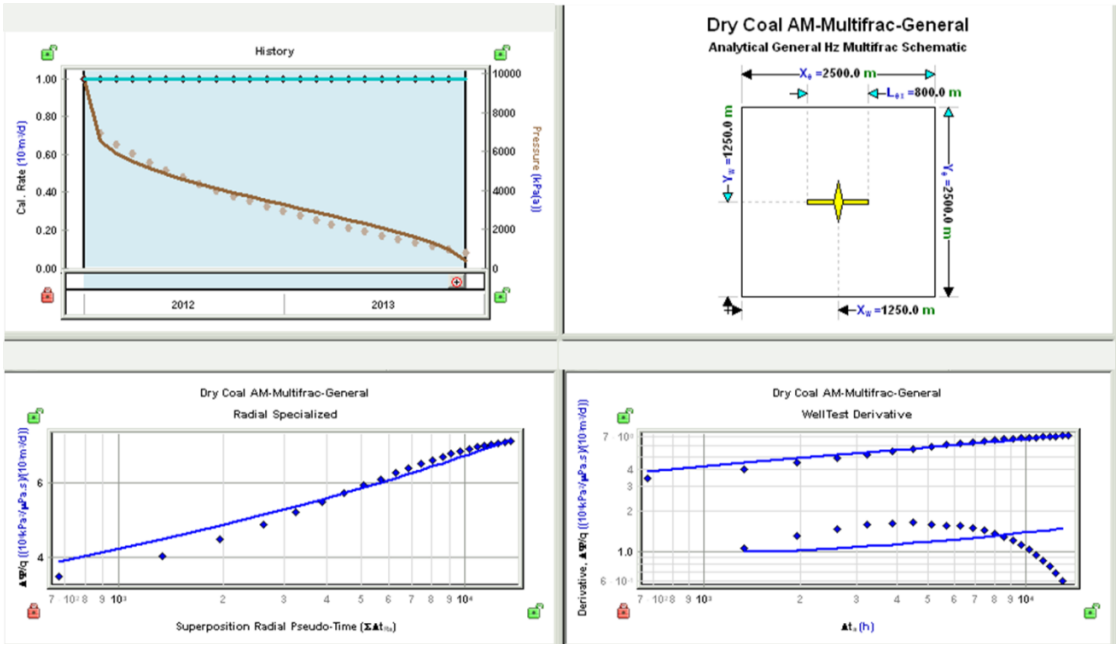

Figure 6. 6 Fekete Horizontal Multifrac General CBM Model for single stage hydraulic stage – 1000 m3/day production: a) history plot; b) SRV model Shematic c) semilog plot; d) RNP log-log derivative plot

Table 6. 6 Horizontal General Multifrac CBM Model under different fracture stage and flowing conditions

Fekete Horizontal Multifrac General –CBM Model		k (mD)	x_f (m)	$k_f w_f$ (mD*m)	k_f (mD)	F_{CD}
1stg	1000 m^3/d	1,14E-03	280,5	1,6	31,2	4,95
	500 m^3/d	7,01E-04	293,8	0,9	17,3	4,26
	200 m^3/d	6,83E-04	78,8	0,3	5,7	5,37
2stg	1000 m^3/d	9,29E-04	274,9	0,9	18,0	3,57
	500 m^3/d	5,76E-04	273,9	0,8	16,2	5,22
	200 m^3/d	7,92E-04	258,4	1,1	20,7	5,14
3stg	1000 m^3/d	9,96E-04	202,3	1,0	20,1	5,06
	500 m^3/d	9,74E-04	281,1	1,5	29,9	5,55
	200 m^3/d	1,03E-03	290,3	1,5	28,6	4,84

For production rates of 200 m^3/day (one, two and three stage hydraulic fracture cases) besides the history match, a good match on the RNP log-log derivative plot is observed (Appendix F) which is an indication of radial flow regime. Development of the particular flow regime is the result of low fracture flow capacity that allows radial flow regime to be achieved (Table 6.6). As for Horizontal SRV (Uniform Frac-s) Model, the only difference between the Horizontal Multifrac General Gas model cases is the lower estimated matrix permeabilities since in CBM case coal has higher volume of gas adsorpted gas for the same adsorption parameters.

6.3 Staight Line Analysis Case

The particular analysis showed to be a very straight forward technique in analyzing the production data of a multi-fractured horizontal well. The incorporation of standard derivative for rate normalized pressure function and ability to distinguish prevailing flow regimes allows to properly interpret the data in a straightforward manner. One of the interesting features was the estimation of elliptical flow regime which is the case for reservoirs with long hydraulic fractures and very low matrix permeability. This particular flow regime made the hydraulic fracture length estimation possible having no formation flow in the system. However, the analysis of the elliptical flow regime was possible only for single-stage fracture case as it showed to be masked for two and three stage fracture cases under different flowing rates due to low fracture spacing. Table 6.7 shows the typical flowing regimes observed under different fracture stage and flowing conditions.

Table 6. 7 Representation of dominating flowing regimes under different fracture stage flowing conditions

Stragiht Line Analysis	1000 m^3/day			500 m^3/day			200 m^3/day		
	1stg	2stg	3stg	1stg	2stg	3stg	1stg	2stg	3stg
Linear Flow	+	+	+	+	+	+	+	+	+
Elliptical	-	-	-	+	-	-	+	-	-
CFL	-	+	+	-	+	+	-	+	+
Radial	+	+	+	+	+	+	+	+	+
BDF	-	-	-	-	-	-	-	-	-

The total of nine analyses were performed under for single, two and three stage hydraulic fracture cases for gas production rate of 1000, 500 and 200 m^3/day for each case separately. Results are distributed in the following table exhibiting fracture and reservoir properties of the particular multi-fractured horizontal shale gas simulation example.

Table 6. 8 Representation of the dominating flow regimes under different flowing and fracture stage conditions

Straight Line Analysis		k (mD)	x_f (m)	w_f sqrt(k_f)	k_f (mD)
1stg	1000 m^3/d	0,01730 (Radial)	-	2,84	3120,89
	500 m^3/d	0,00783 (Radial) 0,00669 (Elliptical)	270,0418	2,22	1908,99
	200 m^3/d	0,0032 (Radial) 0,0022 (Elliptical)	312,975	1,91	1418,11
2stg	1000 m^3/d	0,01407 (Radial)	-	2,99	3474,67
	500 m^3/d	0,00696 (Radial)	-	2,91	3286,05
	200 m^3/d	0,00294 (Radial)	-	2,23	1929,32
3stg	1000 m^3/d	0,01032 (Radial)	-	3,04	3578,91
	500 m^3/d	0,00649 (Radial)	-	3,05	3604,84
	200 m^3/d	0,00289 (Radial)	-	3,03	3546,55

Estimation of hydraulic fracture half-length values were possible on for single fracture horizontal well from elliptical flow at lower production rates. Reservoir permeability values found from elliptical flow shows a good correspondence with the values found using radial flow regime analysis. Due to deviation of the linear flow data from a linear slope corrected pseudo-time function was adopted as it was discussed in the previous section. The aim of its utilization is to handle the deviation at linear flow regime data. Effect of utilization of the corrected pseudo-time function under different fracture stage and flowing conditions is shown below.

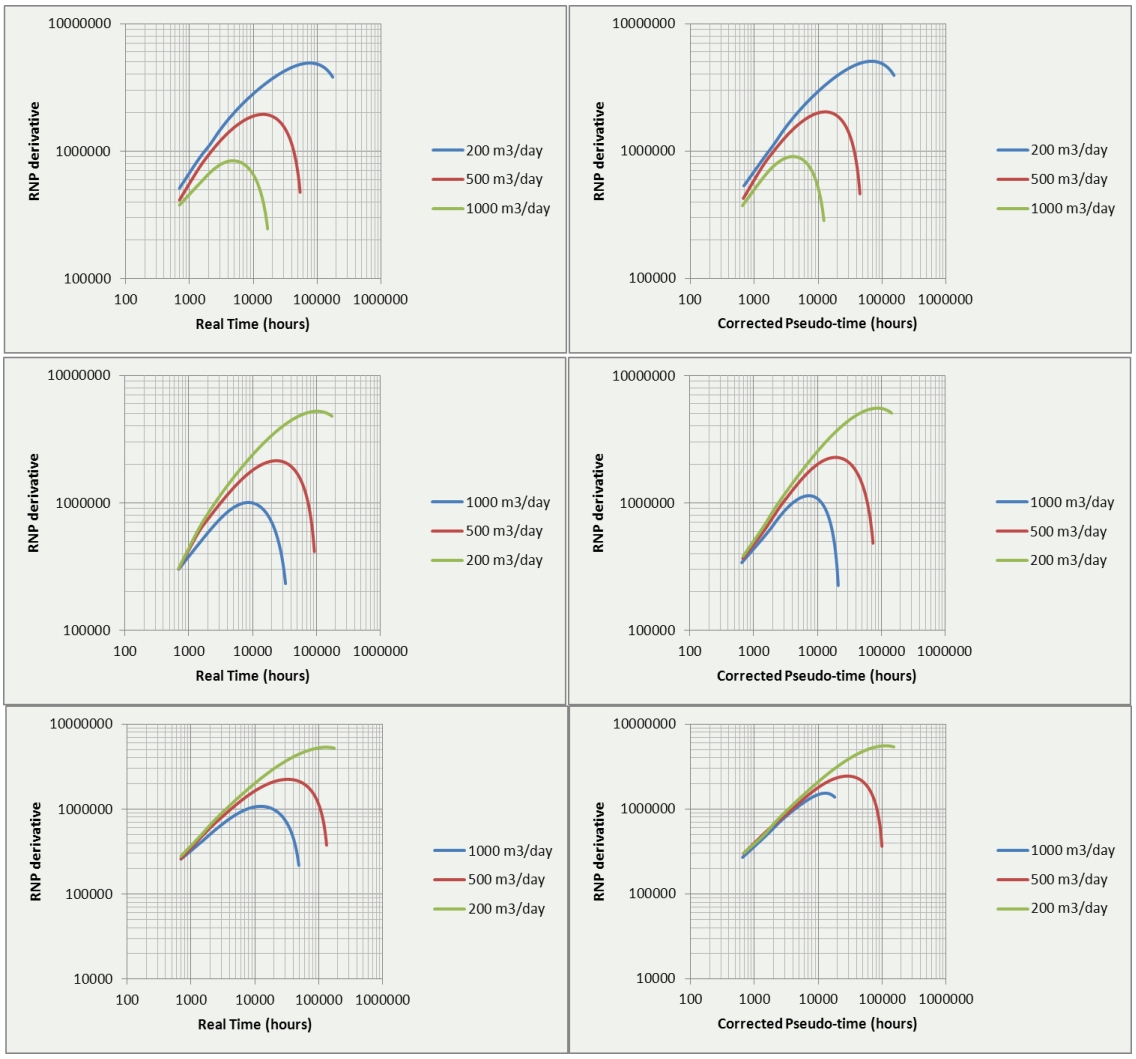

Figure 6. 7 Effect of Corrected pseudo-time on RNP derivative under different flowing rates a) one-, b) two-, c) three-stage hydraulic fracture examples

Fig. 6.7 best describes the behavior of fracture permeabilities (Table 6.8) for different flowing and fracture stage conditions.

CHAPTER 7

CONCLUSION

In this thesis several analytical methods were implemented in order to extract reservoir and hydraulic fracture properties from the shale gas simulation data. Initially, we conducted simulation runs for different production rate and bottom-hole flowing pressures, for each fracture stage condition. Having had the production data, we started with the analyses developed for conventional hydraulically fractured wells using Saphire and Fekete (F.A.S.T) well testing tools. Thereinafter, some advanced analytical built-in functions in Fekete (F.A.S.T) tool was used to handle the SG data interpretation. Finally, as an addition to PTA – Straight Line (Flow Regime) analysis were adopted which specifies advanced production data analysis. Despite the fact that the results estimated from PTA exhibited relatively better correspondence with matrix permeability and fracture half-length, the results for fracture flow capacity were underestimated. Analysis of the Straight Line Analysis results showed relatively overestimated matrix permeability values, however results showed a good coincidence for all other parameters. Following are conclusion drawn from this study:

- Applied Pressure Transient Analysis tools showed poor quality results due to improper handling of flow regime identification for the reservoir system which is mostly associated with the fact that models account for only linear, bilinear and boundary dominated conditions
- The reasonable history match can be achieved with different set of solution parameters so that a good initial guess must be taken in order to get a correct solution
- Straight Line (Flow Regime) Analysis showed to be a more precise and straightforward way of handling the data interpretation and exhibited a good correspondence with original values
- Corrected Pseudo-time has partially decreased deviation of RNP derivative for increasing flowing rates
- RNP derivative revealed elliptical flow regime which is the case for long hydraulic fractures with low reservoir permeability
- Elliptical Flow regime were masked for two- and three- stage fractures for all production rates indicating very close fracture spacing

- Straight Line Analysis has not revealed boundary dominated flow for constant flowing rates and the late time region is considered to be the consequence of the compressibility effects due to gas desorption
- For Constant Pressure Straight Line Analysis both boundary dominated flow and gas desorption effects were observed

REFERENCES

Agarwal, R. G., "Real Gas Pseudo-Time,", Presented at 54th Annual Technical Conference and Exhibition of the Society of Petroleum Engineers of AIME, Las Vegas, NV, SPE 8279, September 1979

Aguilera, R., "Well Test Analysis of Naturally Fractured Reservoirs," SPEFEJ, pp. 239–252, September 1987.

Ahmed T., "Reservoir Engineering Handbook", 2010

Al-Hussainy, R., Ramey, H. J., Jr., Crawford, P. B., "The Flow of Real Gases Through Porous Media," Trans. AIME, pp. 237, 624; 1966.

Anderson D. M., Mattar L., Fekete Assosiates Inc. "An Improved Pseudo-Time for Gas Reservoirs With Significant Transient Flow", Canadian Petroleum Conference, June 7-9, 2005

Bourdet, D., Alagoa, A., Ayoub, J. A., and Pirard, Y. M., "New Type Curves Aid Analysis of Fissured Zone Well Tests," World Oil, pp. 111–124, April 1984

Bourdet, D., Ayoub, J.A., Pirard, Y.M., "Use of pressure derivative in well-test interpretation", Society of Petroleum Engineers Formation Evaluation 4 (2), 293–302, 1989.

Bourdet, D., Gringarten, A. C., "Determination of Fissure Volume and Block Size in Fractured Reservoirs by Type-Curve Analysis," SPE Paper 9293, Presented at the Annual Technical Conference and Exhibition, Dallas, TX, September 21–24, 1980.

Bourdet, D., Whittle, T.M., Douglas, A.A., Pirard, Y.M., "A new set of type curves simplifies well test analysis", World Oil 95–106, May 1983.

Chen, C.C., Raghavan, R., "A multiply-fractured horizontal well in a rectangular drainage region", Society of Petroleum Engineers Journal 2 (4), 455–465, 1997.

Cheng, Y. "A New Approach for Reliable Estimation of Hydraulic Fracture Properties Using Elliptical Flow Data in Tight Gas Wells" SPE, West Virginia University; and W.J. Lee, SPE, and D.A. McVay, SPE-105767, 2009

Cinco, H., Samaniego, F., "Effect of Wellbore Storage and Damage on the Transient Pressure Behavior for a Well with a Finite Conductivity Vertical Fractures," SPEJ, pp. 253–266, August 1978.

Cinco-Ley, H. Samaniego-V. F., "Transient Pressure analysis for Fractured Wells". JPT 33 (9): 1749–1766, SPE-7490-PA, 1981

Cinco, H., Samaniego, F., "Transient Pressure Analysis for Finite Conductivity Fracture Case versus Damage Fracture Case," SPE 10179, 1981.

Clarkson C.R., "Production data analysis of unconventional gas wells: Review of theory and best practices", International Journal of Coal Energy, 2013

Clarkson, C.R., Beierle, J.J., "Integration of microseismic and other post-fracture surveillance with production analysis: a tight gas study", Journal of Natural Gas Science and Engineering 3, 382–401, 2011.

Clarkson, C.R., Jensen, J.L., Blasingame, T.A., "Unconventional gas reservoir evaluation: what do we have to consider?", Journal of Natural Gas Science& Engineering 8, 9 33; 2012a.

Cook, C.E., "Conductivity of Fracture Proppants in Multiple Layers," SPE 4117, JPT, May 1973.

Dake, L. P., "The Practice of Reservoir Engineering". Amsterdam: Elsevier, 1994.

Economides, C., "Use of the Pressure Derivative for Diagnosing Pressure- Transient Behavior," JPT, October 1988.

Environmental Protection Agency (EPA), "Evaluation of Impacts to Underground Sources of Drinking Water by Hydraulic Fracturing of Coalbed Methane Reservoirs," EPA 816-R-04-003 Report, June 2004.

Erturk M. C., "Production Performance Analysis of Coal Bed Methane, Shale Gas and Tight Gas Reservoirs with Different Well Trajectories and Completion Techniques", February 2013

Fekete F.A.S.T WelltestTM v7.70, help section

Gale, J.F.W., Robert M.R., Holder, J., "Natural Fractures in the Barnett Shale and their Importance for Hydraulic Fracture Treatments," AAPG Bulletin, Vol. 91, No. 4 603-622, April, 2007.

Gilman, J., and Kazemi, H., "Improvements in Simulation of Naturally Fractured Reservoirs," SPEJ, pp. 695–707, August 1983.

Gringarten, A.C. "From Straight Lines to Deconvolution: The Evolution of the State of the Art in Well Test Analysis," SPEREE, 11-1, pp 41–62, February 2008

Gringarten, A. C., Scientific Software-Intercomp, "Type-Curve Analysis: What It Can and Cannot Do", 1987

Gringarten, A. C., Ramey, H. J., Jr., Raghavan, R., "Unsteady-State Pressure Distributions Created by a Well with a Single Infinite-Conductivity Vertical Fracture," Soc. Pet. Eng. J., pp. 347–360, August 1974.

Hale, B.W. and Evers, J.F., "Elliptical Flow Equations for Vertically Fractured Gas Wells", JPT 33 (12): 2489–2497; Trans., AIME, 271 SPE-8943-PA. DOI: 10.2118/8943-PA, 1981.

Jones, L.G., Reservoir Reserve Tests. JPT 15 (3): 333–337; Trans., AIME, 228. SPE-402-PA. DOI: 10.2118/402-PA, 1963.

Kappa Shaphire Well Testing v4.02, help section

Kazemi, H., "Pressure Transient Analysis of Naturally Fractured Reservoirs with Uniform Fracture Distribution," Society of Petroleum Engineers J., pp. 451–462, December 1969.

Kruysdijk V., C.J.P.W., Dullaert, G.M., "A boundary element solution of the transient pressure response of multiple fractured horizontal wells", Paper Presented at the 2nd European Conference on the Mathematics of Oil Recovery, Cambridge, England, 1989.

Lee, J. W., "Well Testing", Dallas, TX: Society of Petroleum Engineers, 1982.

Mayerhofer, M.J., Lolon, E.P., Warpinski, N.R., Cipolla, C.L., Walser, D., Rightmire, C.M., "What is stimulated reservoir volume? ", Society of Petroleum Engineering Production & Operations 1 (25), 89–98, 2010.

Meyer, B.R. and Jacot, R.H., "Pseudosteady-State analysis of Finite-Conductivity Vertical Fractures", Paper SPE 95941 presented at the SPE Annual Technical Conference and Exhibition, Dallas, 9–12 October. DOI: 10.2118/95941-MS, 2005.

Moghadam, S., Jeje, O., Mattar L., Fekete Associates Inc. "Advanced Gas Material Balance in Simplified Format", SPE 139428, 2011

Montgomery, S.L., Daniel, M.J., Kent, A.B., Richard, M.P.: "Mississippian Barnet Shale, Fort Worth Basin, North-Central Texas: Gas-Sahle Paly with Multi-Trillion Cubic Foot Potential," AAPG Bulletin, Vol. 89, No. 2, pp. 155-175, February, 2005

Nobakht M., Clarkson C.R., University of Calgary, 2Fekete Associates Inc., "A New Analytical Method for Analyzing Production Data from Shale Gas Reservoirs Exhibiting Linear Flow: Constant Rate Production", SPE 143990, 2011

Nobakht, M., Clarkson, C.R., Kaviani, "New type-curves for analyzing horizontal well with multiple fractures in shale gas reservoirs", Journal of Natural Gas Science and Engineering 10, 99–112, 2012.

Nobakht M., Clarkson C.R., Kaviani D., "New and Improved Methods for Performing Rate-Transient Analysis of Shale Gas Reservoirs", SPE 147869, 2011

Nobakht, M., Mattar, L., "Analyzing production data from unconventional gas reservoirs with linear flow and apparent skin", Journal of Canadian Petroleum Society 51 (1), 52–59, 2012.

Olivier Houze, Eric Tauzin, Vincent Artus, Leif Larsen, "The analysis of dynamic data in shale gas reservoirs – part 1", 2010

Palmer, L., and Mansoori, J.: "How Permeability Depends on Stress and Pore Pressure in Coalbeds: A New Model," paper SPE 36737 presented at the Annual Technical Conference and Exhibition, Denver, Colorado, 6-9 October, 1996.

Prats, M. "Effect of Vertical Fractures on Reservoir Behavior— Incompressible Fluid Case". SPEJ 1 (2): 105–118; Trans., AIME, 222. SPE-1575-G. DOI: 10.2118/1575-G, 1961

Raghavan, R., Chen, C.C., Agarwal, B., "An analysis of horizontal wells intercepted by multiple fractures", Society of Petroleum Engineers Journal 2 (3), 235–245, 1997.

Ramirez, B., Kazemi, H., Ozkan, E., and Atan, S. "A Critical Review for Proper Use of Water/Oil/Gas Transfer Functions in Dual-Porosity NFR," SPE 109295. Presented at the SPE Annual Technical Conference, Anaheim/CA, 11–14 November 2007

Samandarli O., "Production Analysis in Unconventional Reservoirs with Rate Normalized Pressure (RNP): Theory, Methodology and Applications", SPE-155614, 2012

Schenk, Christopher J.: "Geologic Definition and Resource assessment of Continuous (Unconven-tional) Gas Accumulations – the U.S. Experience," AAPG 66086 presented at the Ancient Oil-New Energy Conference, Cairo, October 27-30, 2002.

Schlumberger, "Well Testing Interpretation Manual", 2002.

Shanqiang L., Neal L., Arulampalam P., McDonough J. C., Hess Corporation, "Flow Regime Analysis of Multi-stage Hydraulically-Fractured Horizontal Wells with Reciprocal Rate Derivative Function: Bakken Case Study", SPE 137514, 2010

Soliman M.Y., Kabir C.S., "Testing unconventional formations", Journal of Petroleum Science and Engineering pp 92–93, 102–109, 2012

Warren, J. E., and Root, P. J., "The Behavior of Naturally Fractured Reservoirs," Society of Petroleum Engineers J., pp. 245–255, September 1963.

APPENDICES

APPENDIX A: SAPHIRE FINITE CONDUCTIVITY MODEL RESULTS

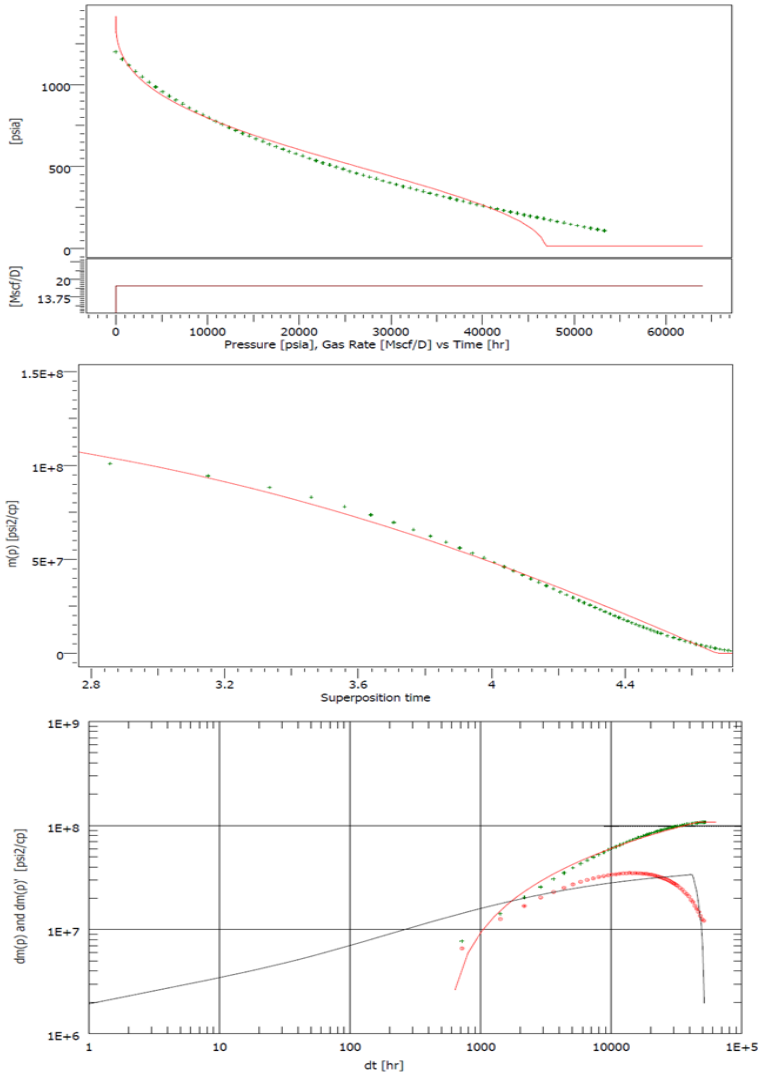

Figure A. 1 Saphire Finite Conductivity Model for single stage hydraulic fracture - 500 m^3/day production: a) history plot; b) semilog plot; c) presudo-pressure log-log derivative plot

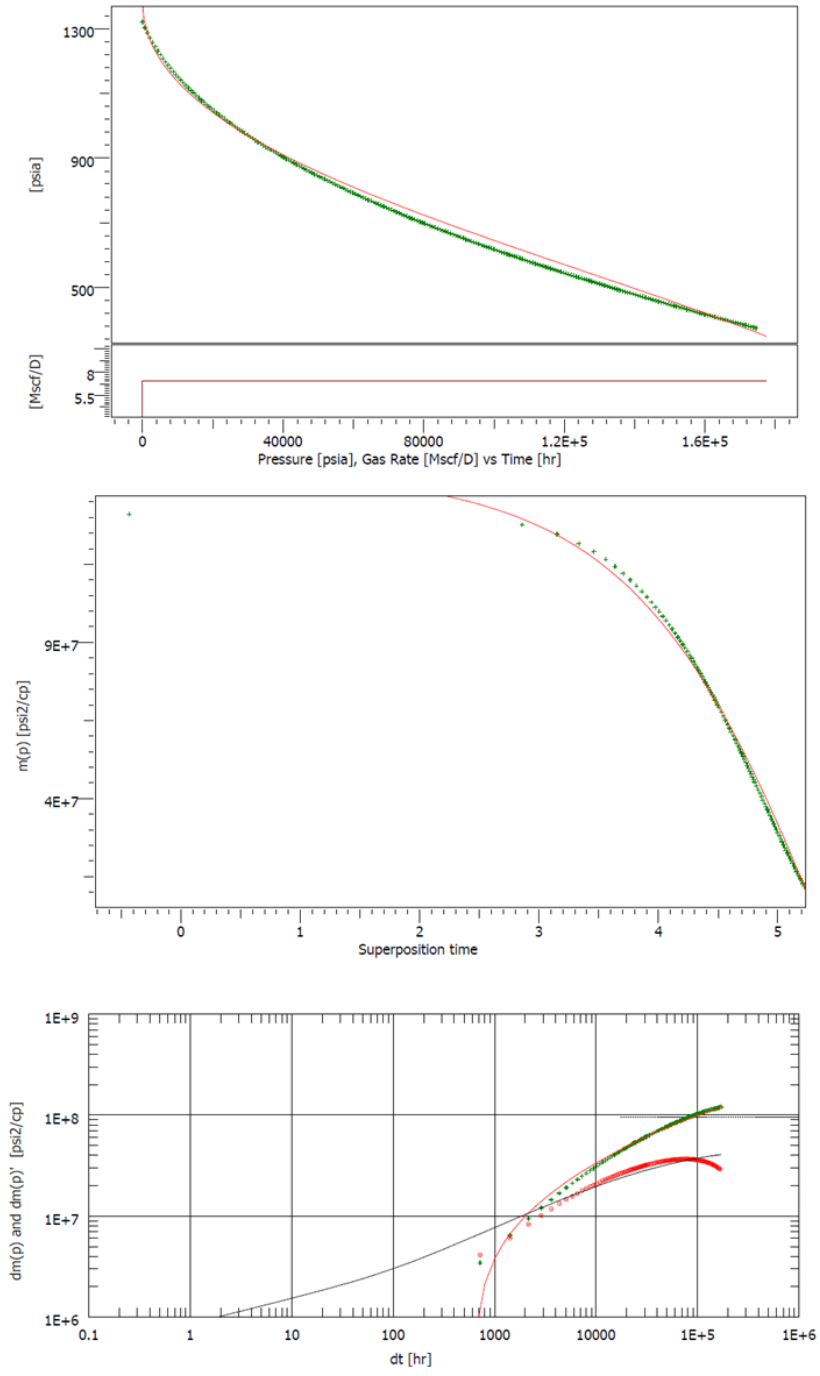

Figure A. 2 Saphire Finite Conductivity Model for single stage hydraulic fracture - 200 m3/day production: a) history plot; b) semilog plot; c) presudo-pressure log-log derivative plot

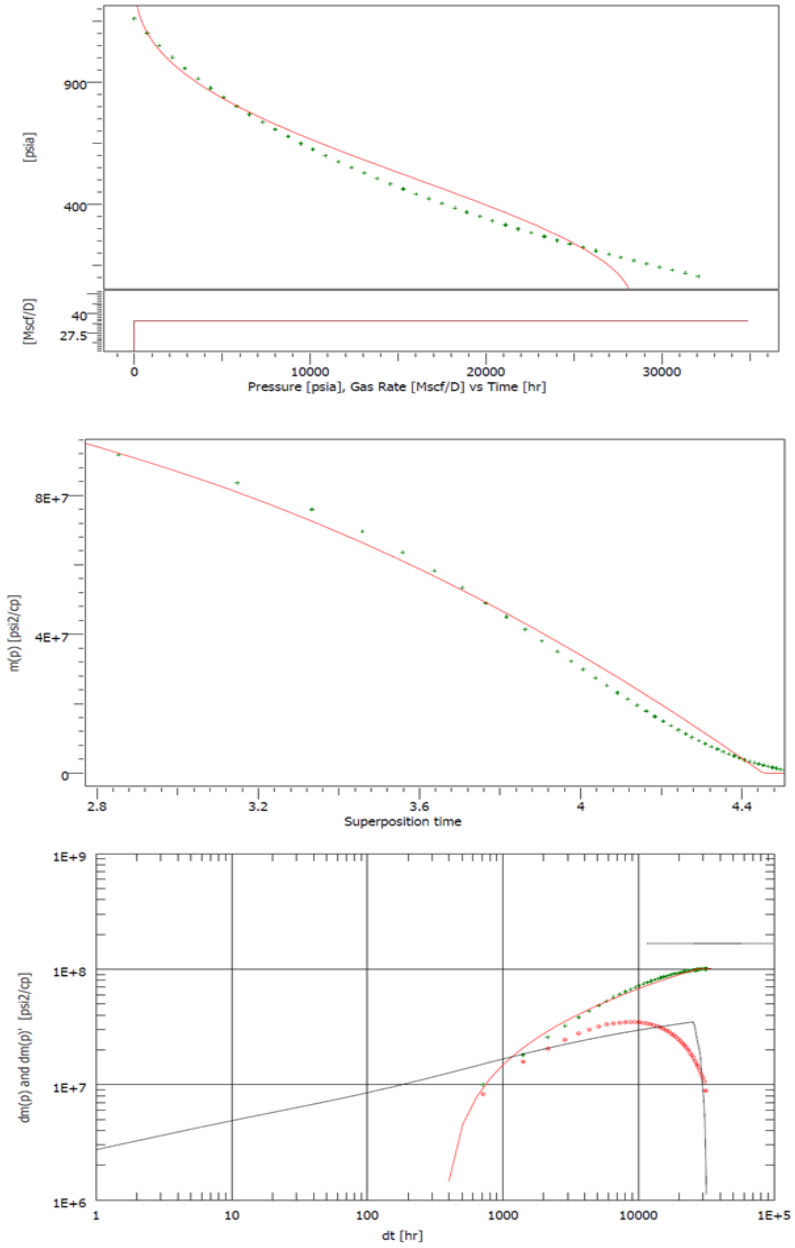

Figure A. 3 Saphire Finite Conductivity Model for two stage hydraulic fracture - 1000 m3/day production: a) history plot; b) semilog plot; c) presudo-pressure log-log derivative plot

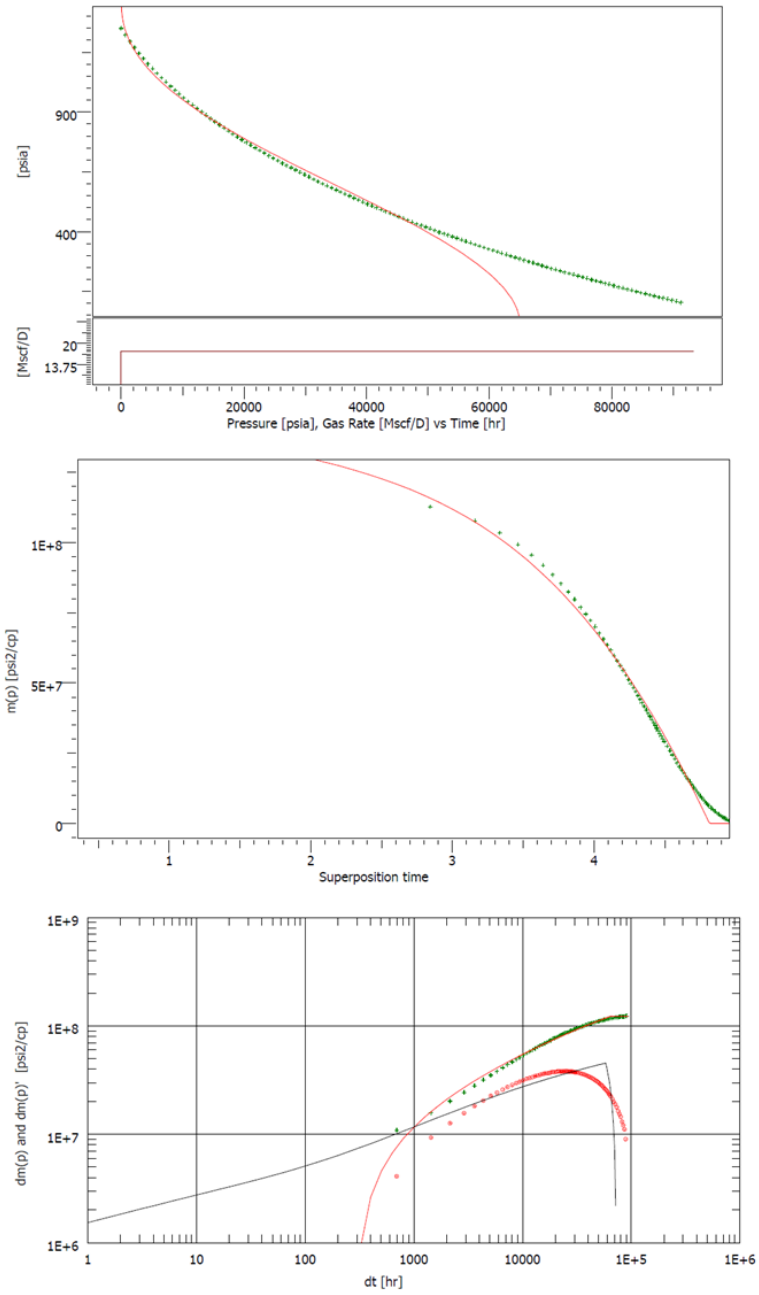

Figure A. 4 Saphire Finite Conductivity Model for two stage hydraulic fracture - 500 m3/day production: a) history plot; b) semilog plot; c) presudo-pressure log-log derivative plot

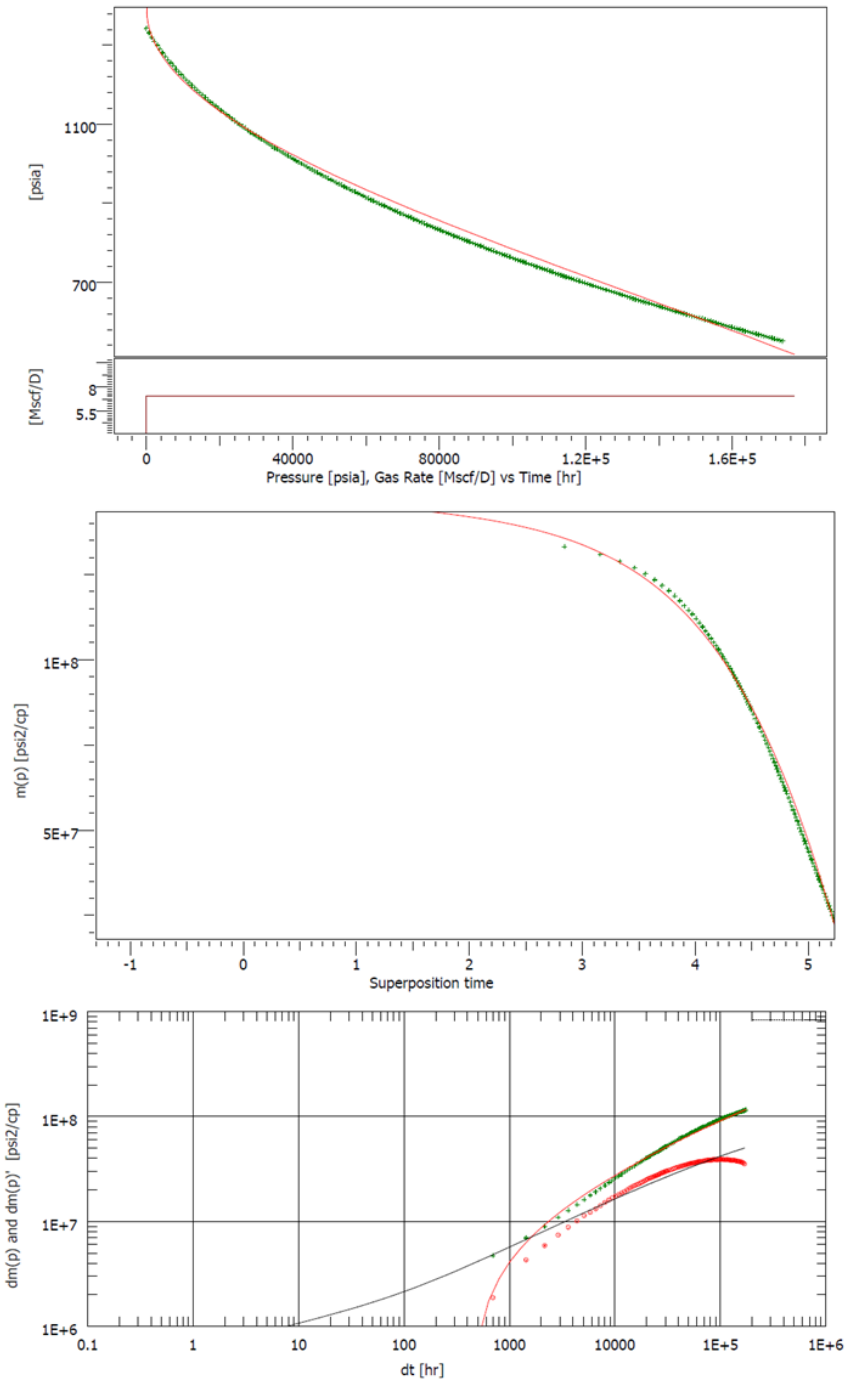

Figure A. 5 Saphire Finite Conductivity Model for two stage hydraulic fracture - 200 m3/day production: a) history plot; b) semilog plot; c) presudo-pressure log-log derivative plot

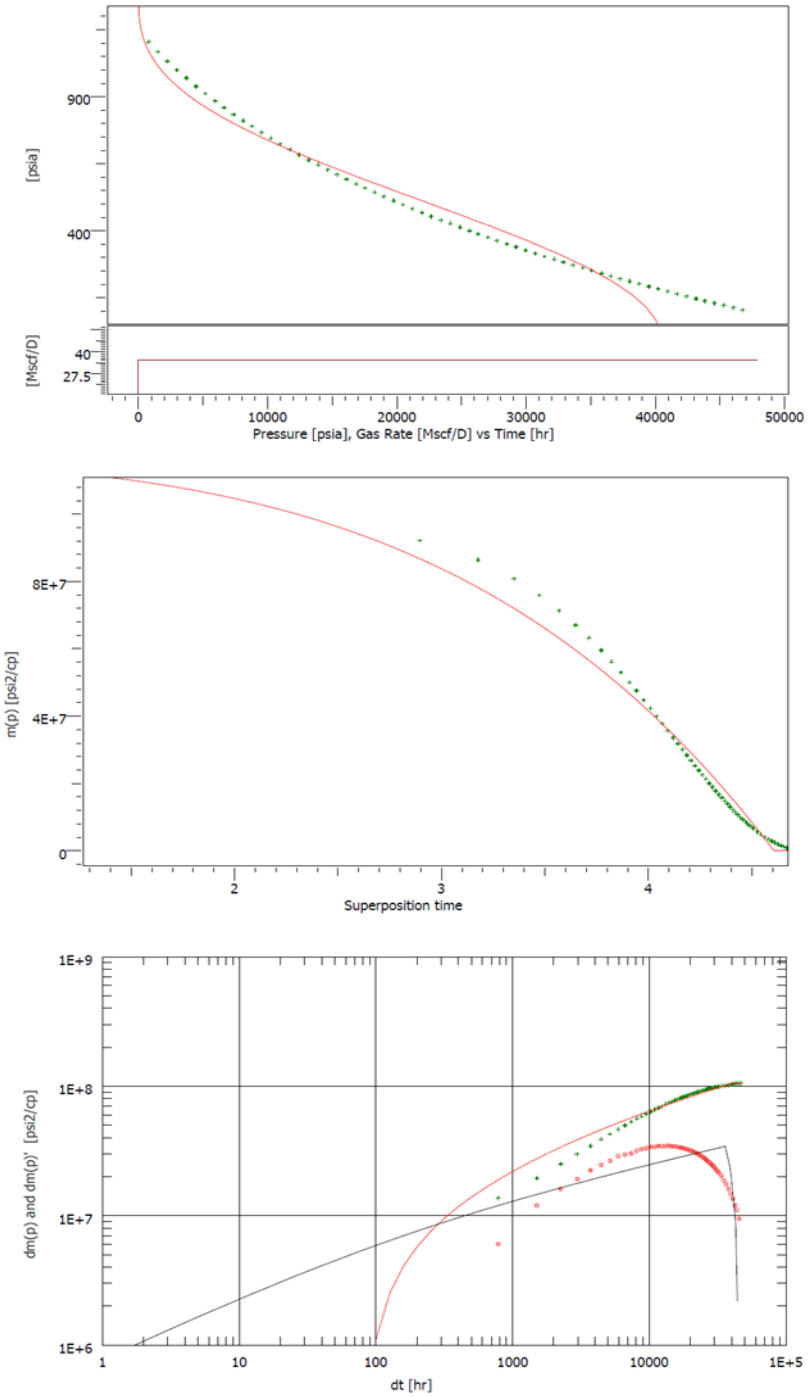

Figure A. 6 Saphire Finite Conductivity Model for three stage hydraulic fracture - 1000 m3/day production: a) history plot; b) semilog plot; c) presudo-pressure log-log derivative plot

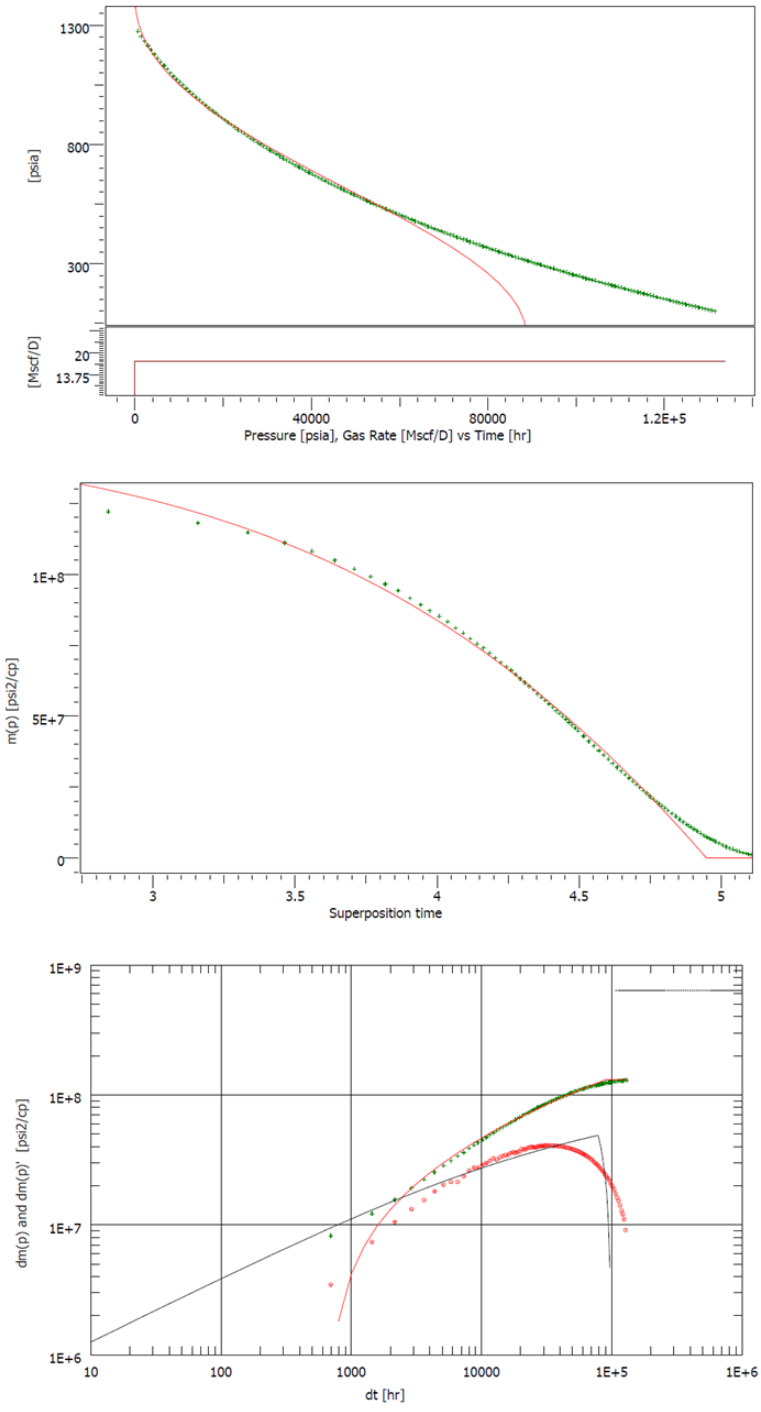

Figure A. 7 Saphire Finite Conductivity Model for three stage hydraulic fracture - 500 m3/day production: a) history plot; b) semilog plot; c) presudo-pressure log-log derivative plot

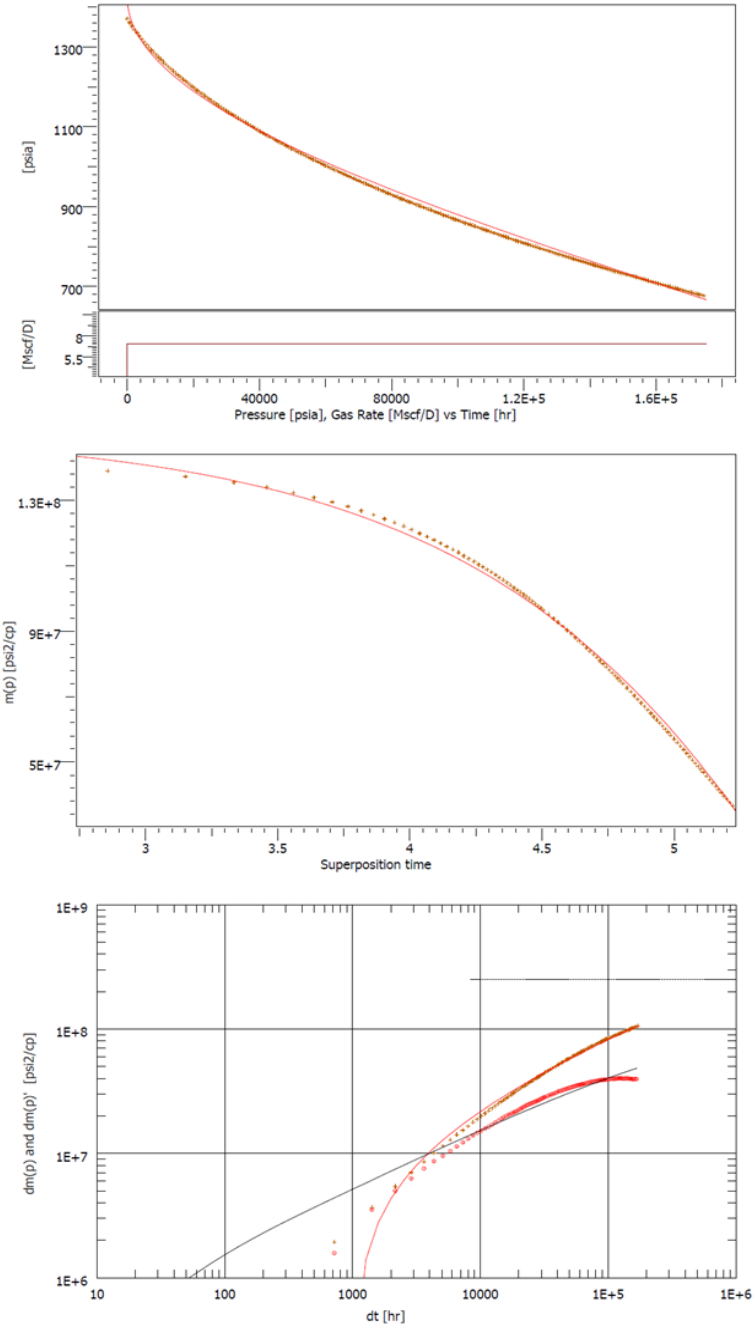

Figure A. 8 Saphire Finite Conductivity Model for three stage hydraulic fracture - 200 m3/day production: a) history plot; b) semilog plot; c) presudo-pressure log-log derivative plot

APPENDIX B: F.A.S.T FINITE CONDUCTIVITY MODEL RESULTS

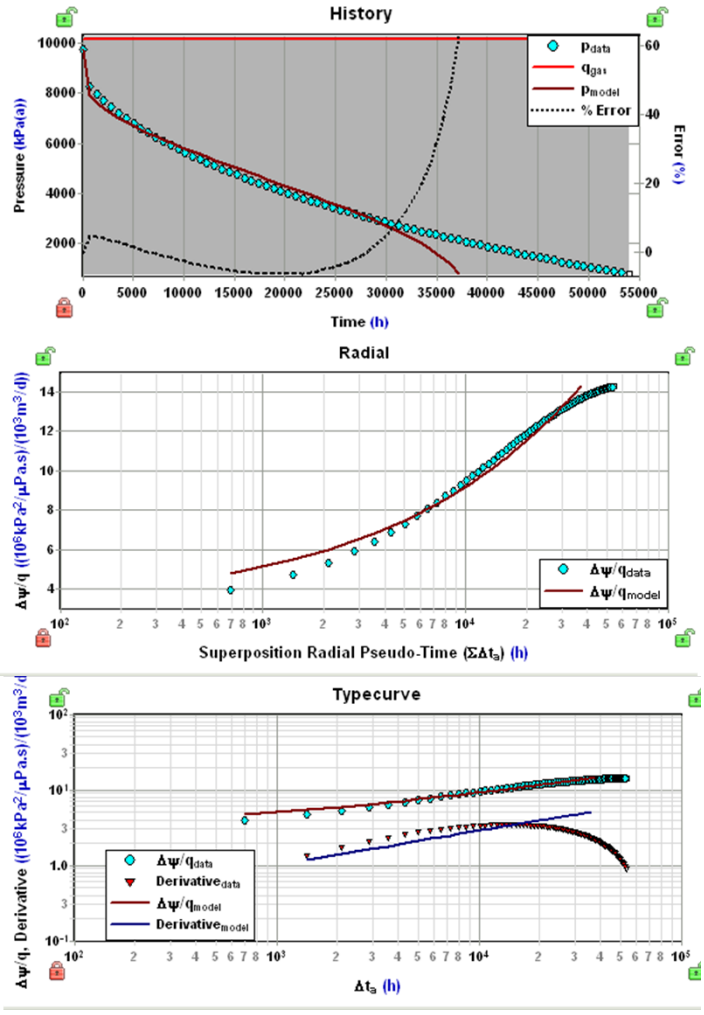

Figure B. 1 Fekete Finite Conductivity Model for single stage hydraulic fracture - 500 m^3/day production: a) history plot; b) semilog plot; c) RNP log-log derivative plot

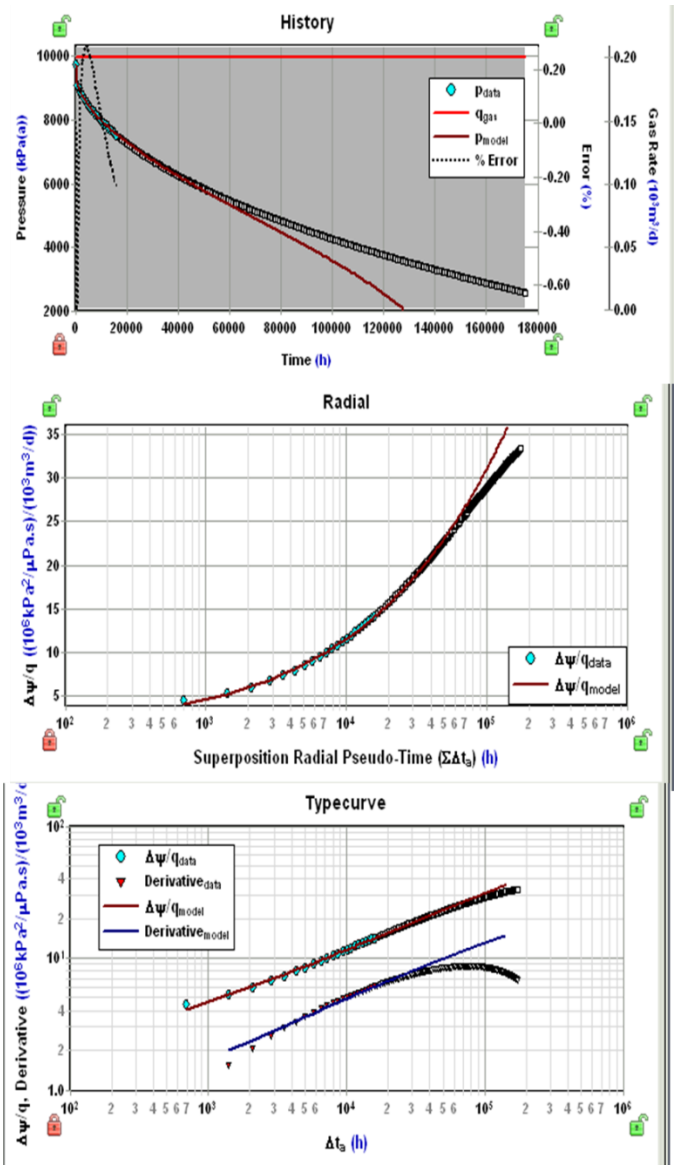

Figure B. 2 Fekete Finite Conductivity Model for single stage hydraulic fracture - 200 m^3/day production: a) history plot; b) semilog plot; c) RNP log-log derivative plot

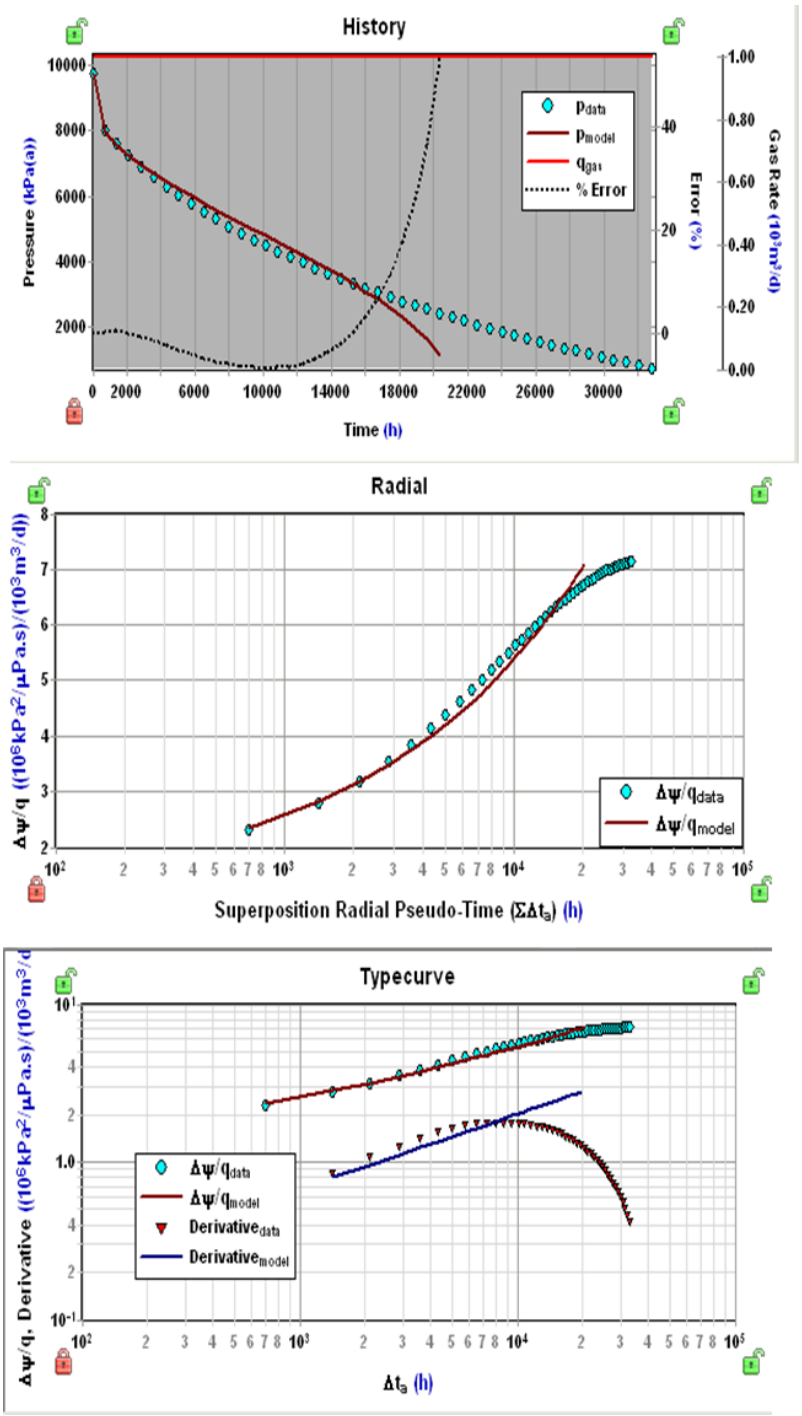

Figure B. 3 Fekete Finite Conductivity Model for two stage hydraulic fracture - 1000 m^3/day production: a) history plot; b) semilog plot; c) RNP log-log derivative plot

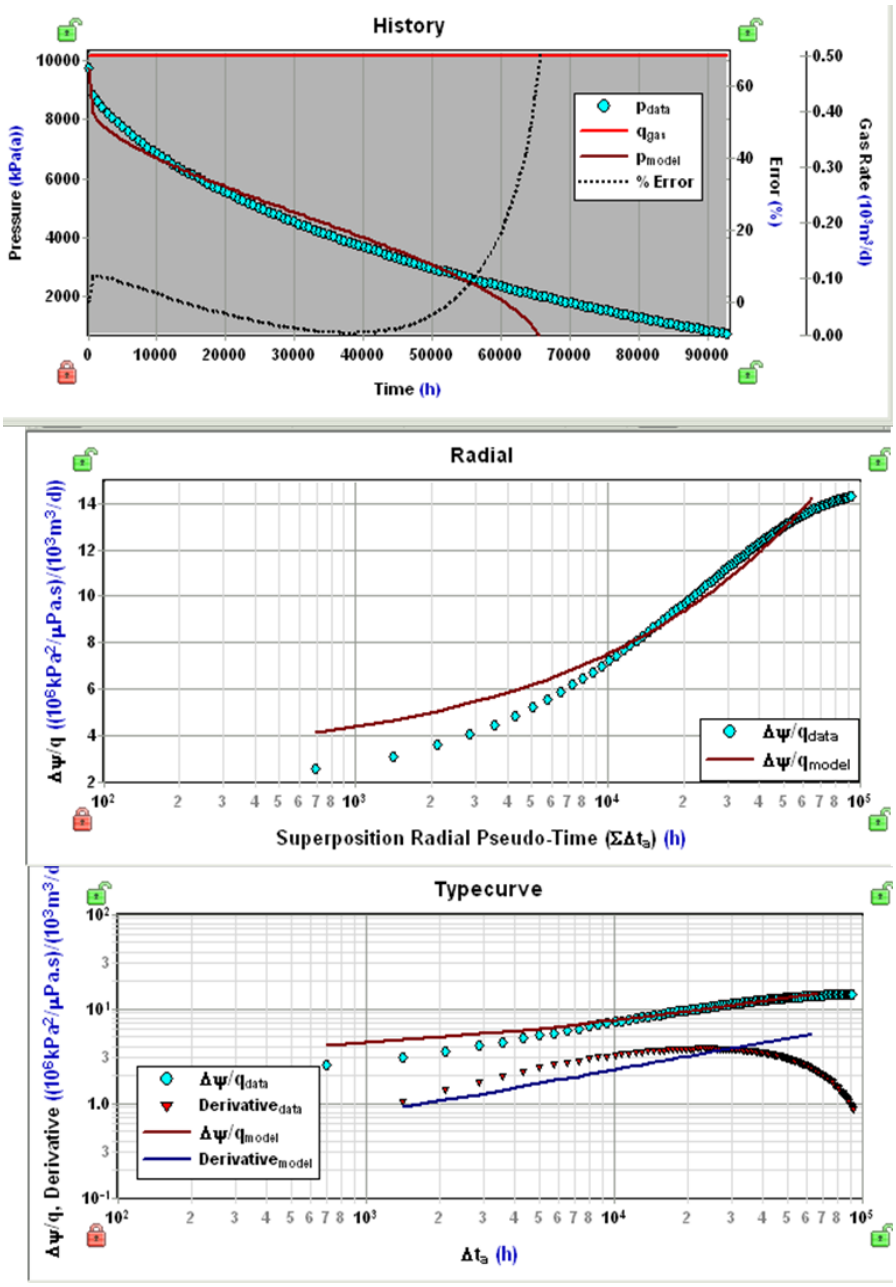

Figure B. 4 Fekete Finite Conductivity Model for two stage hydraulic fracture - 500 m3/day production: a) history plot; b) semilog plot; c) RNP log-log derivative plot

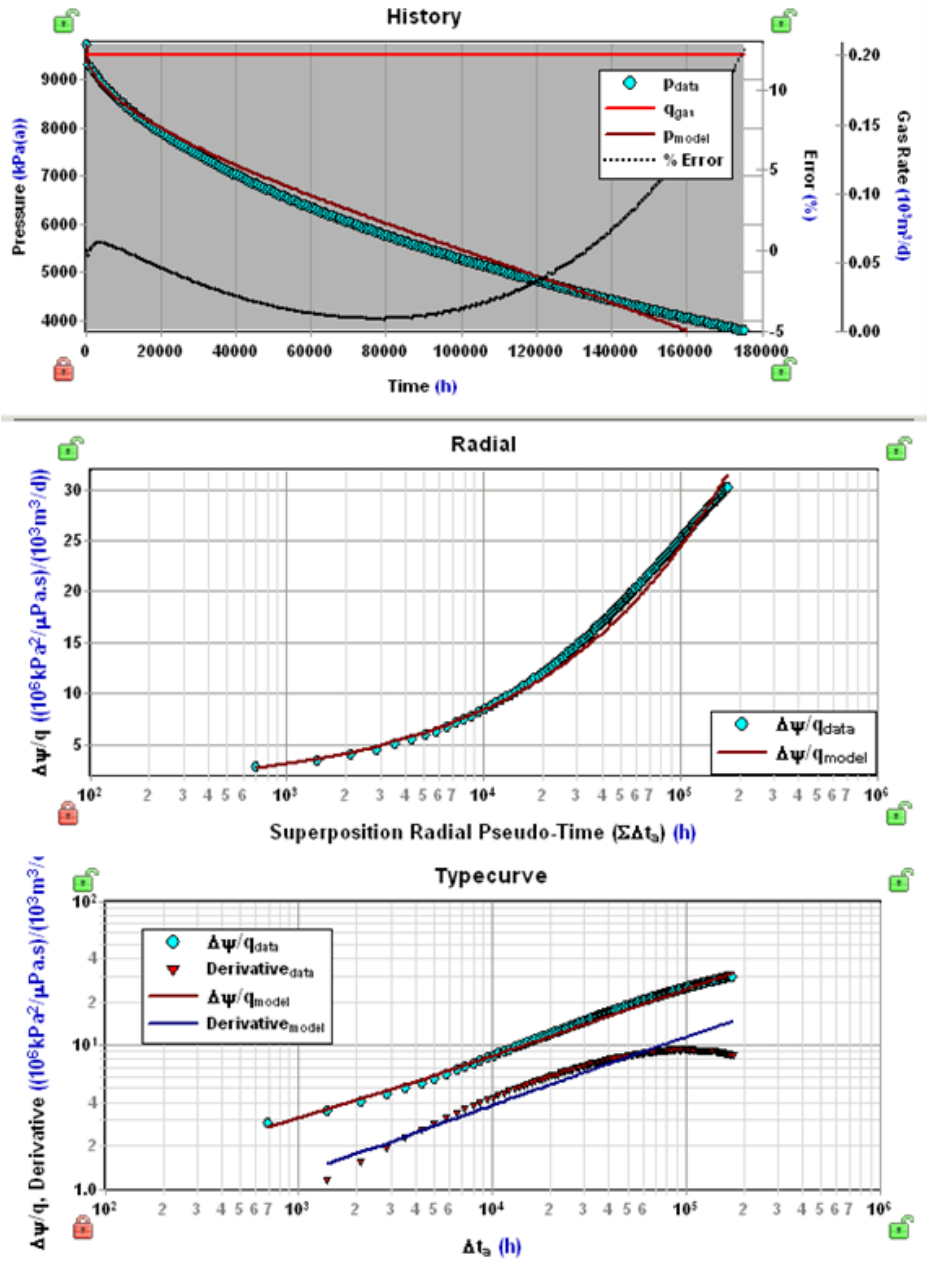

Figure B. 5 Fekete Finite Conductivity Model for two stage hydraulic fracture - 200 m3/day production: a) history plot; b) semilog plot; c) RNP log-log derivative plot

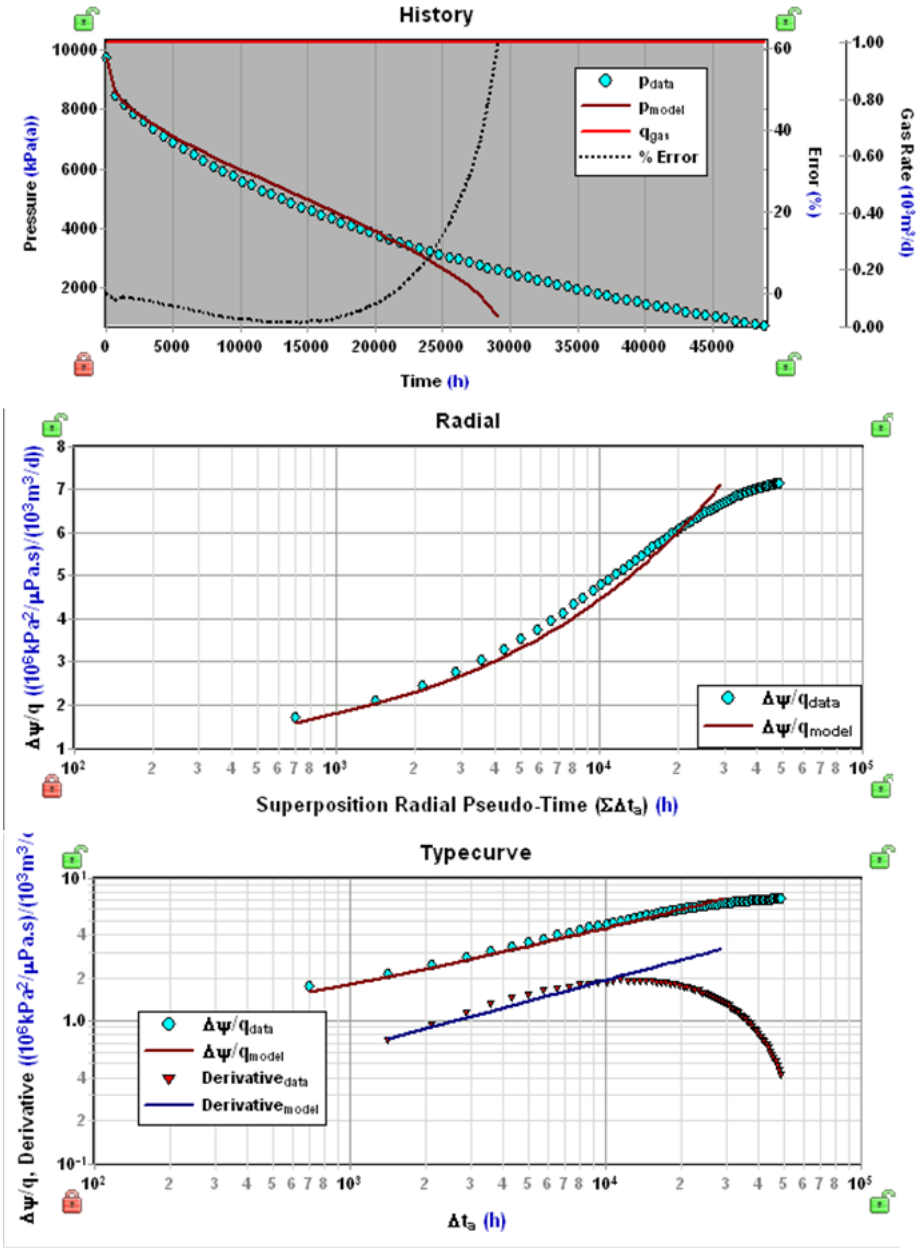

Figure B. 6 Fekete Finite Conductivity Model for three stage hydraulic fracture - 1000 m3/day production: a) history plot; b) semilog plot; c) RNP log-log derivative plot

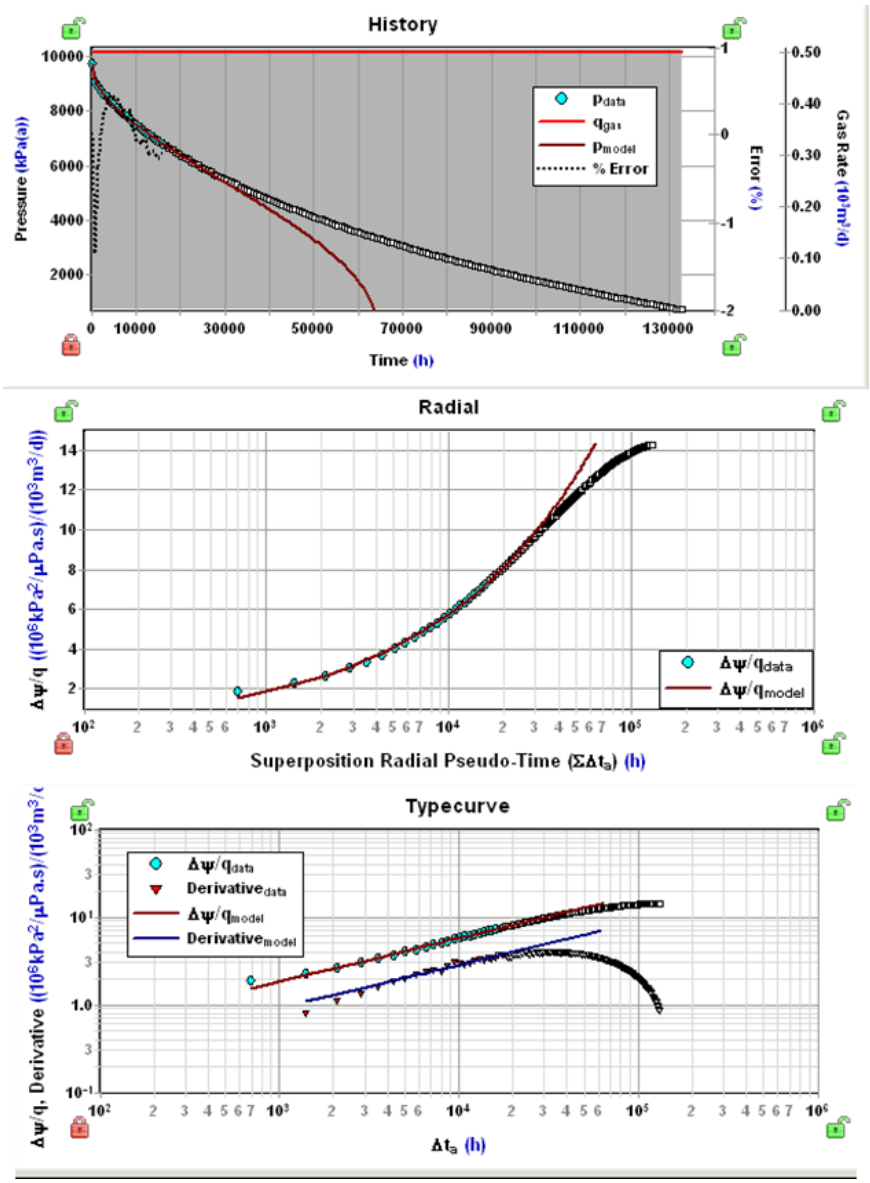

Figure B. 7 Fekete Finite Conductivity Model for three stage hydraulic fracture - 500 m3/day production: a) history plot; b) semilog plot; c) RNP log-log derivative plot

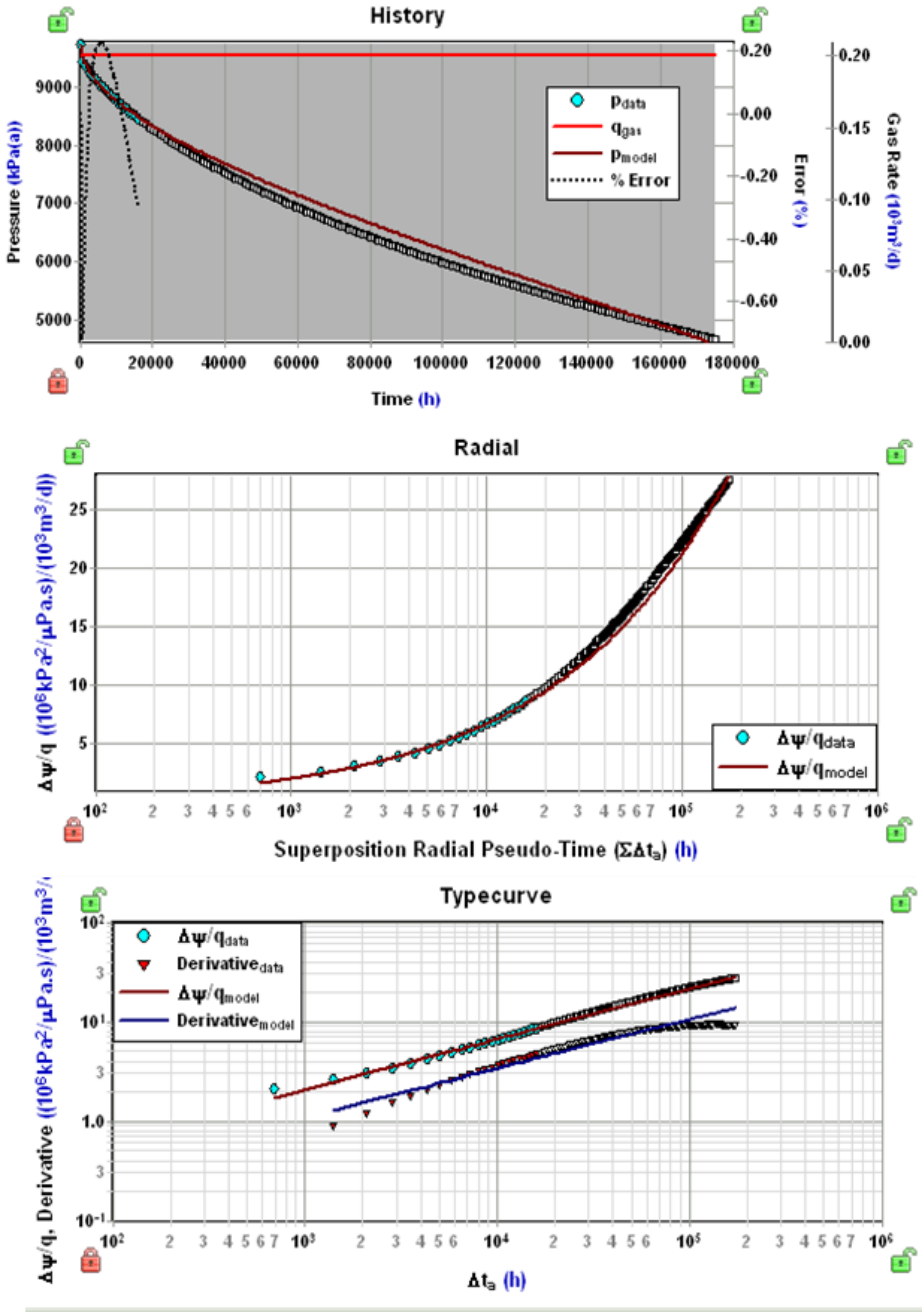

Figure B. 8 Fekete Finite Conductivity Model for three stage hydraulic fracture - 200 m3/day production: a) history plot; b) semilog plot; c) RNP log-log derivative plot

APPENDIX C: HORIZONTAL MULTIFRAC SRV (GAS) MODEL RESULTS

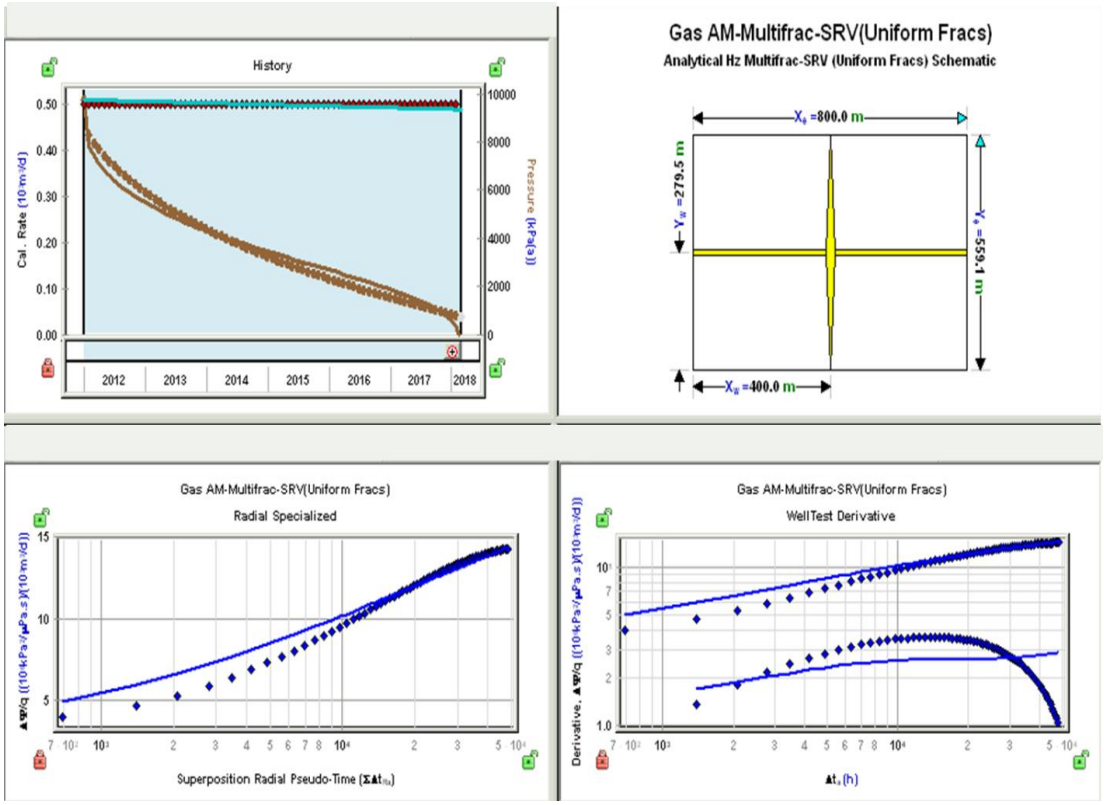

Figure C. 1 Fekete Horizontal Multifrac SRV (Uniform Frac-s) Gas Model for single stage hydraulic fracture - 500 m3/day production: a) history plot; b) SRV model Shematic c) semilog plot; d) RNP log-log derivative plot

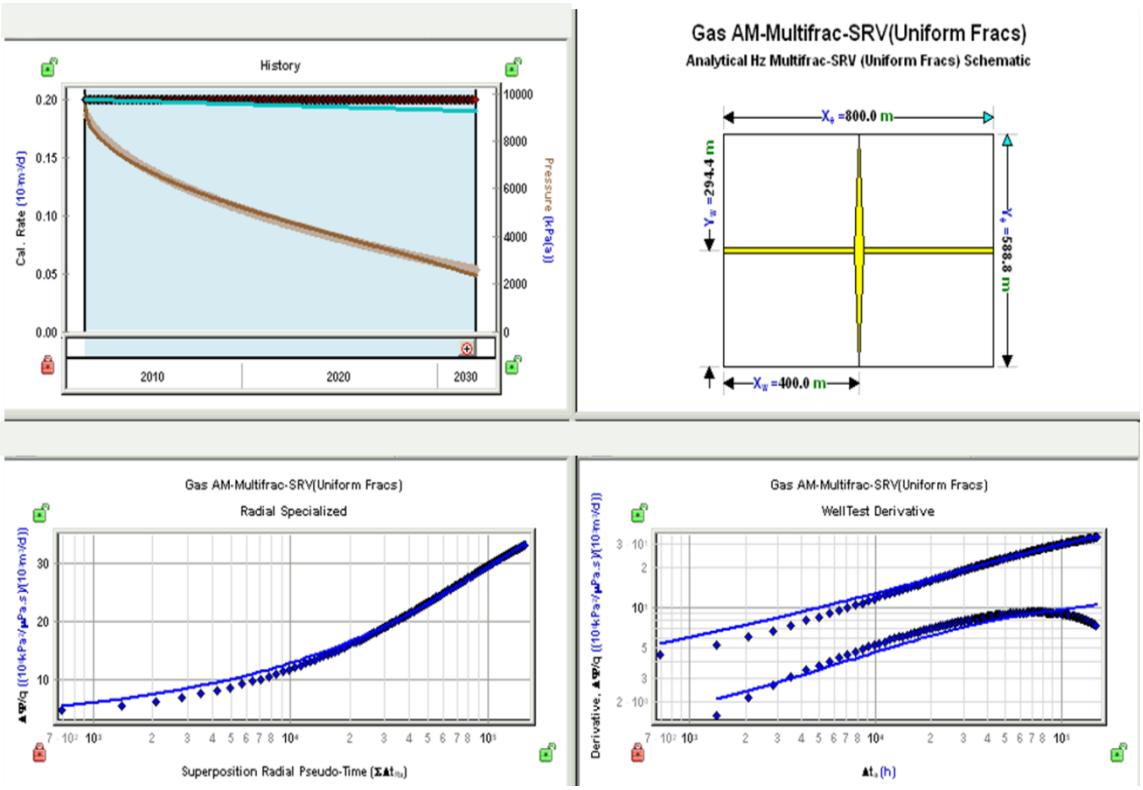

Figure C. 2 Fekete Horizontal Multifrac SRV (Uniform Frac-s) Gas Model for single stage hydraulic fracture - 200 m3/day production: a) history plot; b) SRV model Shematic c) semilog plot; d) RNP log-log derivative plot

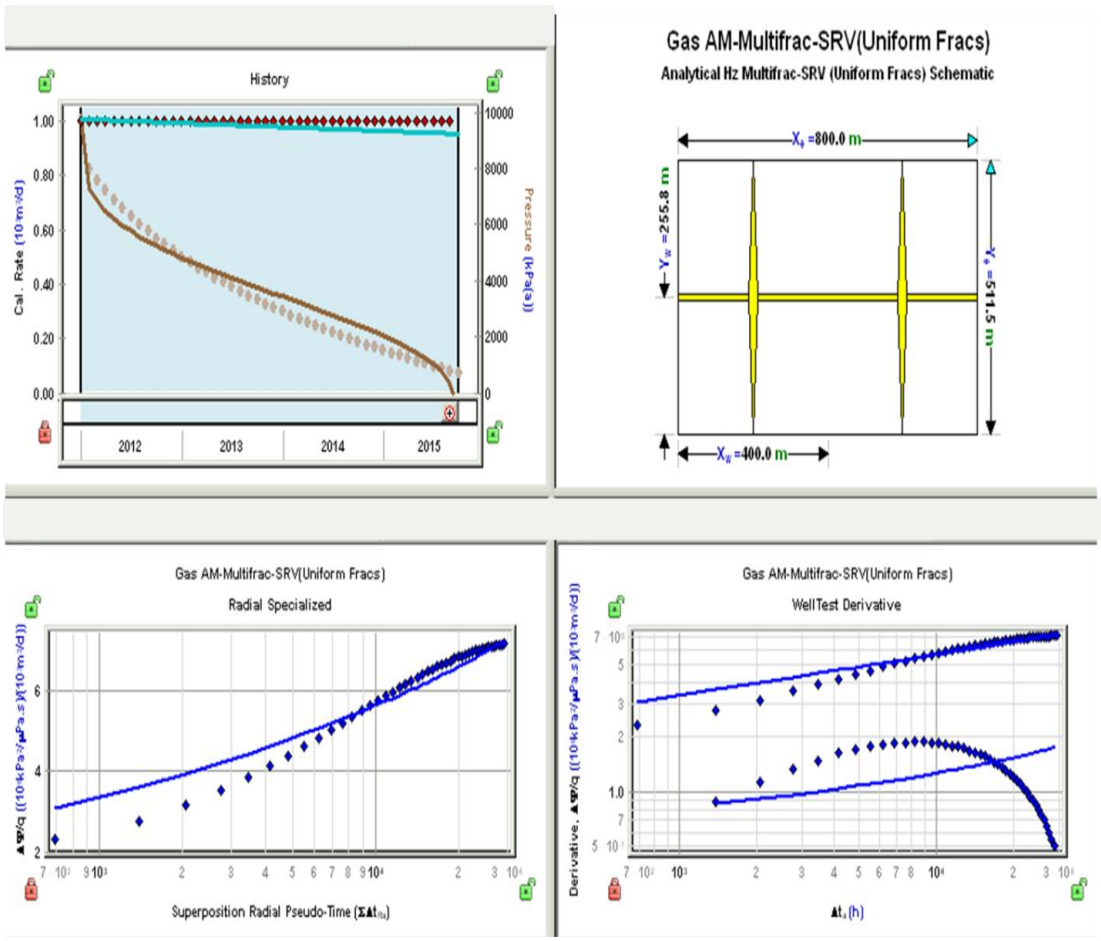

Figure C. 3 Fekete Horizontal Multifrac SRV (Uniform Frac-s) Gas Model for two stage hydraulic fracture - 1000 m3/day production: a) history plot; b) SRV model Shematic c) semilog plot; d) RNP log-log derivative plot

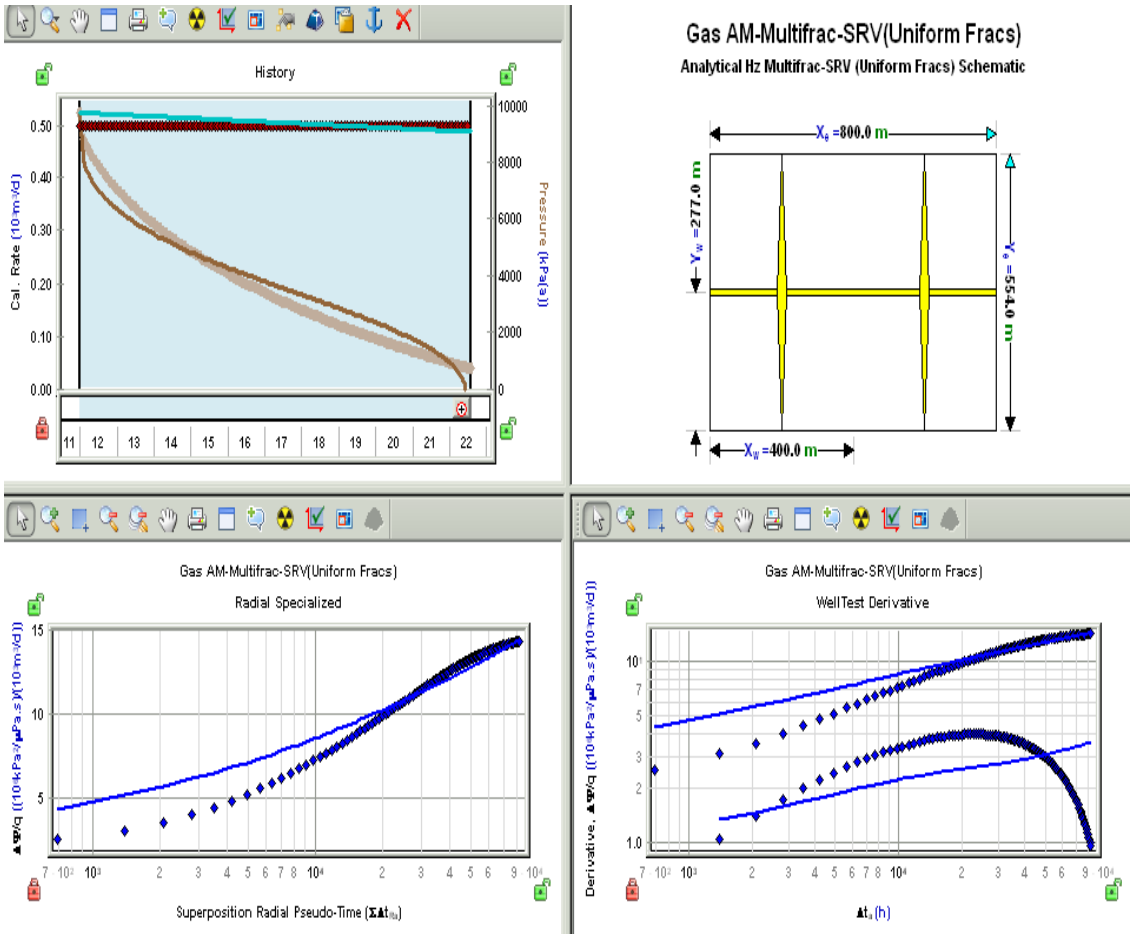

Figure C. 4 Fekete Horizontal Multifrac SRV (Uniform Frac-s) Gas Model for two stage hydraulic fracture - 500 m3/day production: a) history plot; b) SRV model Shematic c) semilog plot; d) RNP log-log derivative plot

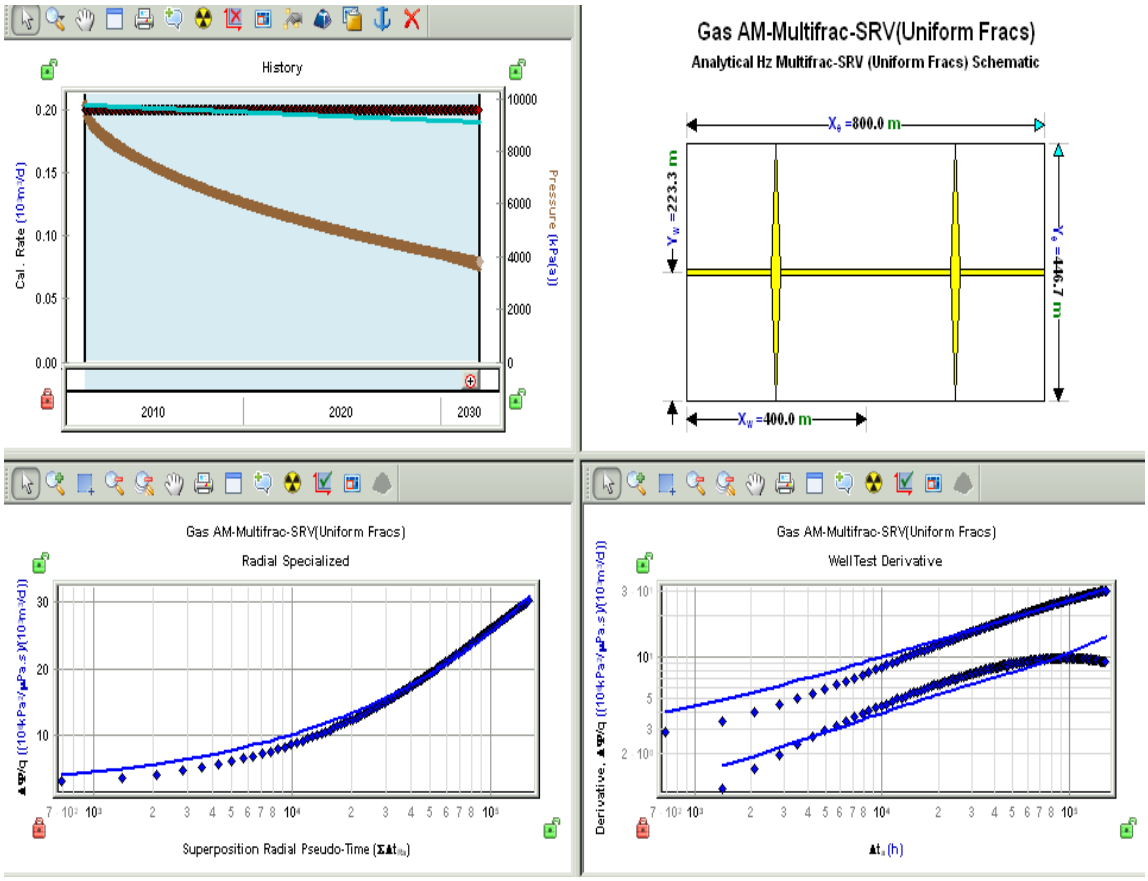

Figure C. 5 Fekete Horizontal Multifrac SRV (Uniform Frac-s) Gas Model for two stage hydraulic fracture - 200 m3/day production: a) history plot; b) SRV model Shematic c) semilog plot; d) RNP log-log derivative plot

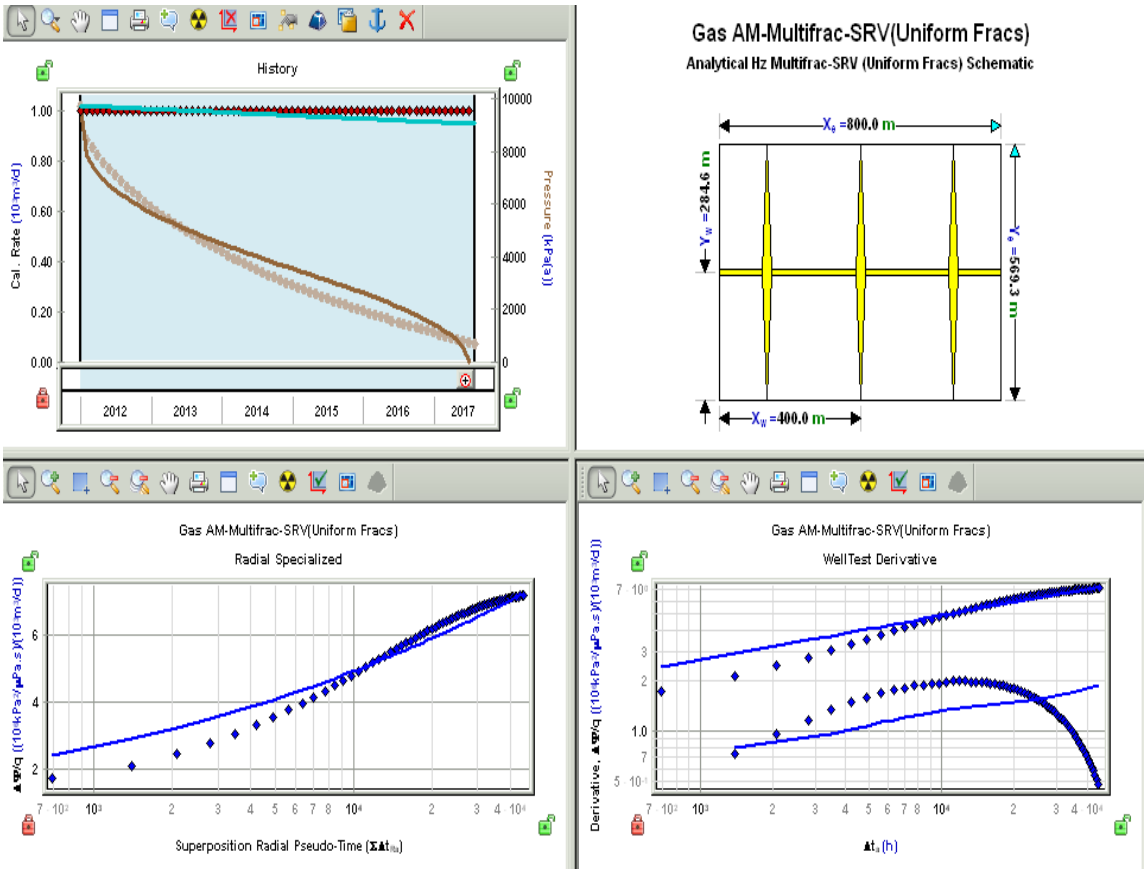

Figure C. 6 Fekete Horizontal Multifrac SRV (Uniform Frac-s) Gas Model for three stage hydraulic fracture - 1000 m3/day production: a) history plot; b) SRV model Shematic c) semilog plot; d) RNP log-log derivative plot

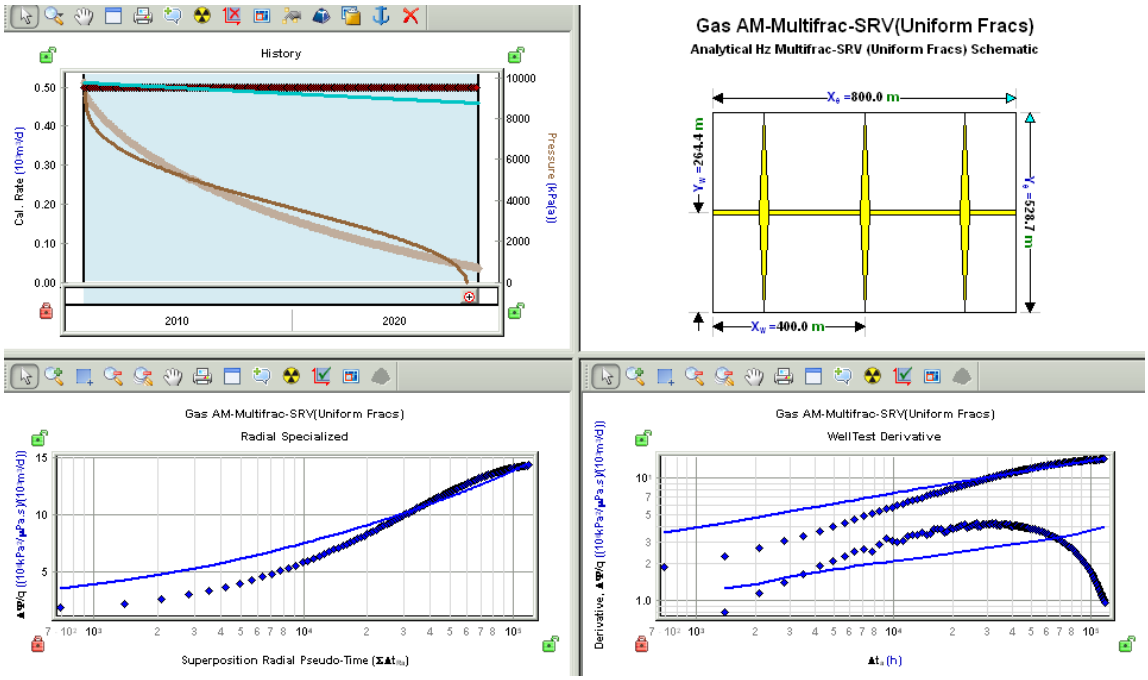

Figure C. 7 Fekete Horizontal Multifrac SRV (Uniform Frac-s) Gas Model for three stage hydraulic fracture - 500 m3/day production: a) history plot; b) SRV model Shematic c) semilog plot; d) RNP log-log derivative plot

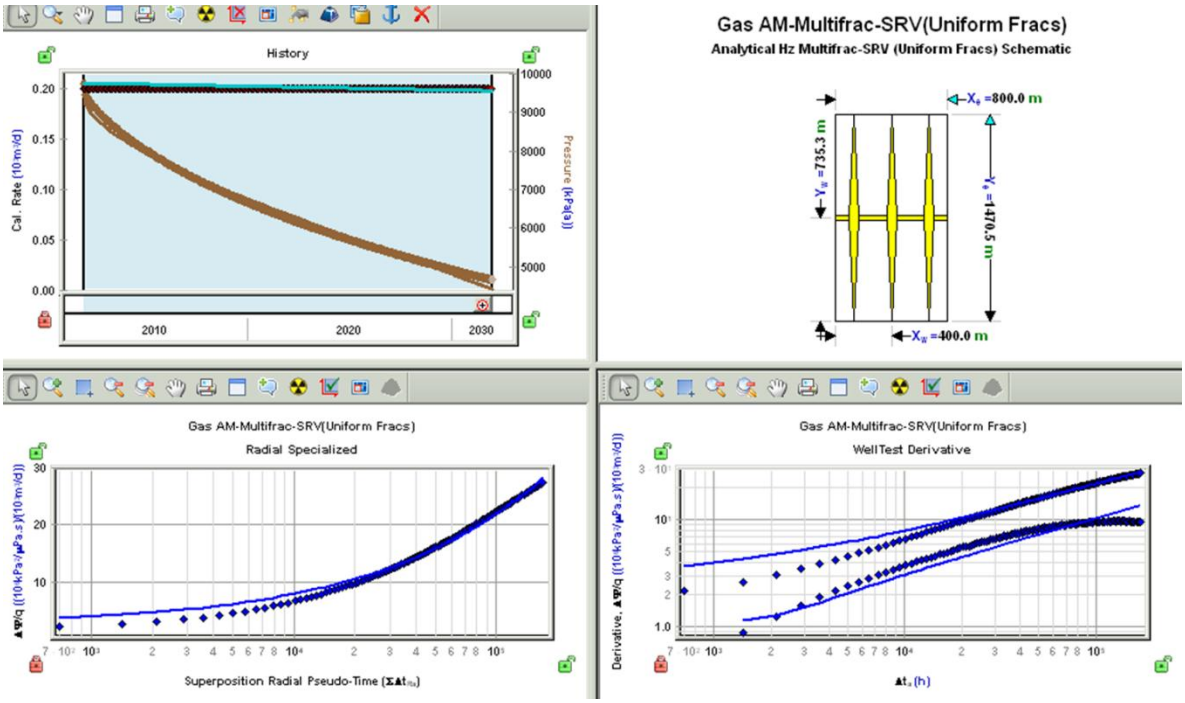

Figure C. 8 Fekete Horizontal Multifrac SRV (Uniform Frac-s) Gas Model for three stage hydraulic fracture - 200 m3/day production: a) history plot; b) SRV model Shematic c) semilog plot; d) RNP log-log derivative plot

APPENDIX D: HORIZONTAL MULTIFRAC SRV (CBM) MODEL RESULTS

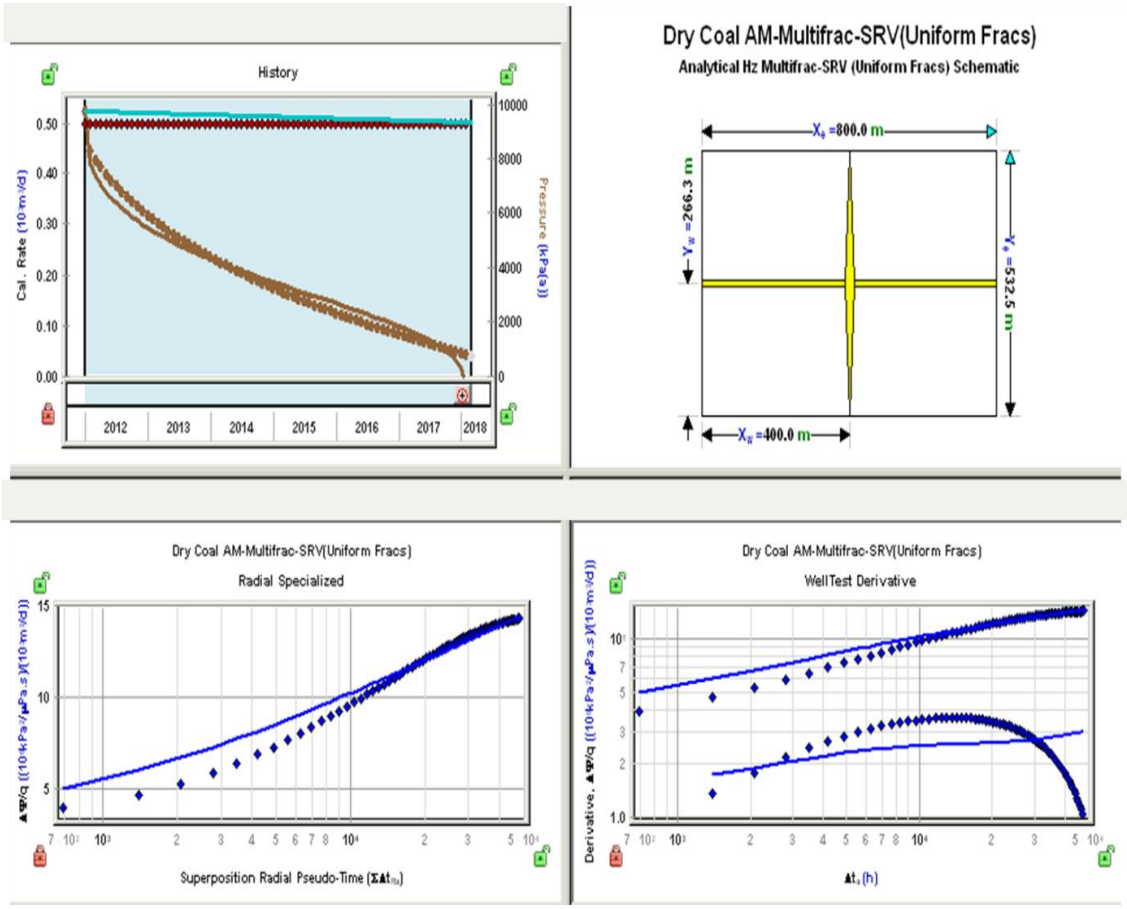

Figure D. 1 Fekete Horizontal Multifrac SRV (Uniform Frac-s) CBM Model for single stage hydraulic fracture - 500 m3/day production: a) history plot; b) SRV model Shematic c) semilog plot; d) RNP log-log derivative plot

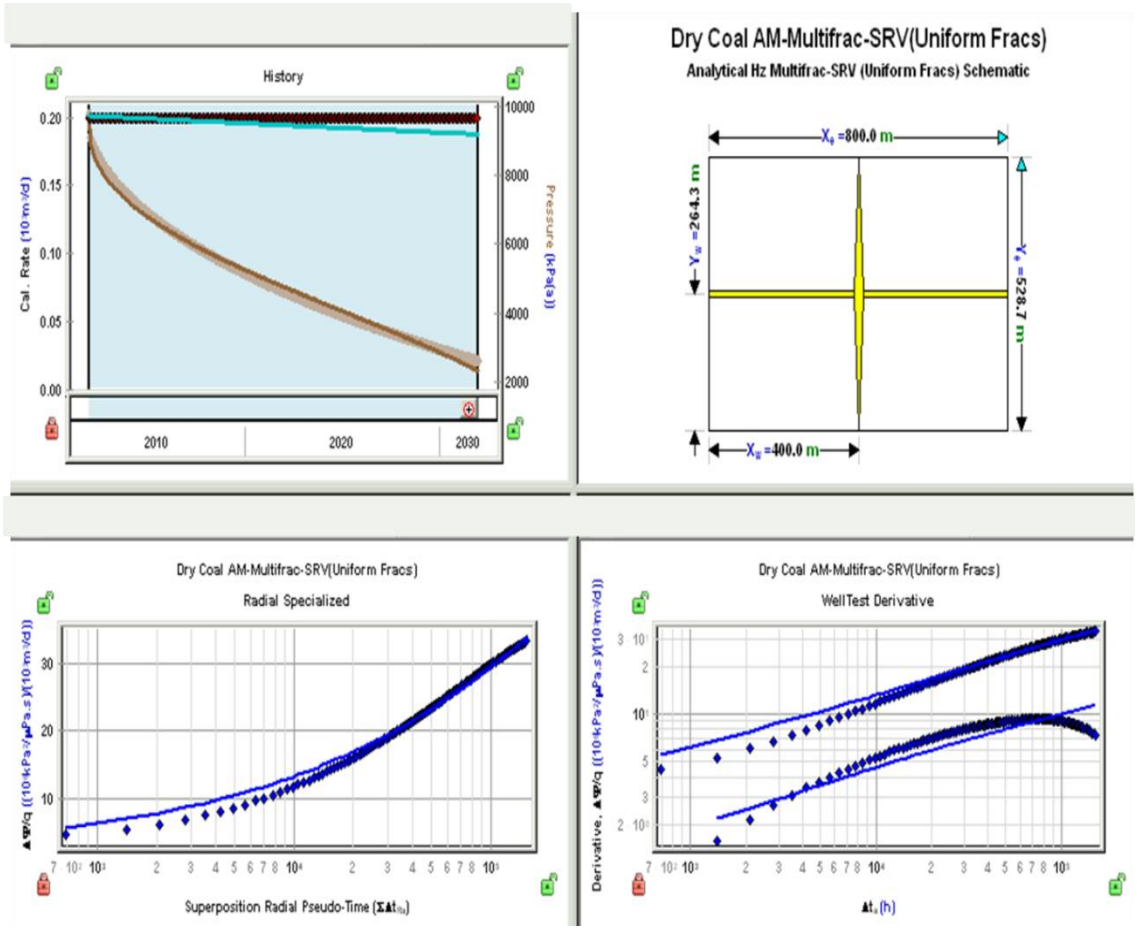

Figure D. 2 Fekete Horizontal Multifrac SRV (Uniform Frac-s) CBM Model for single stage hydraulic fracture - 200 m3/day production: a) history plot; b) SRV model Shematic c) semilog plot; d) RNP log-log derivative plot

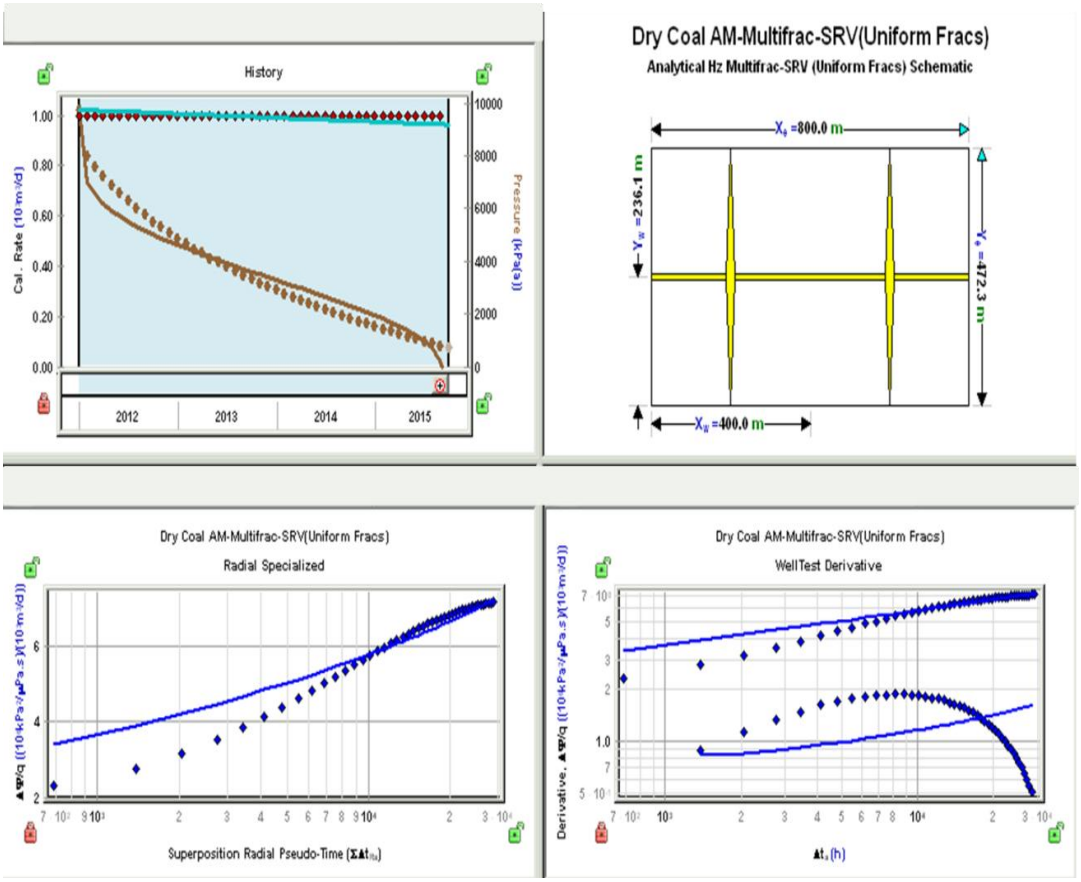

Figure D. 3 Fekete Horizontal Multifrac SRV (Uniform Frac-s) CBM Model for two stage hydraulic fracture - 1000 m3/day production: a) history plot; b) SRV model Shematic c) semilog plot; d) RNP log-log derivative plot

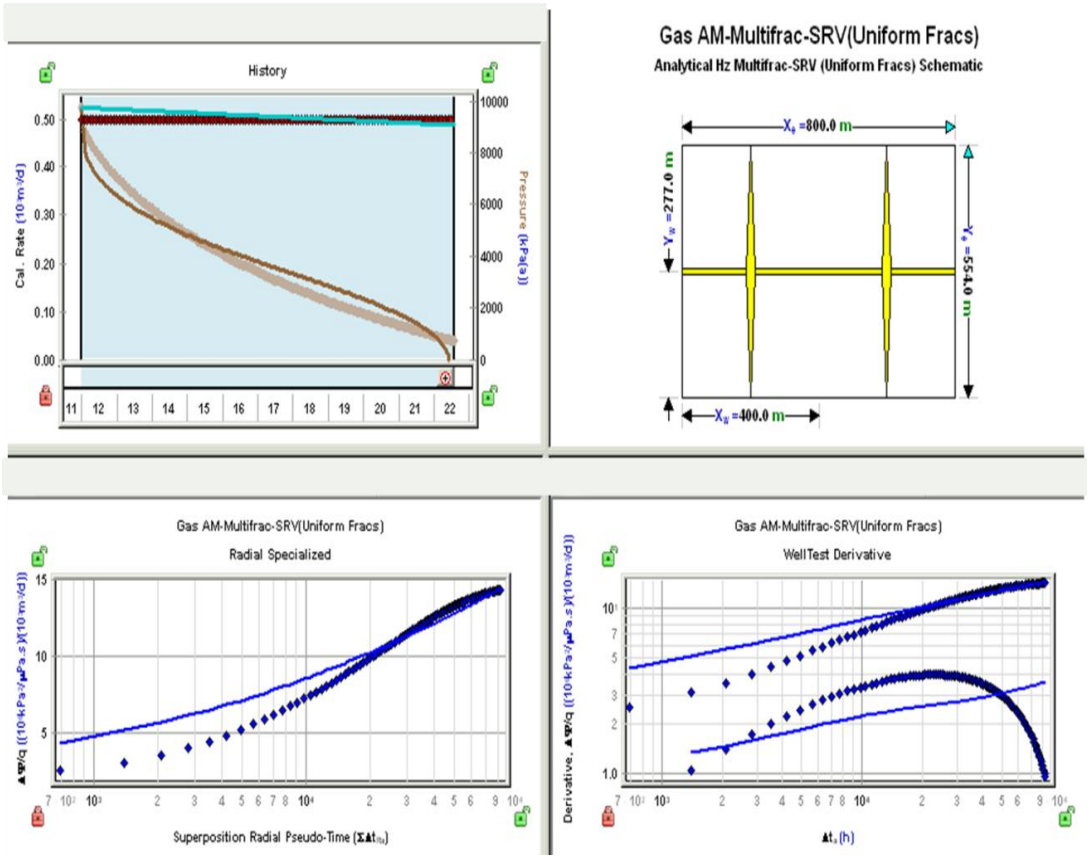

Figure D. 4 Fekete Horizontal Multifrac SRV (Uniform Frac-s) CBM Model for two stage hydraulic fracture - 500 m3/day production: a) history plot; b) SRV model Shematic c) semilog plot; d) RNP log-log derivative plot

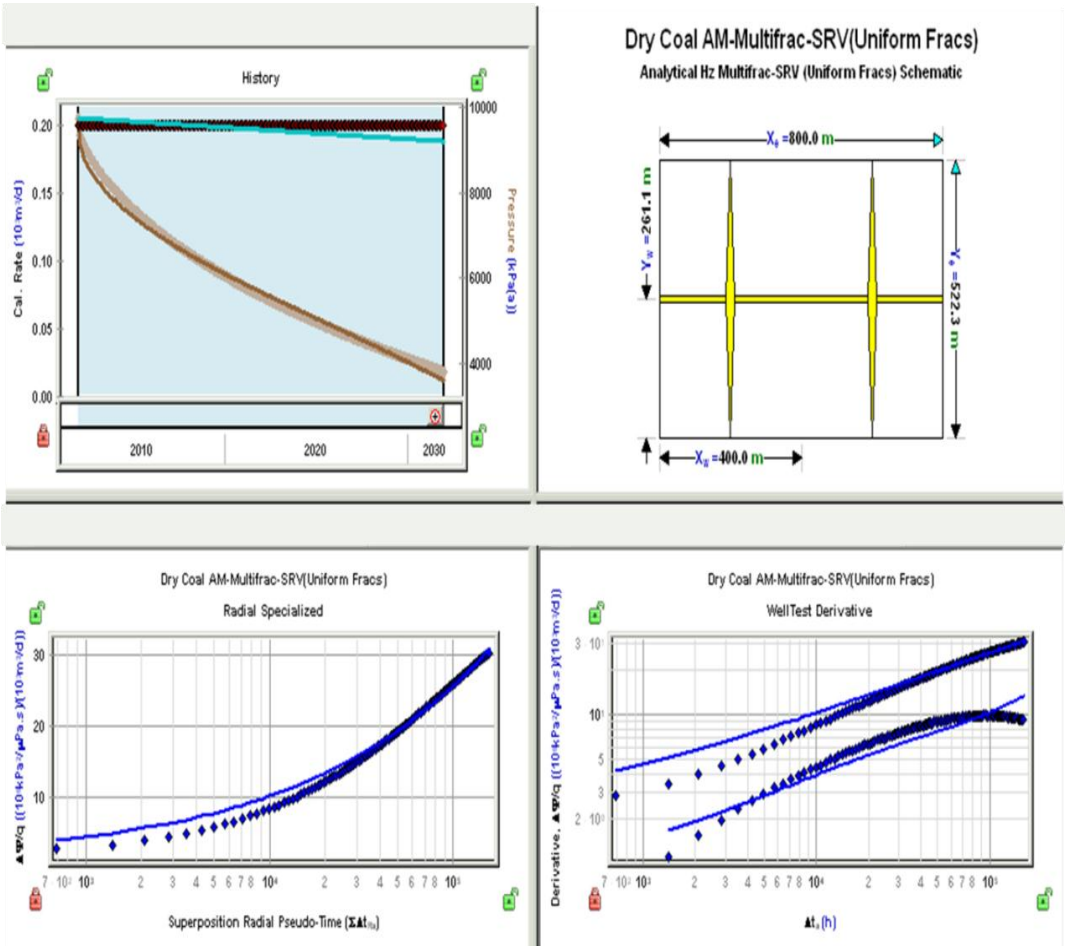

Figure D. 5 Fekete Horizontal Multifrac SRV (Uniform Frac-s) CBM Model for two stage hydraulic fracture - 200 m3/day production: a) history plot; b) SRV model Shematic c) semilog plot; d) RNP log-log derivative plot

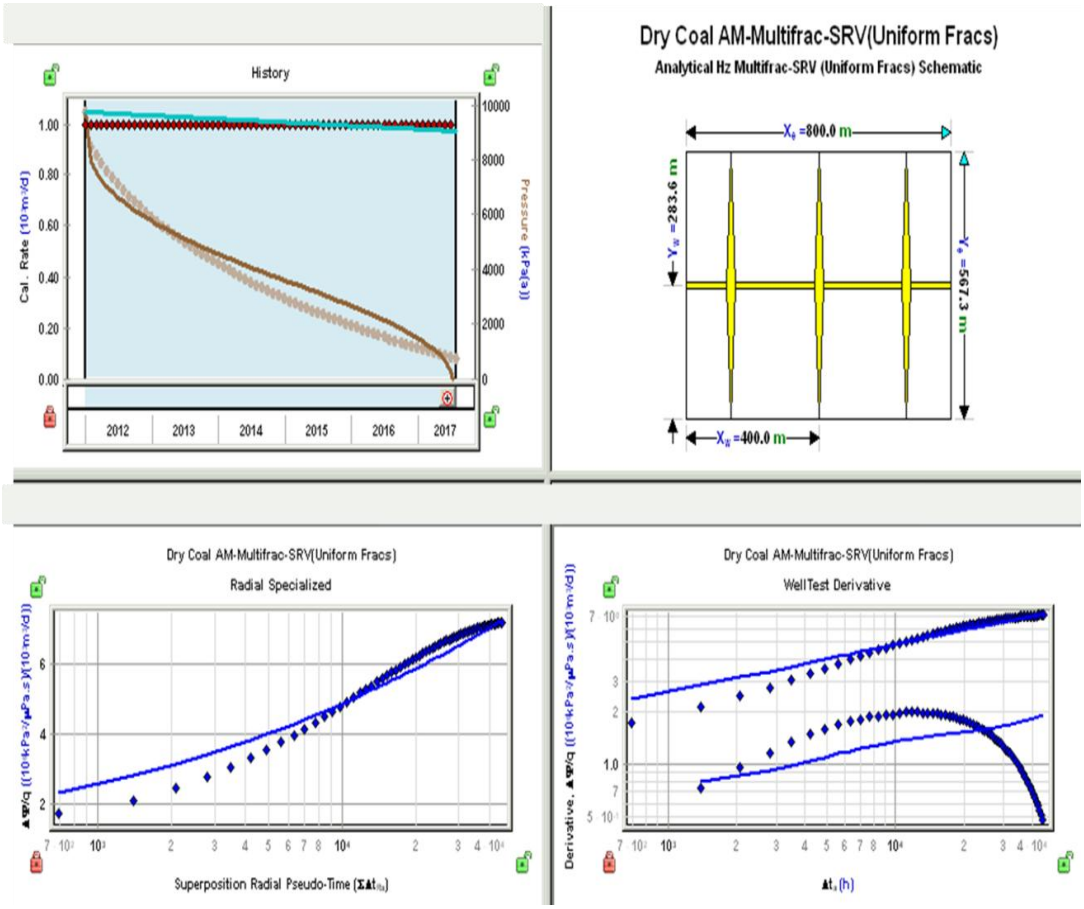

Figure D. 6 Fekete Horizontal Multifrac SRV (Uniform Frac-s) CBM Model for three stage hydraulic fracture - 1000 m3/day production: a) history plot; b) SRV model Shematic c) semilog plot; d) RNP log-log derivative plot

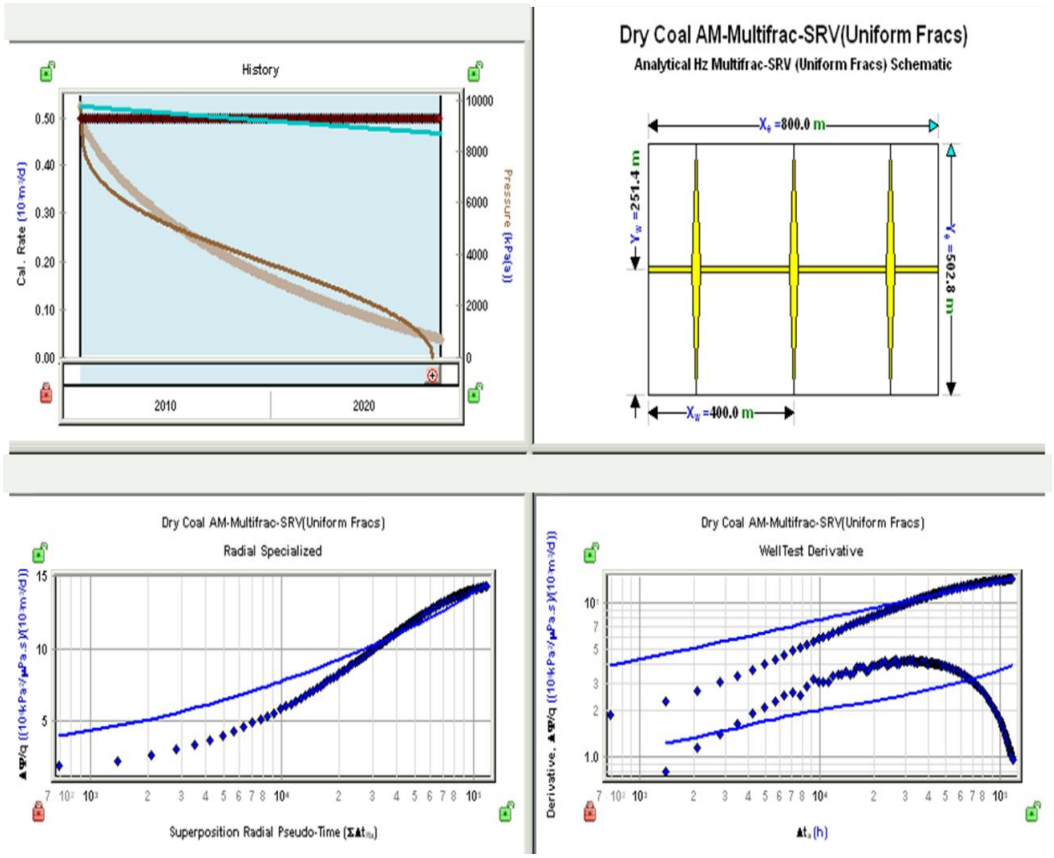

Figure D. 7 Fekete Horizontal Multifrac SRV (Uniform Frac-s) CBM Model for three stage hydraulic fracture - 500 m3/day production: a) history plot; b) SRV model Shematic c) semilog plot; d) RNP log-log derivative plot

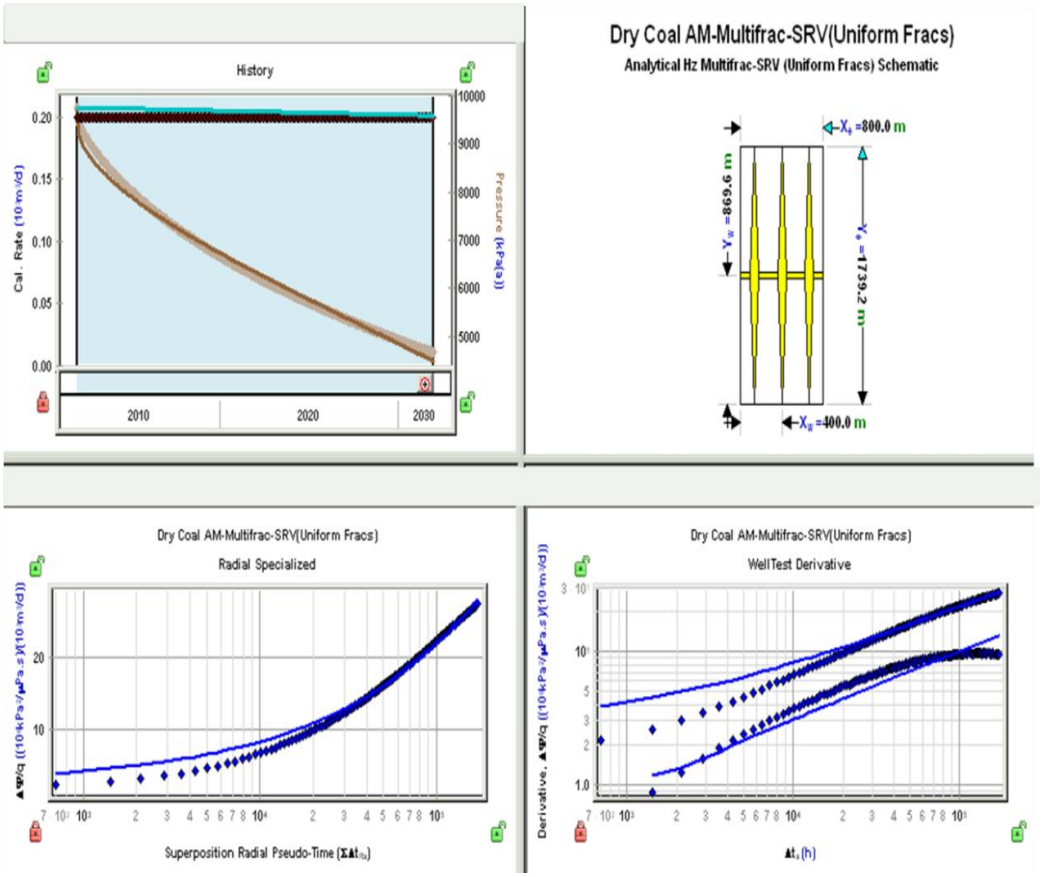

Figure D. 8 Fekete Horizontal Multifrac SRV (Uniform Frac-s) CBM Model for three stage hydraulic fracture - 200 m3/day production: a) history plot; b) SRV model Shematic c) semilog plot; d) RNP log-log derivative plot

APPENDIX E: HORIZONTAL MULTIFRAC GENERAL (GAS) MODEL RESULTS

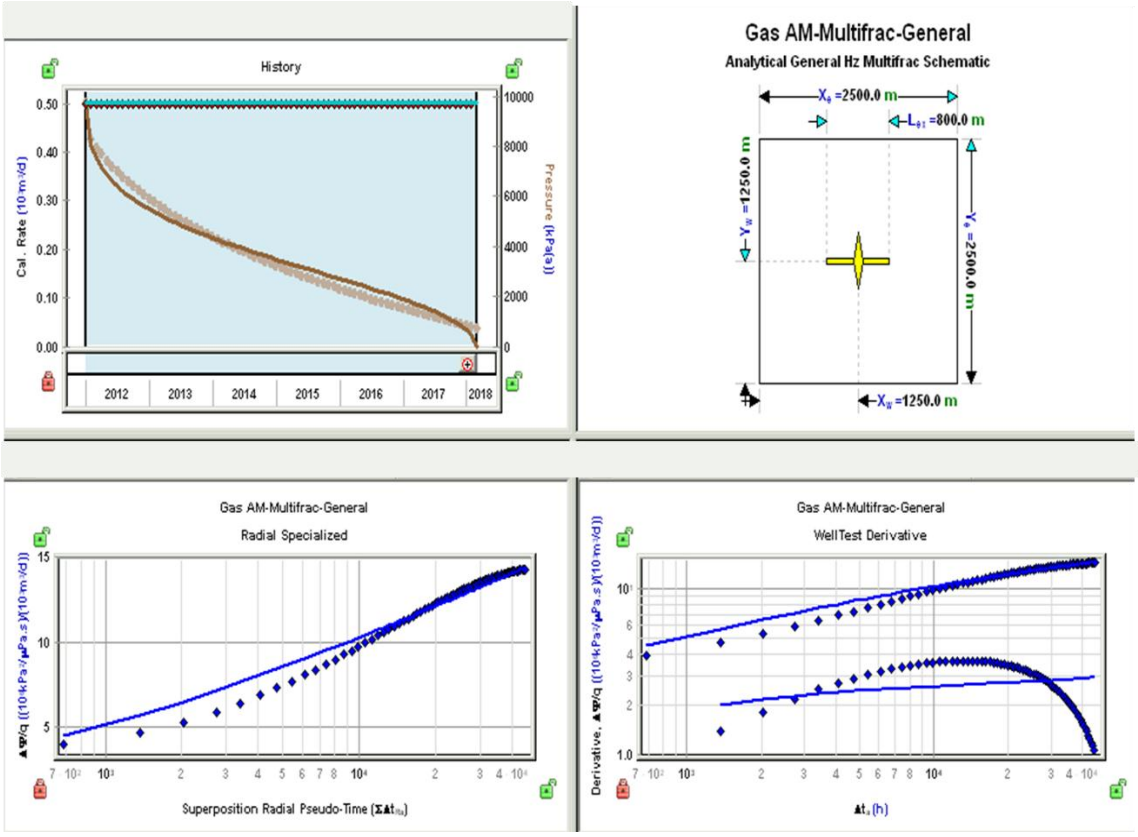

Figure E. 1 Fekete Horizontal Multifrac General Gas Model for single stage hydraulic fracture - 500 m3/day production: a) history plot; b) SRV model Shematic c) semilog plot; d) RNP log-log derivative plot

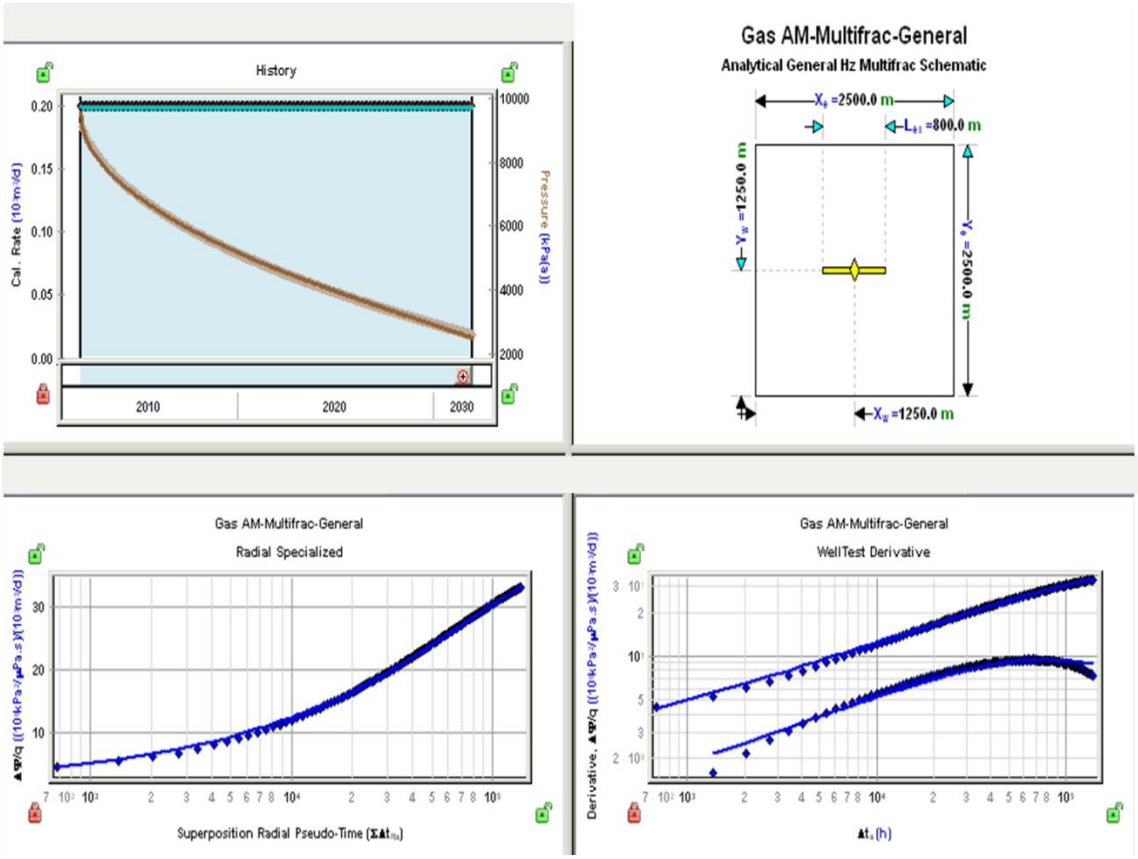

Figure E. 2 Fekete Horizontal Multifrac General Gas Model for single stage hydraulic fracture - 200 m3/day production: a) history plot; b) SRV model Shematic c) semilog plot; d) RNP log-log derivative plot

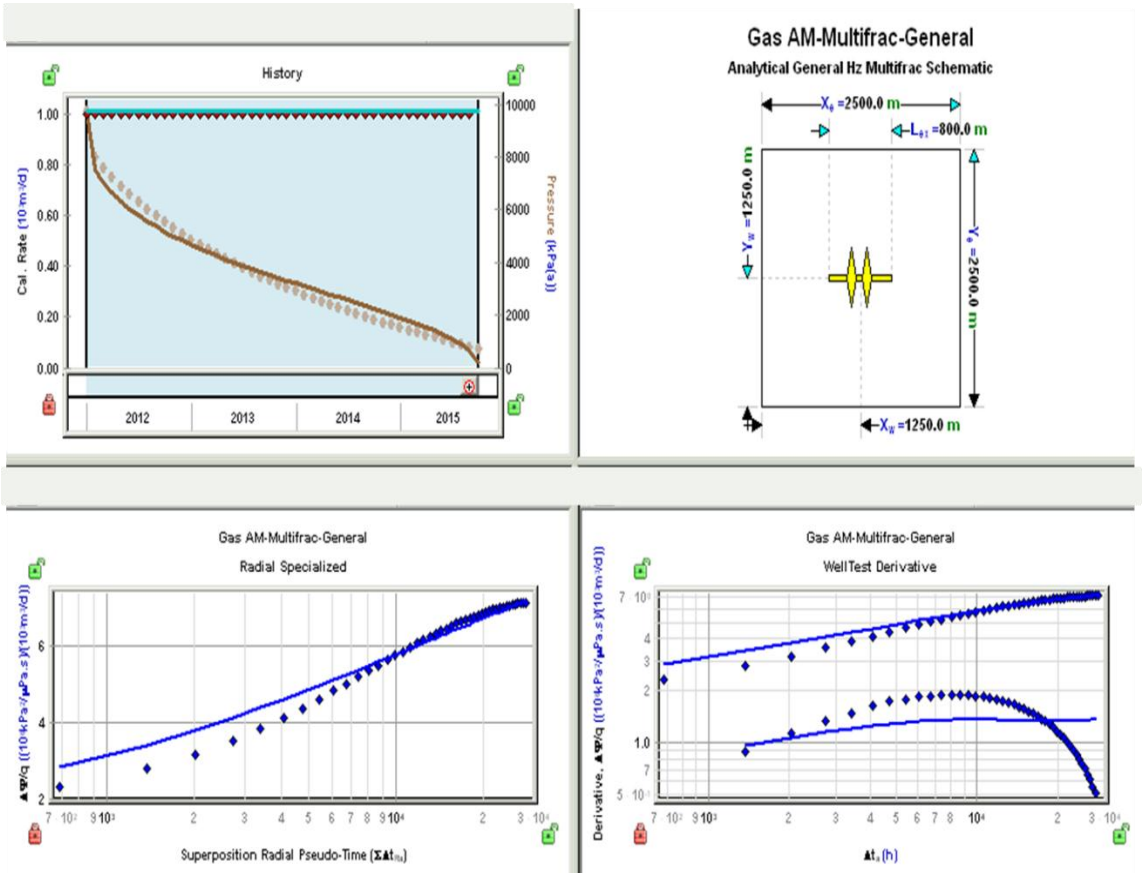

Figure E. 3 Fekete Horizontal Multifrac General Gas Model for two stage hydraulic fracture - 1000 m3/day production: a) history plot; b) SRV model Shematic c) semilog plot; d) RNP log-log derivative plot

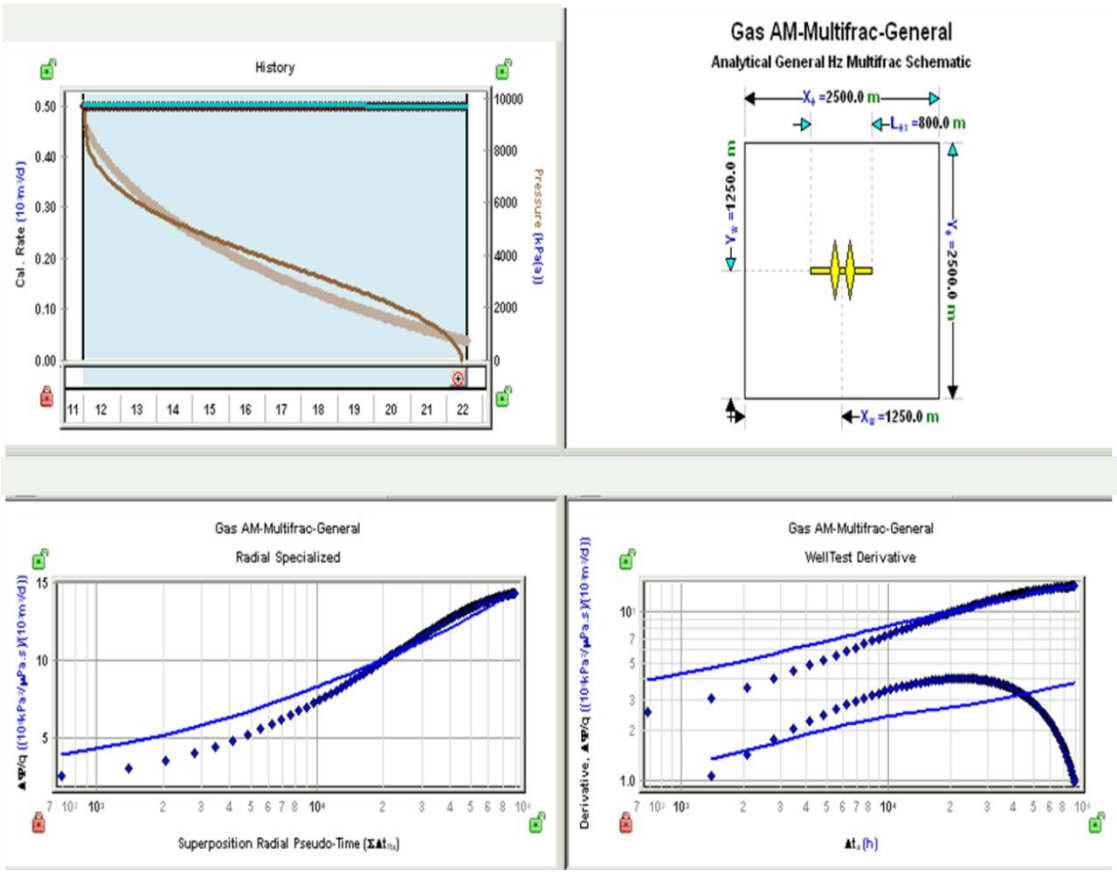

Figure E. 4 Fekete Horizontal Multifrac General Gas Model for two stage hydraulic fracture - 500 m3/day production: a) history plot; b) SRV model Shematic c) semilog plot; d) RNP log-log derivative plot

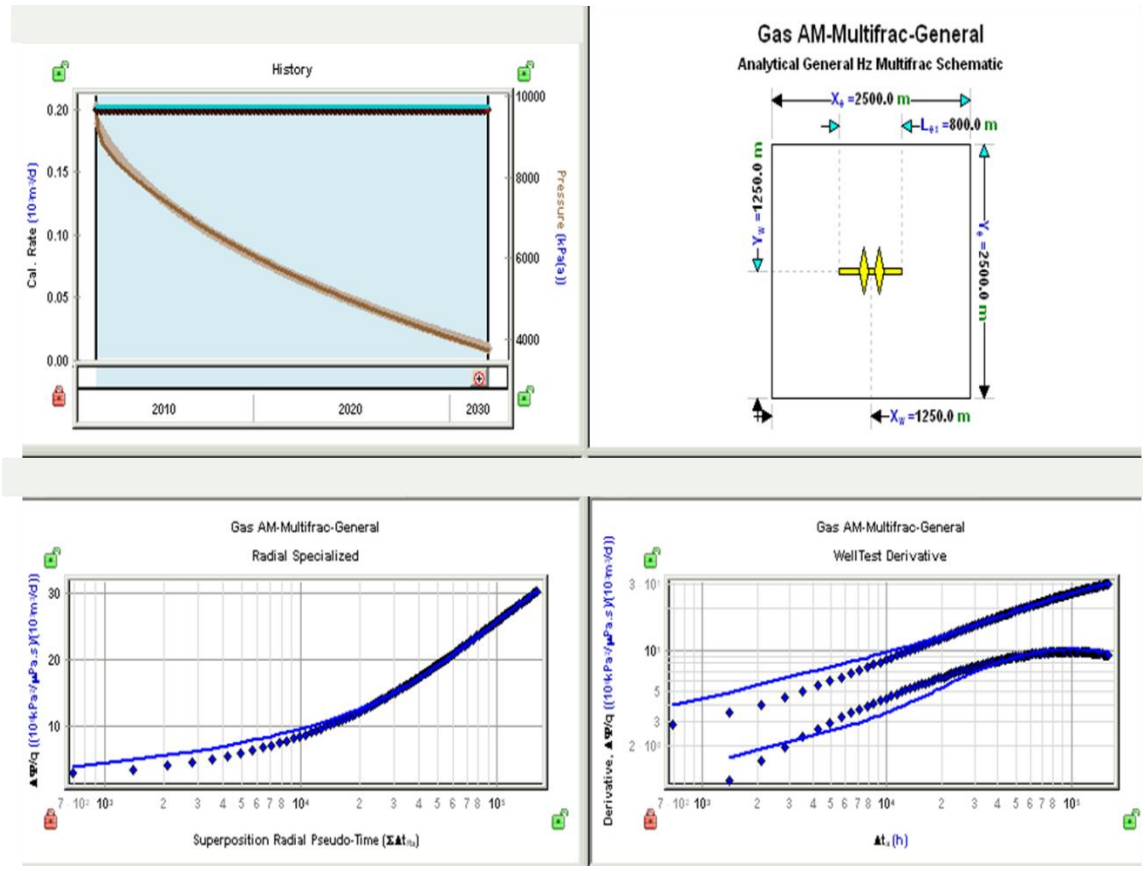

Figure E. 5 Fekete Horizontal Multifrac General Gas Model for two stage hydraulic fracture - 200 m3/day production: a) history plot; b) SRV model Shematic c) semilog plot; d) RNP log-log derivative plot

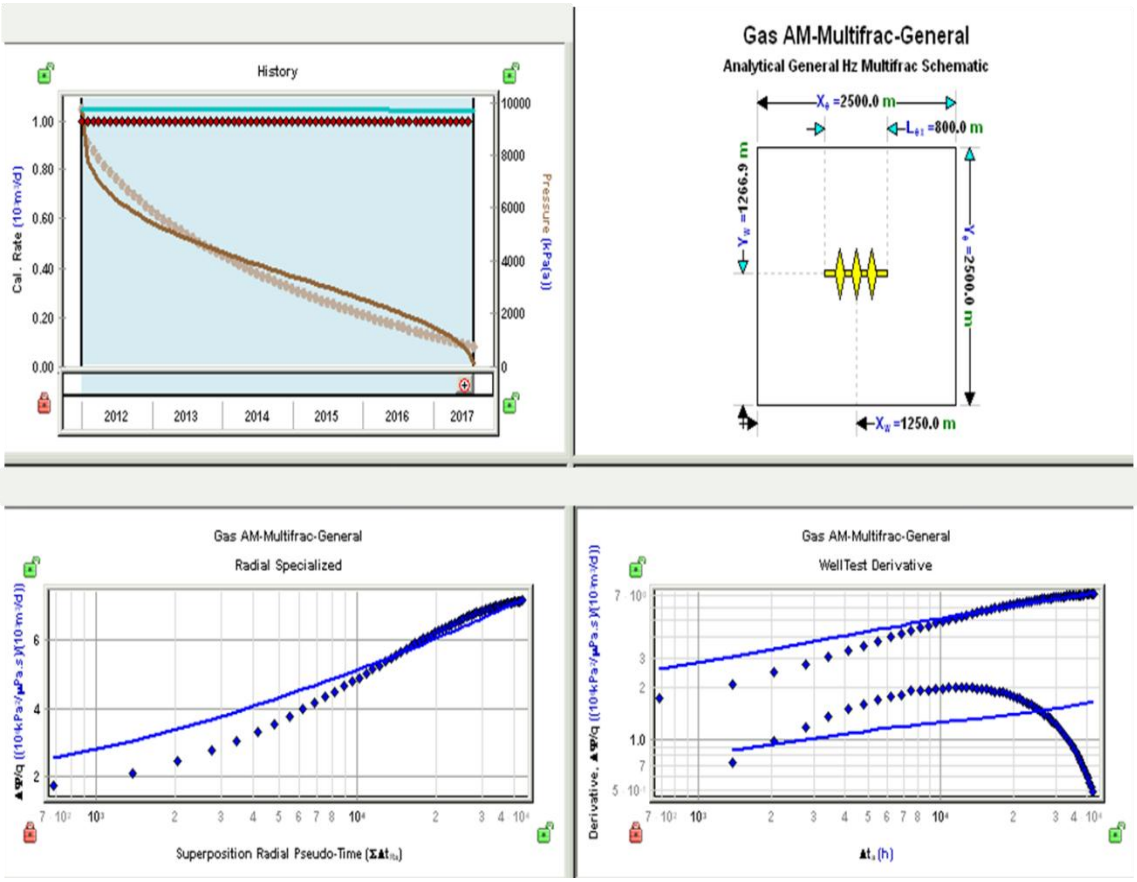

Figure E. 6 Fekete Horizontal Multifrac General Gas Model for three stage hydraulic fracture - 1000 m3/day production: a) history plot; b) SRV model Shematic c) semilog plot; d) RNP log-log derivative plot

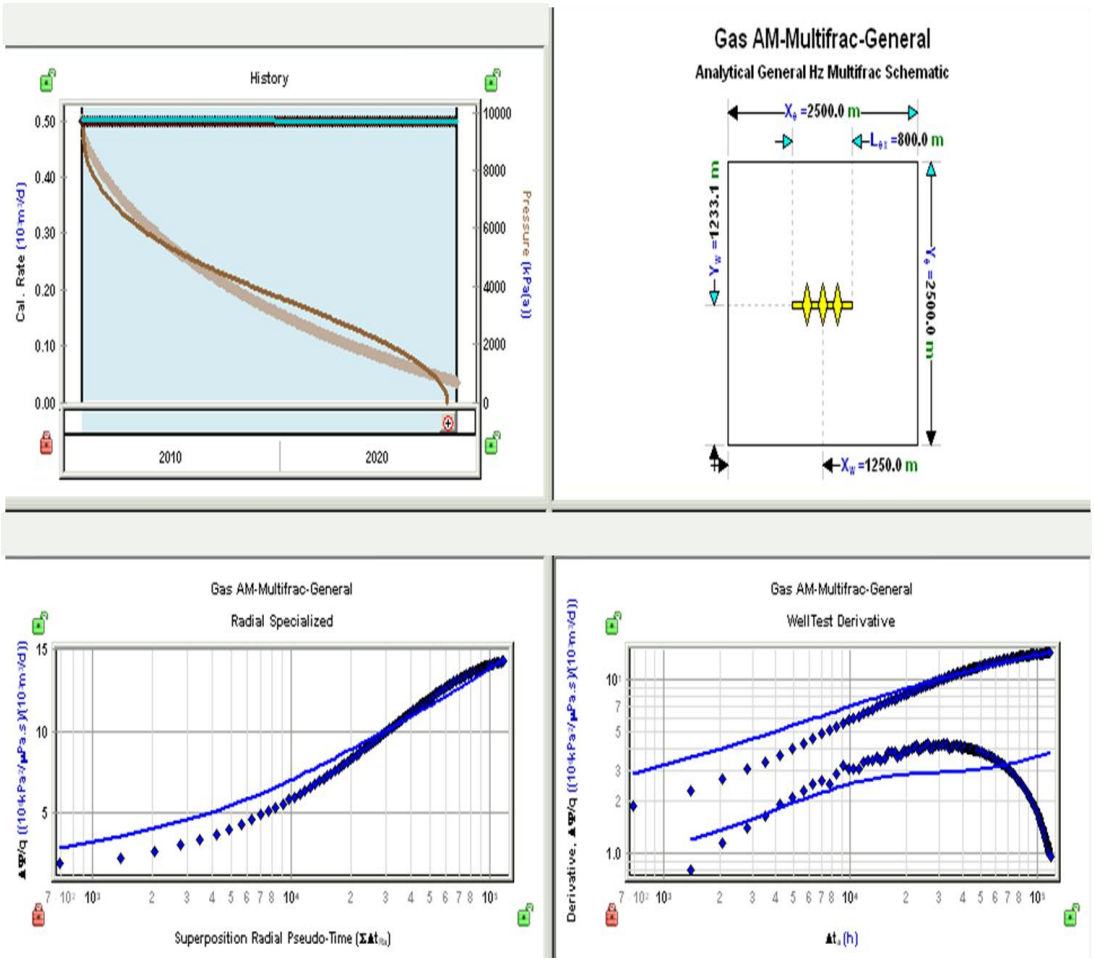

Figure E. 7 Fekete Horizontal Multifrac General Gas Model for three stage hydraulic fracture - 500 m3/day production: a) history plot; b) SRV model Shematic c) semilog plot; d) RNP log-log derivative plot

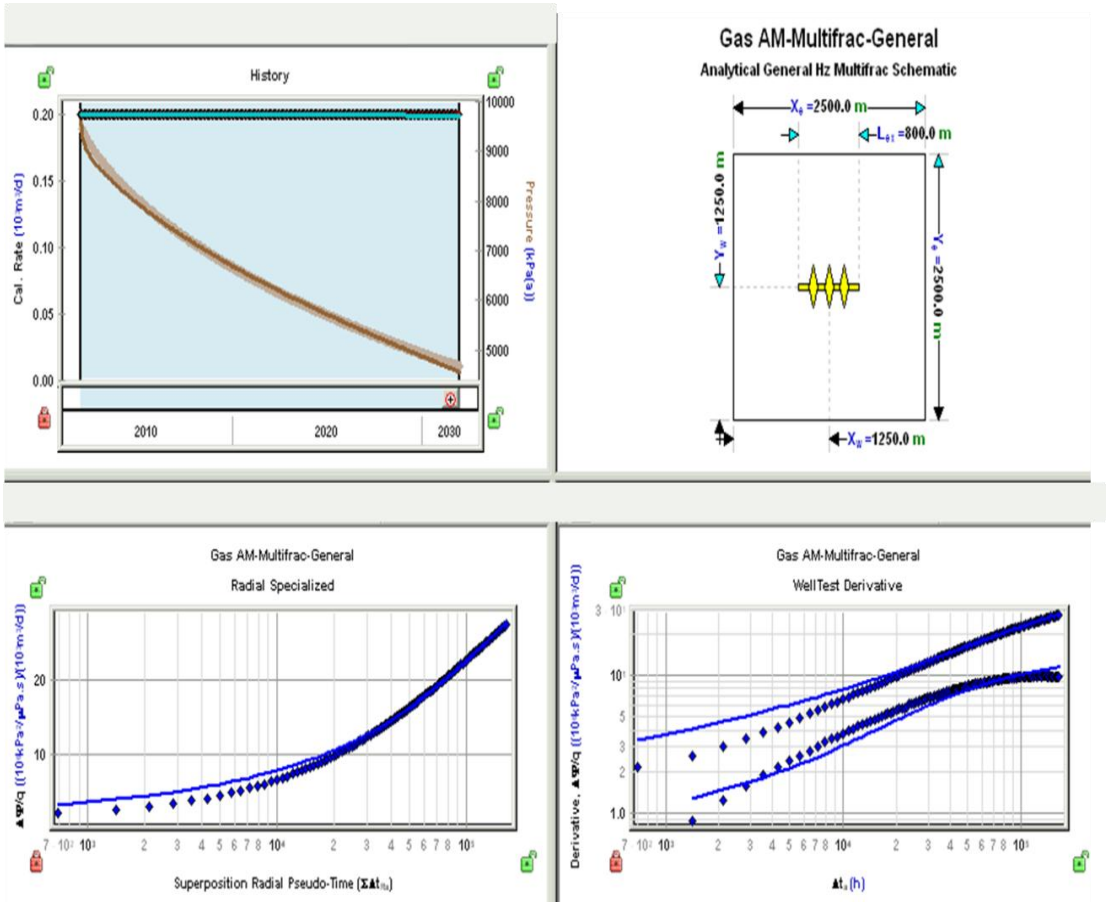

Figure E. 8 Fekete Horizontal Multifrac General Gas Model for three stage hydraulic fracture - 200 m3/day production: a) history plot; b) SRV model Shematic c) semilog plot; d) RNP log-log derivative plot

APPENDIX F: HORIZONTAL MULTIFRAC GENERAL (CBM) MODEL RESULTS

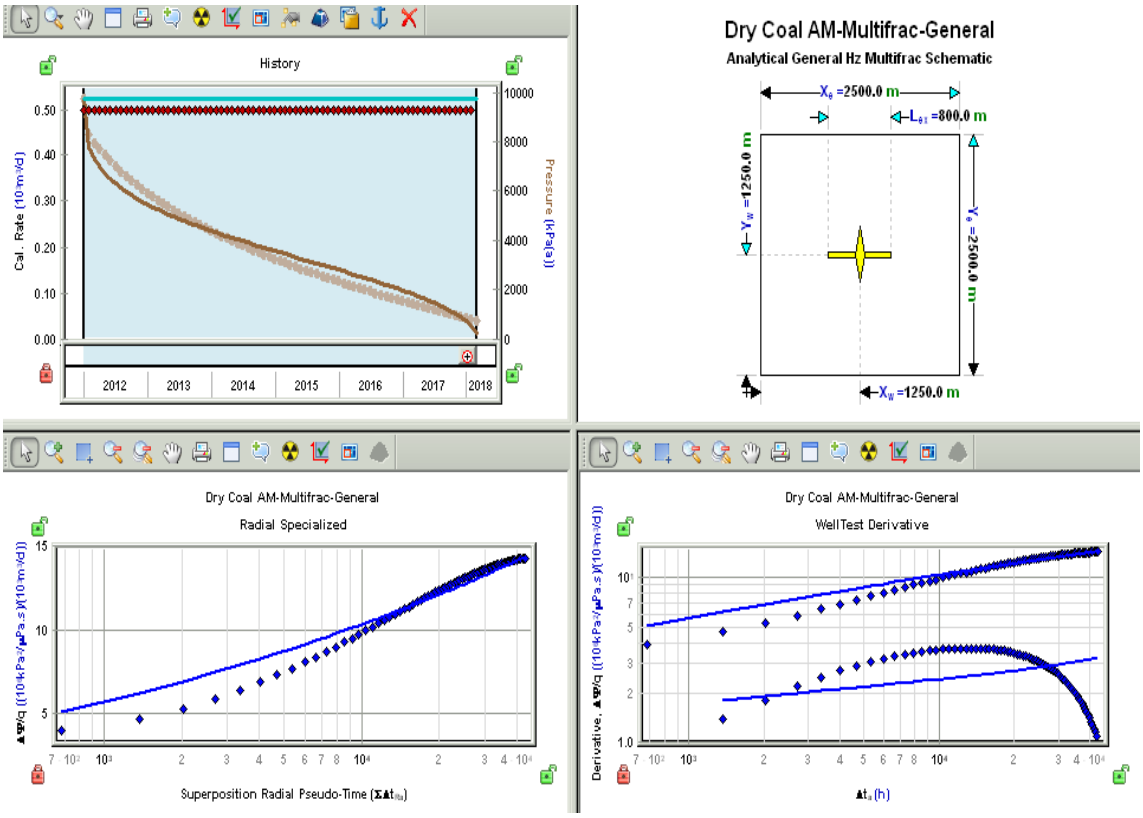

Figure F. 1 Fekete Horizontal Multifrac General CBM Model for single stage hydraulic fracture - 500 m3/day production: a) history plot; b) SRV model Shematic c) semilog plot; d) RNP log-log derivative plot

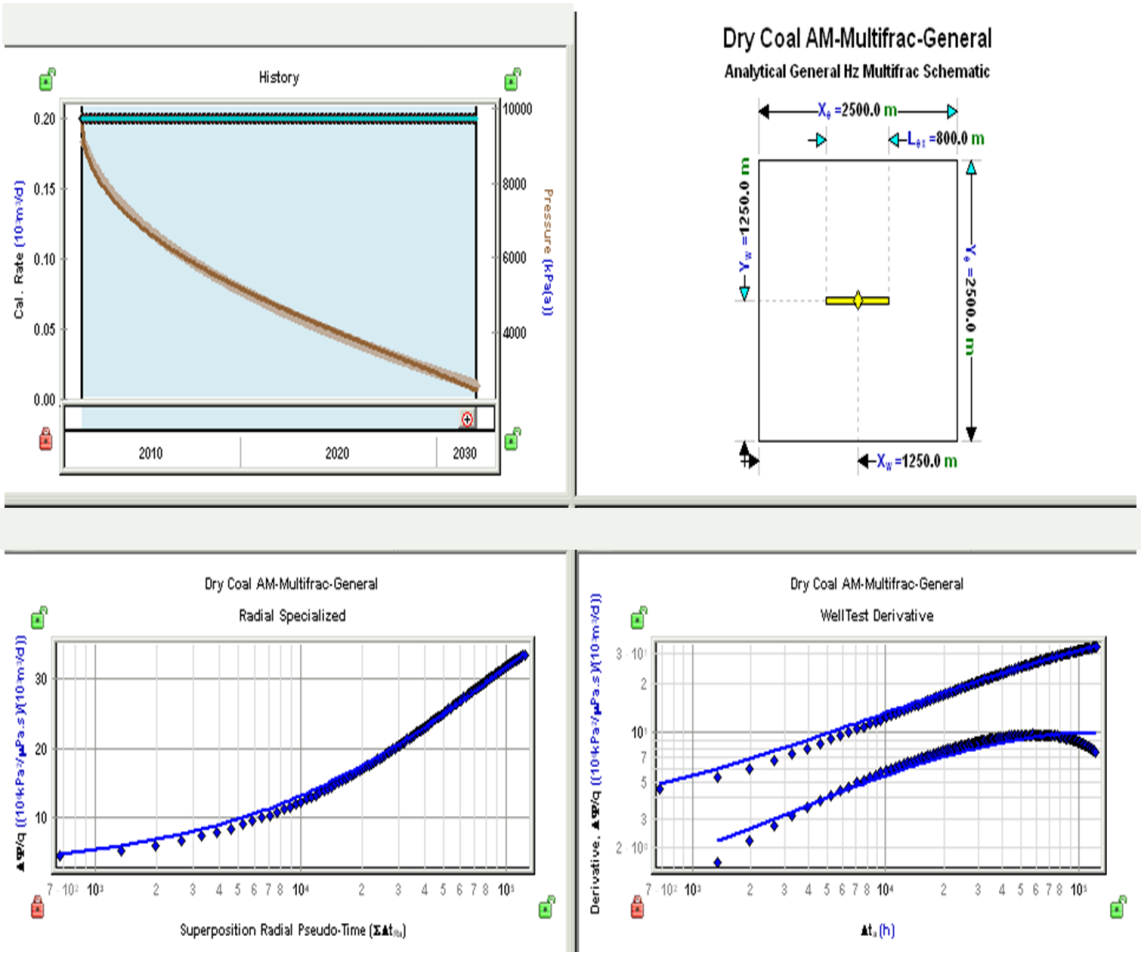

Figure F. 2 Fekete Horizontal Multifrac General CBM Model for single stage hydraulic fracture - 200 m3/day production: a) history plot; b) SRV model Shematic c) semilog plot; d) RNP log-log derivative plot

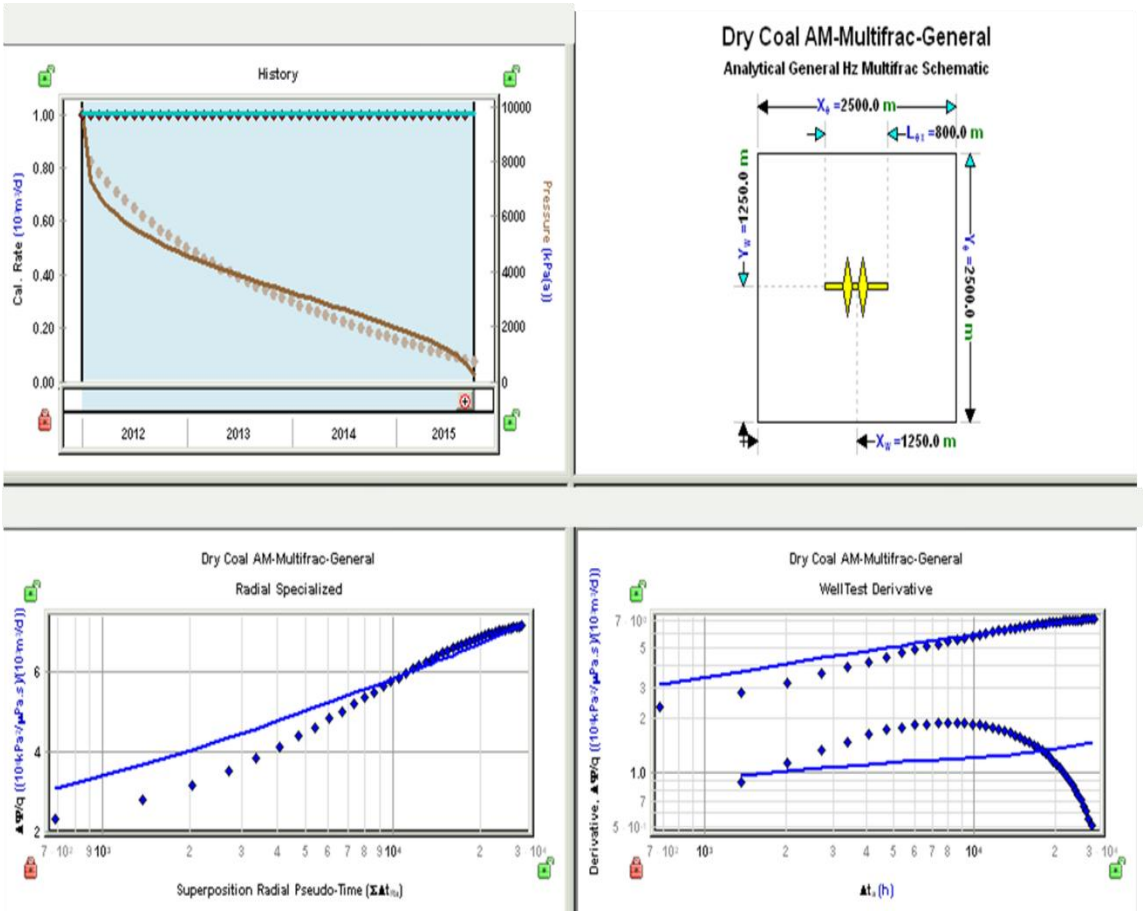

Figure F. 3 Fekete Horizontal Multifrac General CBM Model for two stage hydraulic fracture - 1000 m3/day production: a) history plot; b) SRV model Shematic c) semilog plot; d) RNP log-log derivative plot

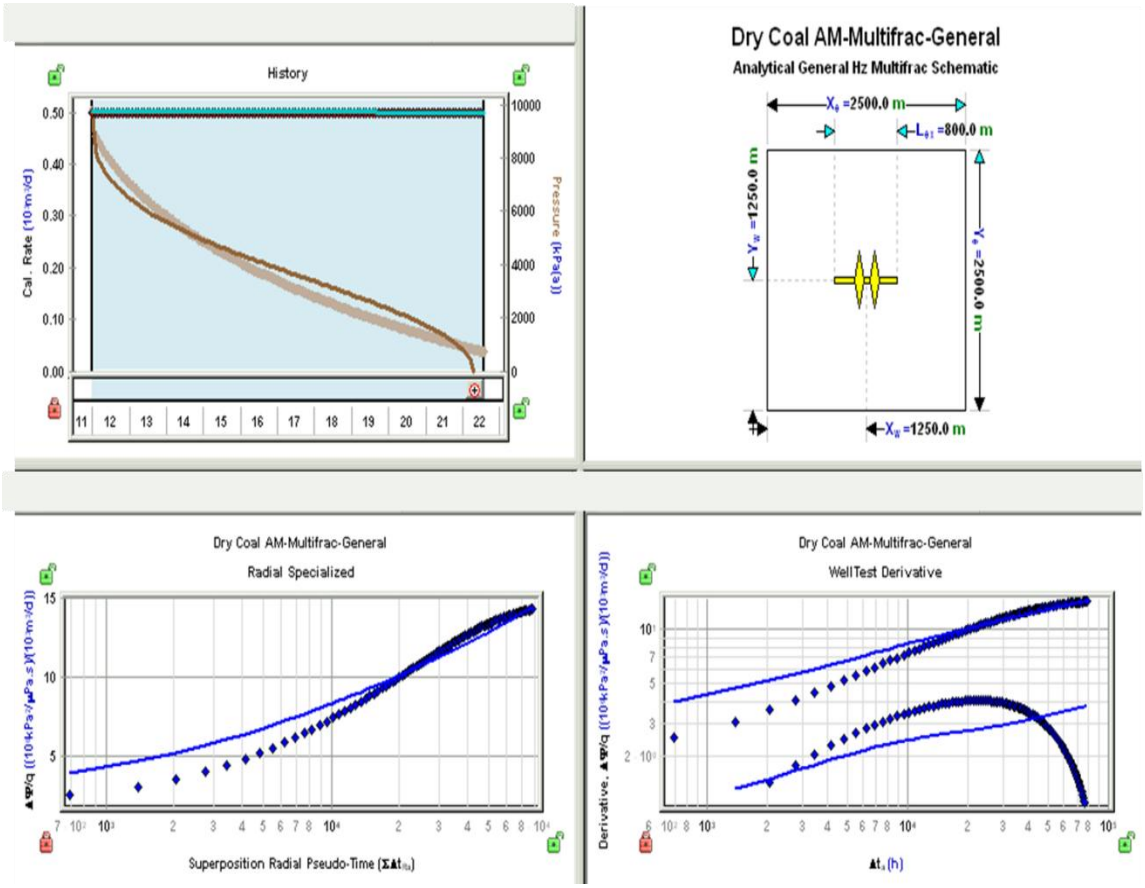

Figure F. 4 Fekete Horizontal Multifrac General CBM Model for two stage hydraulic fracture - 500 m3/day production: a) history plot; b) SRV model Shematic c) semilog plot; d) RNP log-log derivative plot

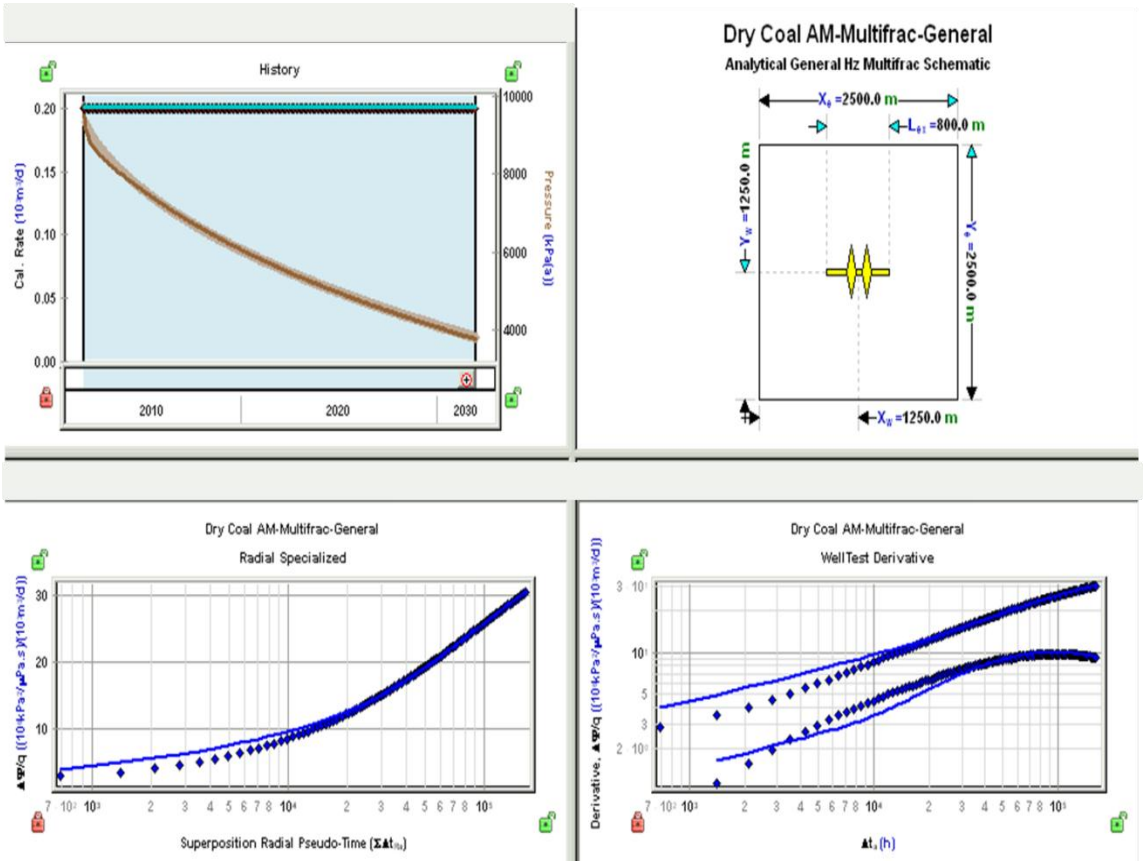

Figure F. 5 Fekete Horizontal Multifrac General CBM Model for two stage hydraulic fracture - 200 m3/day production: a) history plot; b) SRV model Shematic c) semilog plot; d) RNP log-log derivative plot

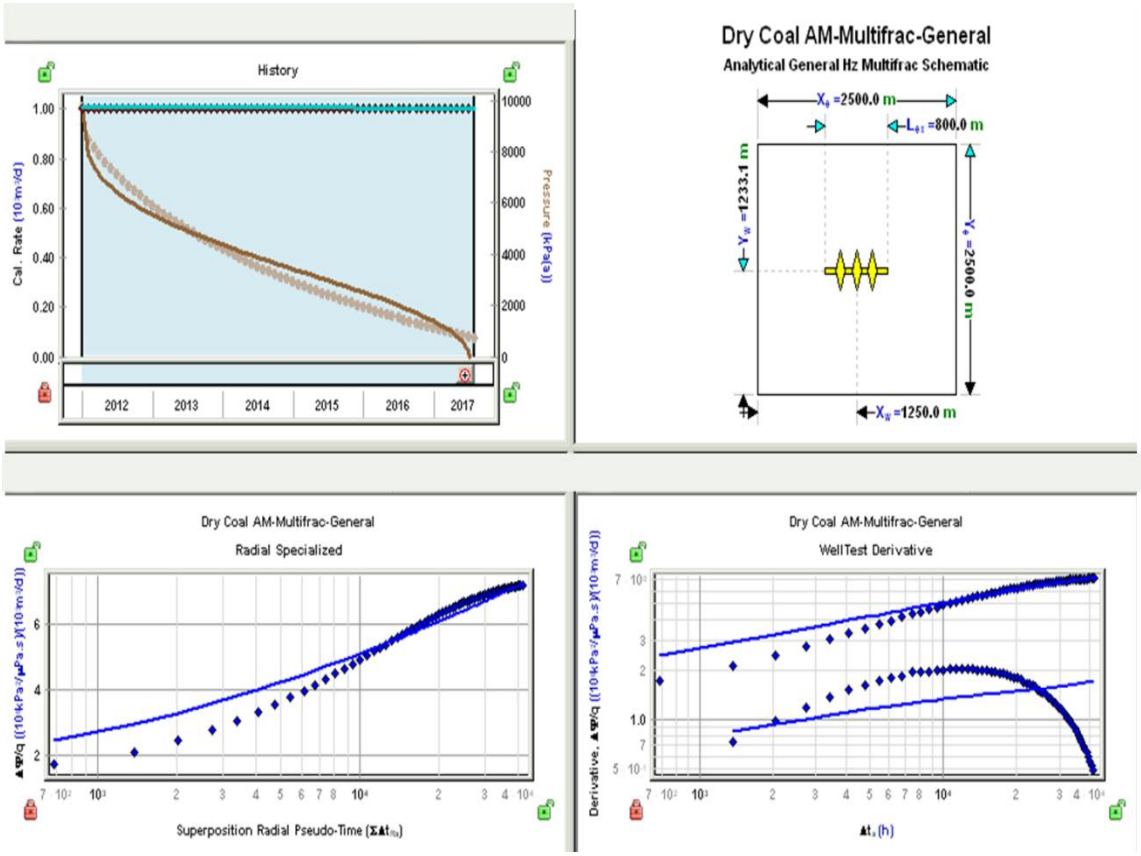

Figure F. 6 Fekete Horizontal Multifrac General CBM Model for three stage hydraulic fracture - 1000 m3/day production: a) history plot; b) SRV model Shematic c) semilog plot; d) RNP log-log derivative plot

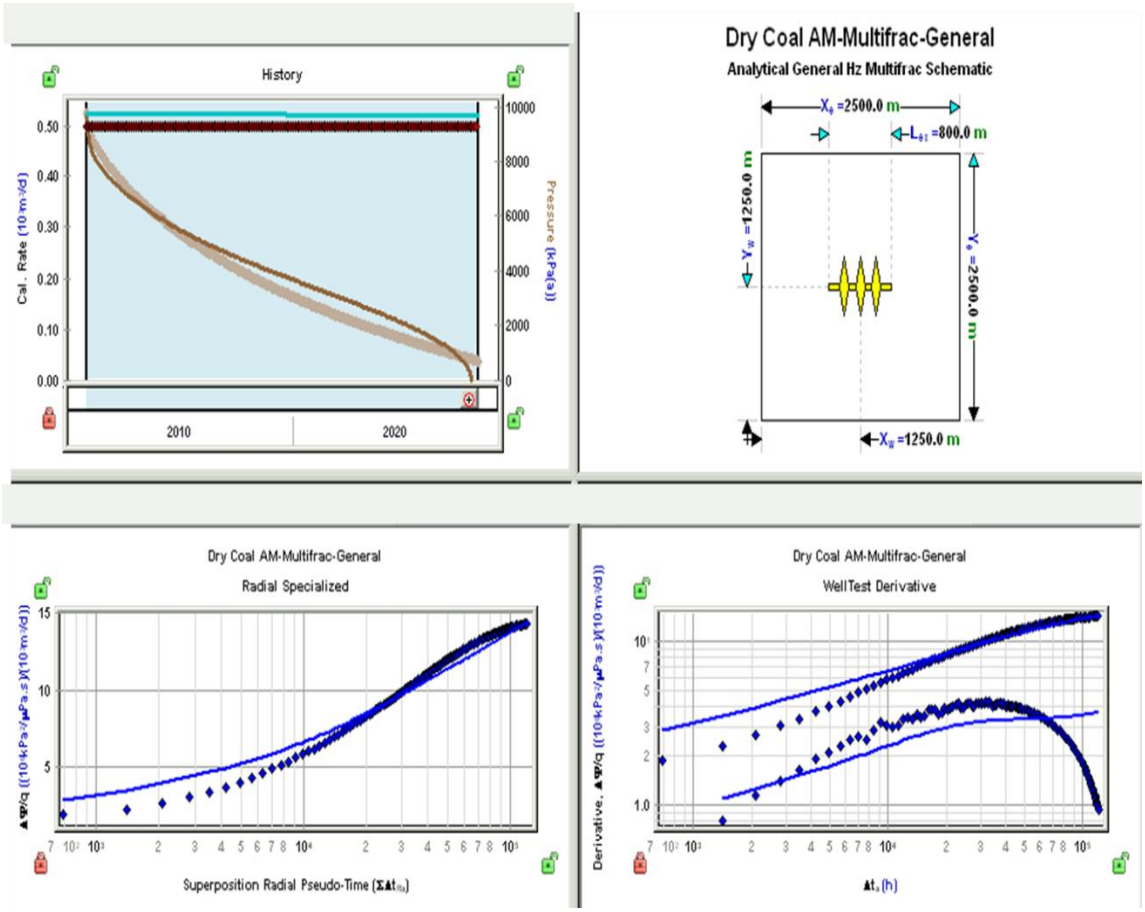

Figure F. 7 Fekete Horizontal Multifrac General CBM Model for three stage hydraulic fracture - 500 m3/day production: a) history plot; b) SRV model Shematic c) semilog plot; d) RNP log-log derivative plot

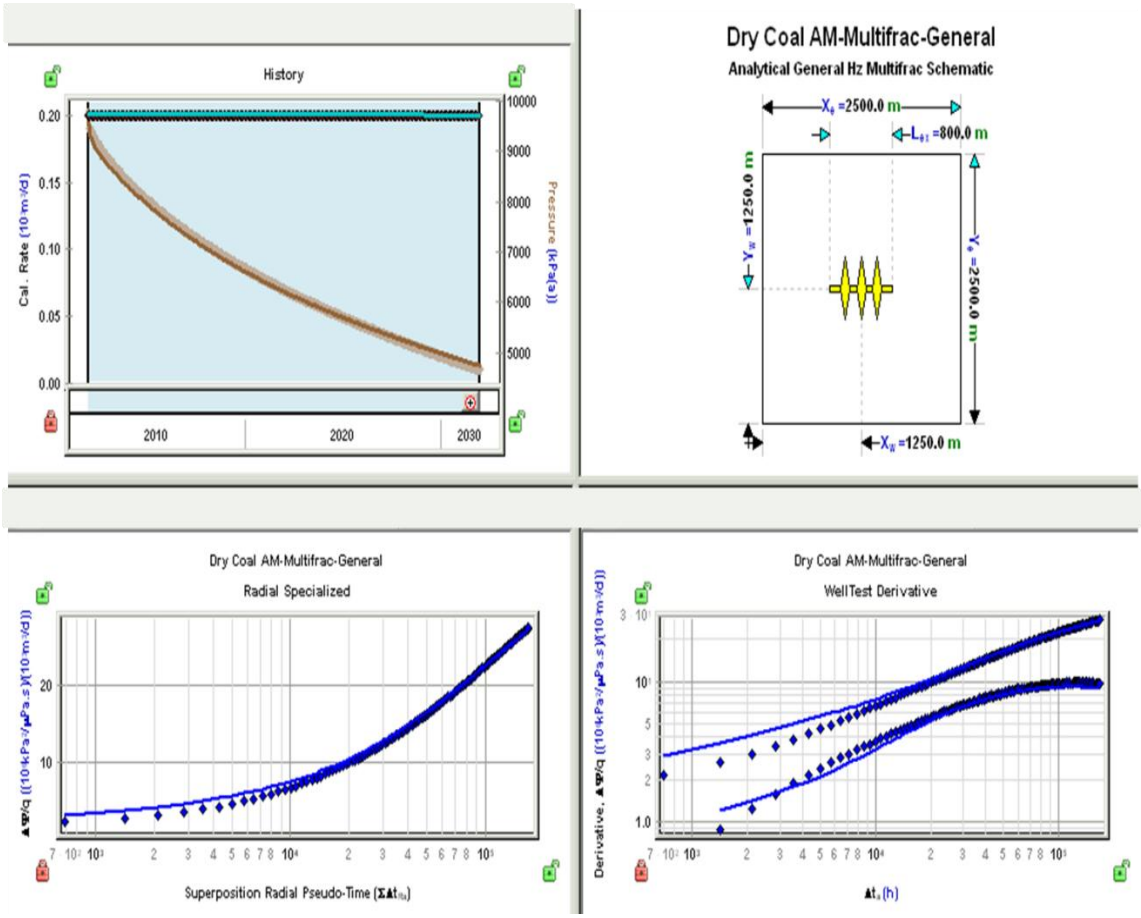

Figure F. 8 Fekete Horizontal Multifrac General CBM Model for three stage hydraulic fracture - 200 m3/day production: a) history plot; b) SRV model Shematic c) semilog plot; d) RNP log-log derivative plot

APPENDIX G: HORIZONTAL MULTIFRAC GENERAL (CBM) MODEL RESULTS

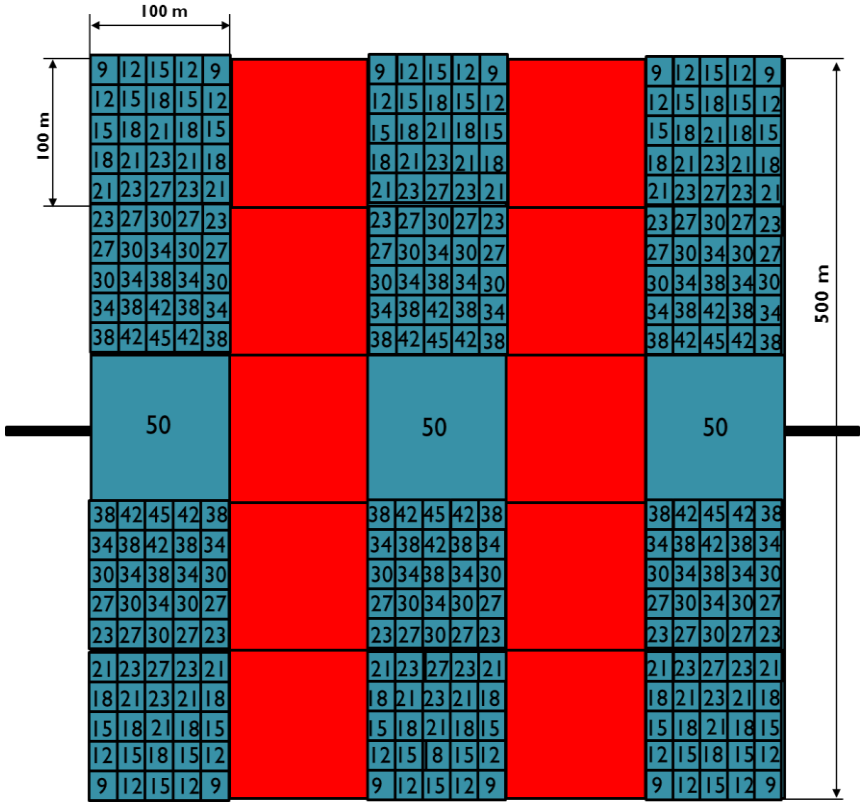

Figure G. 1 Permeability distribution for the refined grid blocks; blue- hydraulic fractured region, red – matrix (values are indicated in mD units)